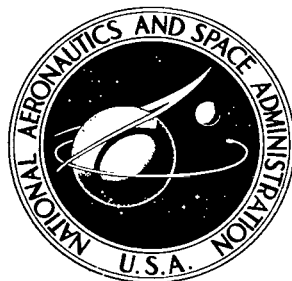


NASA TECHNICAL
REPORT



NASA TR R-289

C.1



LOAN COPY: RETURN TO
AFWL (WLIL-2)
KIRTLAND AFB, N MEX.

THEORY AND RESULTS ON
COLLECTIVE AND COLLISIONAL
EFFECTS FOR A ONE-DIMENSIONAL
SELF-GRAVITATING SYSTEM

by Frank Hohl
Langley Research Center
Langley Station, Hampton, Va.



TECH LIBRARY KAFB, N/



0068412

THEORY AND RESULTS ON COLLECTIVE AND COLLISIONAL EFFECTS
FOR A ONE-DIMENSIONAL SELF-GRAVITATING SYSTEM

By Frank Hohl

Langley Research Center
Langley Station, Hampton, Va.

NATIONAL AERONAUTICS AND SPACE ADMINISTRATION

For sale by the Clearinghouse for Federal Scientific and Technical Information
Springfield, Virginia 22151 - CFSTI price \$3.00

CONTENTS

	Page
SUMMARY	1
INTRODUCTION	1
SYMBOLS	3
THEORY OF SELF-GRAVITATING STELLAR SYSTEMS	6
Stationary Solutions	8
The Virial Theorem	9
Waterbag Distribution	10
Multiple-Contour Waterbag Distributions	13
Maxwellian Distribution	15
Energy Considerations	16
The Minimum-Energy Principle	18
Generalized Minimum-Energy Property	20
COMPUTER SIMULATION OF STELLAR SYSTEMS	22
Description of the One-Dimensional Model	23
Initial Distributions Near Equilibrium	27
Initial Distributions Far From Equilibrium	30
Initially "Cold" Systems	31
Unstable Stationary States	33
Thermalization Effects In a One-Dimensional Stellar System	34
CONCLUDING REMARKS	37
REFERENCES	40
FIGURES	43

THEORY AND RESULTS ON COLLECTIVE AND COLLISIONAL EFFECTS FOR A ONE-DIMENSIONAL SELF-GRAVITATING SYSTEM

By Frank Hohl
Langley Research Center

SUMMARY

The equilibrium properties of one-dimensional self-gravitating systems are investigated analytically. One-dimensional models are used to perform computer experiments tracing the evolution of stellar systems. The stationary solution of the Vlasov equation for a one-dimensional system of stars as computed for an interesting class of initial conditions is found to correspond to a minimum-energy configuration. The results of the numerical experiments are compared with theory. For initial energies far from the minimum equilibrium energy the system becomes unstable and breaks up into smaller clusters. A variational principle was applied to the one-dimensional stellar system to show that stationary distribution functions which decrease monotonically in going outward from the center of the system are stable. That other stationary distributions may be unstable is illustrated by means of computer experiments. The one-dimensional model is of interest as an approximation to the distribution of velocity and mass normal to the galactic plane of a greatly flattened galactic system. Observational results for the gravitational force normal to the galactic plane of the Galaxy agree with the results obtained from the one-dimensional model. Thermalization effects for systems containing small numbers of stars were investigated. The fluctuation of the kinetic energy was found to be inversely proportional to the square root of the number of particles in the system.

INTRODUCTION

Many problems in stellar dynamics involve phenomena occurring in inhomogeneous systems in which the interaction between the particles is fully described by a self-consistent field operating in phase space. Because the particles interact by means of the long-range Coulomb force, each particle is under the simultaneous influence of a large number of other particles. Therefore, stellar systems will respond to any perturbation in a collective manner, and a study of such systems is concerned essentially with the N-body problem.

The collective phenomena do not depend on two-body collisions such as occur in ordinary gases, and therefore the collective effects will be present in collisionless

systems. Since the number of particles in the system is large, a distribution function can be used to describe the density of particles in phase space. The distribution function must then satisfy the Vlasov equation (the self-consistent set of the Maxwell equations plus the collisionless Boltzmann equation). In using the Vlasov equation to describe a stellar system the number of masses which make up the system is assumed to become infinite while the total mass remains constant. Although such an approach allows description of the system by means of a distribution function which must satisfy the Vlasov equation, solutions to the time-dependent nonlinear Vlasov equation are, in general, very difficult to obtain. An attempt is therefore made to condense the 10^{11} stars which a galaxy may contain into about 10^3 superparticles. Numerical or computer models are then used to perform computer experiments simulating Vlasov phenomena by following the simultaneous motion of a number of superparticles of the order of 10^3 . One-dimensional models are used to effectively solve the time-dependent nonlinear Vlasov equation for various systems.

Computer models used to study plasmas and stellar systems are essentially of two types. The first type is the Lagrangian model in which the self-consistent motion of large numbers of particles in phase space is followed. In such a model the number of particles which can be treated is limited by computer storage and time. The second type of computer model is the Eulerian model in which the system behaves like a fluid in phase space. The macroscopic quantities describing the system are then obtained by solving the appropriate partial differential equations on the computer. In the present study the main interest is in systems which can be described by the Vlasov equation. However, it was found advantageous to use a Lagrangian model to simulate the time development of the systems investigated. Thus, the main interest is not in solving the Vlasov equation for the macroscopic quantities describing a system but rather in performing numerical experiments by solving the N-body problem.

Direct solutions of the N-body problem have become possible only with the advent of high-speed electronic computers. Since the pioneering work of Pasta and Ulam (ref. 1), many workers have used computer models in their investigations of the N-body problem.

The simplest system of stars which can be considered is a one-dimensional system with the stars stratified into plane parallel layers. All parameters then vary only in one direction. With the exception of the work done by Lecar (ref. 2) with small numbers of sheets, the author is not aware of any previous numerical experiments to simulate stellar systems with a one-dimensional sheet model. Hénon (ref. 3) used a computer model of concentric spherical mass shells to study the dynamical mixing of spherical star clusters. Recently, Hockney (ref. 4) and Hohl (ref. 5) have used two-dimensional rod models to simulate a cylindrical galaxy. The results obtained with the two-dimensional model show that filamentary and spiral structure can be obtained by purely

gravitational effects. However, these calculations should be repeated by using point masses confined to move in a plane. Lindblad (ref. 6) calculated the two-dimensional motion of a number (up to 192) of mutually attracting mass points in a given central field of force. By placing the mass points initially in a system of concentric rings with circular velocities, Lindblad investigated the mutual disturbances in such a system to simulate the spiral structure of galaxies. The remaining numerical calculations in stellar dynamics appear to be three-dimensional calculations for systems with small numbers of stars. Thus, von Hoerner (refs. 7 and 8) made extensive calculations with up to 25 stars. In such a system the effects of the individual encounters are large and cannot be smoothed by averaging over many calculations. Aarseth (ref. 9) performed similar three-dimensional calculations with up to 100 stars and applied the results to clusters of galaxies. The irreversibility in stellar systems with up to 32 stars was investigated by Miller (ref. 10).

SYMBOLS

A	constant defined by equations (19) and (42)
a	acceleration
a_{ij}	matrix elements defined by equation (85)
C	energy correlation function
c	speed of light in vacuum
D	Debye length, $v_T(4\pi G\rho)^{-1/2}$
E	gravitational field
F	energy distribution function
f	distribution function
G	gravitational constant
g	total energy density
g_p	potential energy density

\mathcal{E}_T	kinetic energy density
H	Heaviside unit step function
M	mass
m	mass per unit area
N	total number of particles in system
n	particle density
P	potential energy
r	radial coordinate
T	kinetic energy
t	time
U	total particle energy, $\frac{1}{2}mv^2 + m\phi$
V_+, V_-	contours defined in figure 2
V_n	normalized equilibrium contour
v	velocity
v_T	thermal velocity
$W = T + P$	
x	position coordinate
x'	position defined by $\phi(x') = \epsilon_0$
z	dummy variable
α	constant defined as $16\pi G_K m^2 A \sqrt{\frac{\pi}{2m\kappa}}$ and variable used in equation (66)

δ	Dirac delta function
ϵ	potential energy defined by equation (22)
ϵ_1, ϵ_2	energies defined by equation (118)
ξ	integration variable
η	function used in variational method
θ	variable, $\int_{-x_s}^x V_+(x) dx$
κ	thermal energy
μ	relative fluctuation of kinetic energy
ν	energy ratio
ρ	mass density
τ	dimensionless time
τ_c	characteristic period, $(4\pi G\rho)^{-1/2}$
Φ	dimensionless gravitational potential
φ	gravitational potential
χ	dimensionless position coordinate
χ'	dimensionless position coordinate defined by $\Phi(\chi') = \nu$
$\langle \rangle$	time-averaged quantity

Subscripts:

eq	equilibrium
i,j,k,n	summation indices

min	minimum
o	initial
s	system boundary

Superscript:

k	summation index defining waterbag contours or ordering index
---	--

THEORY OF SELF-GRAVITATING STELLAR SYSTEMS

The analytical portion of the present study is confined to an investigation of steady states for stellar systems. A computer model is used to simulate the time behavior of the system and to study its approach to an equilibrium state. The simplest star system is one in which the stars are stratified into plane parallel layers. The velocity distribution and density then vary only in one direction. For such a model the stars can be represented by a large number of mass sheets. The motion of such sheets is sufficiently simple that the trajectories of several thousand stars can be followed on an electronic computer. Thus numerical experiments to investigate the evolution of a stellar system can be performed and the results compared with the equilibrium conditions obtained from the Vlasov equation.

As indicated by Michie (ref. 11) the importance of orbital (or phase) mixing in the initial evolution of a system of stars needs to be investigated. As the system of stars evolves, the gravitational field changes with time and the stars follow complicated trajectories along which the individual stellar energies are not conserved. Hénon (ref. 3) has recently performed numerical experiments with a system of concentric spherical shells to study the relaxation of the mean gravitational field and the resulting approach to equilibrium for a spherically symmetric star cluster. The analogy between models in which the material is stratified in parallel planes and those in which the material is distributed in concentric spherical shells has been examined by Woolley (ref. 12).

According to Oort (ref. 13) the velocities of stars normal to the galactic plane are decoupled from the other velocity components. Since the force on a star is approximately normal to the galactic plane, the stars will oscillate perpendicular to the galactic plane with a period independent of the revolution of the galactic system. A one-dimensional model representing a system stratified in infinite parallel planes can therefore be used as an approximation to the distribution of velocity and density of stars normal to the galactic plane of a greatly flattened galactic system. Camm (ref. 14) has considered steady solutions of the collisionless Boltzmann and the Poisson equations for such a model,

and his results compared favorably with the observed densities. More recently Lindblad (ref. 15), Woolley (ref. 16), and Oort (ref. 17) have used a one-dimensional analysis to study greatly flattened galactic systems. Prendergast (ref. 18) has investigated the general solutions of the steady-state one-dimensional self-gravitating system.

The present study is concerned primarily with the conditions under which a system will approach a stationary state and for which a system will become unstable and break up into smaller systems. The relaxation, or characteristic, time for a system of stars is given by

$$\tau_c = (4\pi G\rho)^{-1/2} \quad (1)$$

where G is the gravitational constant and ρ is the mass density. The characteristic length of interest is the Jeans or Debye length D which is defined by

$$D = v_T \tau_c \quad (2)$$

where v_T is the thermal velocity of the system of stars. The dimension of a system of stars near equilibrium is of the order of a Debye length. Thus, for a three-dimensional system the number of stars within the Debye sphere is very large, that is, $nD^3 \gg 1$ where n is the average density of stars. For example, a galaxy contains somewhere from 10^8 to 10^{12} stars so that $nD^3 \approx 10^8$ to 10^{12} . Similarly, for the one-dimensional model the number of stars in a Debye length is large, or $nD \gg 1$. The effects of collisions between individual stars can then be neglected, inasmuch as the distance traveled by a star before collisions significantly modified the star's trajectory is much larger than the dimension of the system (that is, the Debye length of the system). Thus, an actual stellar system as well as the one-dimensional model is well within the Vlasov regime. For $nD \gg 1$, the numerical experiments using the one-dimensional model should simulate the time development of the distribution function as given by the Vlasov equation.

It should be mentioned that computer calculations such as those performed by von Hoerner (refs. 7 and 8) and by Aarseth (ref. 9) involving the three-dimensional motion of up to 100 stars are not described by the Vlasov equation.

In the one-dimensional model the forces between the sheets are long range and the sheet model includes individual as well as collective behavior of the stars since the computer simply solves the equations of motion of the stars in the system. The exact behavior of a system depends on the graininess and will be affected by going to the "fluid limit" as implied by the Vlasov equation. As shown in a subsequent section, equivalent models with different graininess (or collisions) give identical results for any time scales of present interest; thus, graininess has a negligible effect on the system. Also, since the collective behavior is not affected in going to the fluid limit, good agreement can be expected between the "experimental" results and the theoretical results obtained from the Vlasov equation for the steady state of the system.

The phrase "metaequilibrium" refers to the equilibrium state which is established by the interaction of the stars with the smoothed potential of the system in a time of the order of $2\pi\tau_c$. The metaequilibrium can be considered a steady state only as long as graininess or collisions can be neglected. On a long time scale, binary encounters eventually cause the system to approach a state of statistical or thermal equilibrium. An actual three-dimensional stellar system can never completely attain a state of statistical equilibrium since this would involve a Gaussian velocity distribution. The absence of a potential barrier outside an actual stellar system permits the escape from the system of all stars with positive energies. Thus, the escape of stars will prevent the establishment of a Gaussian distribution necessary for a state of statistical equilibrium. Nevertheless, the time constant with which the three-dimensional system will tend toward a state of statistical equilibrium (even though it can never be completely attained) is of the order $nD^3\tau_c$, where n is the density of stars. This time is of the same order of magnitude as the time constant involved in Chandrasekhar's (ch. II of ref. 19) calculation of the dynamical friction. For the one-dimensional model the behavior is different because of the potential barrier outside the system. Fluctuations due to graininess may now cause the establishment of a state of statistical equilibrium in a time which is at least of the order of $(nD)^2\tau_c$.

Lecar (ref. 2) has performed numerical integrations of a one-dimensional system of stars and has shown that no thermalization exists to order $nD\tau_c$. For a plasma without an external electric field this has been shown analytically by Eldridge and Feix (ref. 20). Presently, only times of order τ_c are of interest, during which collisional effects will be negligible.

Comparison of the gravitational fields acting on stars in a one-, two-, and three-dimensional system shows that they are very similar with the exception of the field acting on stars near the boundary of the system. Figure 1 shows the gravitational field for a one-, two-, and three-dimensional system with constant density. Because of the $1/r^2$ dependence of the field outside the three-dimensional system, stars can escape; this is not possible for the one-dimensional system. However, inside the system the force on a star in all three systems is proportional to the distance from the star to the center of the system.

Stationary Solutions

In problems concerning the structure and evolution of stellar systems Camm (ref. 21) has shown that in the Vlasov limit ($nD \gg 1$), the difference in mass and structure of individual stars can be neglected. Therefore, all the star masses are set equal to m so that a distribution function $f(x,v,t)$ completely defines the state of the system.

When $nD \gg 1$ the effects of graininess are negligible and the distribution function satisfies the usual equation of stellar dynamics, that is, the Vlasov equation

$$\frac{\partial f}{\partial t} + v \frac{\partial f}{\partial x} + E \frac{\partial f}{\partial v} = 0 \quad (3)$$

where $E = -\frac{\partial \varphi}{\partial x}$ is given by the Poisson equation

$$\frac{\partial^2 \varphi}{\partial x^2} = 4\pi Gm \int f dv \quad (4)$$

The limitations of the Vlasov equation in describing stellar systems are discussed by Kurth (ref. 22).

In a study of the time development of a system of stars the distribution function at $t = 0$, that is, $f(x, v, t=0)$, could be used as the initial condition in an attempt to solve the time-dependent nonlinear Vlasov equation. But this problem has not yet been solved analytically for general initial conditions. Therefore, a high-speed computer is used to determine the evolution of the system from Newton's laws instead, and equations (3) and (4) are used only to obtain the steady-state solution for the system.

The Virial Theorem

The virial theorem can be applied to the one-dimensional system to obtain a relation between the potential and kinetic energy of the system in equilibrium. Consider an arbitrary volume of phase space which is convected with the flow. The integral over this volume $\iint x^2 f(x, v) dx dv$ is a well-defined function of time, and according to the transport theorem (p. 131 of ref. 23)

$$\frac{d^2}{dt^2} \iint x^2 f(x, v) dx dv = \iint \frac{D^2}{Dt^2} [x^2 f(x, v)] dx dv \quad (5)$$

where the substantial derivative $\frac{D}{Dt} = \frac{\partial}{\partial t} + v \frac{\partial}{\partial x} + a \frac{\partial}{\partial v}$. By the Liouville theorem $\frac{Df}{Dt} = 0$, and thus equation (5) when multiplied by $m/2$ becomes

$$\begin{aligned} \frac{m}{2} \frac{d^2}{dt^2} \iint x^2 f(x, v) dx dv &= \frac{m}{2} \iint f(x, v) \frac{D^2}{Dt^2} (x^2) dx dv \\ &= \iint m v^2 f(x, v) dx dv + \iint m x a f(x, v) dx dv \end{aligned} \quad (6)$$

If the region of integration spans the entire system of particles, the integral

$\iint x^2 f(x, v) dx dv$ is constant and the left-hand side of equation (6) vanishes. Also

$$\iint m v^2 f(x, v) dx dv = 2T \quad (7)$$

where T is the total kinetic energy of the system. Using $\rho(x) = \int m f dv$ and $a = -\frac{d\varphi}{dx}$ in equation (6) gives the expression

$$0 = 2T - \int x \rho(x) \frac{d\varphi}{dx} dx \quad (8)$$

The Poisson equation can be written as

$$\rho(x) = \frac{1}{4\pi G} \frac{d^2 \varphi}{dx^2} \quad (9)$$

Therefore, an integration by parts yields the result

$$\begin{aligned} \int_{-x_S}^{x_S} x \rho(x) \frac{d\varphi}{dx} dx &= \frac{1}{4\pi G} \int_{-x_S}^{x_S} x \frac{d^2 \varphi}{dx^2} \frac{d\varphi}{dx} dx \\ &= \frac{x}{8\pi G} \left(\frac{d\varphi}{dx} \right)^2 \Big|_{-x_S}^{x_S} - \frac{1}{8\pi G} \int_{-x_S}^{x_S} \left(\frac{d\varphi}{dx} \right)^2 dx \end{aligned} \quad (10)$$

The last expression is simply the potential energy P of the system, normalized so that $P = 0$ when all masses are at the same point. Equation (5) then becomes

$$2T - P = 0 \quad (11)$$

irrespective of the distribution function. In most of these numerical studies it was found that the system very quickly approached conditions such that equation (11) was satisfied.

Waterbag Distribution

In the steady state, $\frac{\partial f}{\partial t} = 0$ and the Vlasov equation takes the form

$$v \frac{\partial f}{\partial x} + E \frac{\partial f}{\partial v} = v \frac{\partial f}{\partial x} - \frac{d\varphi}{dx} \frac{\partial f}{\partial v} = 0 \quad (12)$$

Using the method of characteristics to solve the partial differential equation given by equation (12) results in the subsidiary equation

$$\frac{dx}{v} = - \frac{dv}{d\varphi/dx} \quad (13)$$

which gives the result

$$\frac{1}{2} mv^2 + m\phi = U = \text{Constant} \quad (14)$$

where U is the total energy of a star. Therefore, any solution of equation (12) has the form

$$f(x,v) = F(U) \quad (15)$$

Thus, if a time-independent equilibrium state exists

$$f(x,v,t \rightarrow \infty) = F(U) \quad (16)$$

where $F(U)$ may be any function of U . Of course, only functions $F(U)$ that are stable are of interest in this study. In general, the form of $F(U)$ depends on the initial distribution and must be obtained by following the time development of the Vlasov equation. However, there is one type of initial distribution for which $F(U)$ is known without actually solving the Vlasov equation. For this distribution the initial f is taken to be constant over a certain region of phase space and is zero outside this region. Figure 2 illustrates the distribution. According to equation (12) f remains constant along the different trajectories so that the region can only change its shape with time while keeping its area constant. For this reason the distribution function just described has been called the waterbag model by DePackh (ref. 24). When DePackh considered the waterbag model he was interested primarily in a solution for the linearized oscillations about the equilibrium state. However, a more interesting application of the waterbag model seems to be in the present study of the nonlinear problem. The waterbag model is of interest in this study primarily because it allows calculation of the exact equilibrium configuration of the one-dimensional star gas for comparison with the computer results.

Two initial distributions considered in the present study are the waterbag model and a distribution which has a constant density over a region of the X -axis and has a Maxwellian velocity distribution. For the waterbag model, the stationary distribution function $F(U)$ is known to be constant for $0 \leq U \leq m\epsilon$ and to be zero for U outside of this region; $m\epsilon$ is some maximum energy to be determined later. For the second distribution, $F(U)$ is assumed to be Maxwellian.

The equilibrium solution for the waterbag model is obtained as follows. The initial shape of the waterbag for most of the calculations is taken to be a rectangle defined by the area in phase space between $\pm x_0$ and $\pm v_0$. The function $F(U)$ is now used in the Poisson equation (eq. (4)) and the integration over dv is changed to an integration over dU . Since the density at a given x only is of interest, $dU = mv dv$ or $dv = \frac{dU}{\sqrt{2m(U - m\phi)}}$ is obtained. The Poisson equation then becomes

$$\frac{d^2\varphi}{dx^2} = \frac{8\pi Gm\Lambda}{\sqrt{2m}} \int_{m\varphi}^{m\epsilon} \frac{dU}{\sqrt{U - m\varphi}} = 8\pi\sqrt{2} Gm\Lambda \sqrt{\epsilon - \varphi} \quad (17)$$

where $m\epsilon$ is the energy such that $F(U) = 0$ for $U > m\epsilon$ and $F(U) = A$ for $0 \leq U \leq m\epsilon$. Since the area of the system in phase space remains constant, the value of A for the initially rectangular waterbag is obtained from the relation

$$\iint A \, dx \, dv = N \quad (18)$$

or

$$A = \frac{N}{4x_0 v_0} \quad (19)$$

A first integration of equation (17) gives the result

$$\left(\frac{d\varphi}{dx}\right)^2 = -\frac{8\sqrt{2}\pi GNm}{3x_0 v_0} \left[(\epsilon - \varphi)^{3/2} - \epsilon^{3/2} \right] \quad (20)$$

where $\varphi = \frac{d\varphi}{dx} = 0$ at $x = 0$ has been chosen to determine the constant of integration.

The condition $\left(\frac{d\varphi}{dx}\right)_{x=0} = 0$ is simply the statement that the force on a star vanishes in a plane dividing the system into two equal masses. A second integration gives the final result

$$\pm x = \left(\frac{3x_0 v_0}{8\sqrt{2}\pi GNm} \right)^{1/2} \int_0^\varphi \left[\epsilon^{3/2} - (\epsilon - \xi)^{3/2} \right]^{-1/2} d\xi \quad (21)$$

Let x_S be the coordinate defining the boundary of the one-dimensional system; then $\varphi(x_S) = \epsilon$ and $\left(\frac{d\varphi}{dx}\right)_{x=x_S} = 2\pi GNm$. If these values for φ and $d\varphi/dx$ are used in equation (20), the result is

$$\epsilon = \left(\frac{3\pi GNm x_0 v_0}{2\sqrt{2}} \right)^{2/3} \quad (22)$$

The value of x_S is obtained from equation (21) by taking ϵ as the upper limit of the integral. Thus

$$x_S = \frac{1}{4} \left(\frac{9x_0^2 v_0^2}{\pi GNm} \right)^{1/3} \int_0^1 \left[1 - (1 - \xi)^{3/2} \right] d\xi \approx 0.43 \left(\frac{9x_0^2 v_0^2}{\pi GNm} \right)^{1/3} \quad (23)$$

The value of the maximum velocity is given by the expression

$$v_S = \sqrt{2\epsilon} = \left(3\pi GNm x_0 v_0 \right)^{1/3} \quad (24)$$

Equation (17) shows that the particle density is given by

$$n(x) = \frac{N}{\sqrt{2} x_0 v_0} (\epsilon - \varphi)^{1/2} \quad (25)$$

where use was made of equation (19).

If the dimensionless variables

$$\chi = (2\pi G N m / \epsilon) x \quad (26)$$

and

$$\Phi = \frac{\varphi}{\epsilon} \quad (27)$$

are used in equation (21), the simplified equation obtained is

$$\pm \chi = \int_0^\Phi \left[1 - (1 - \zeta)^{3/2} \right]^{-1/2} d\zeta \quad (28)$$

The resulting Φ and E as functions of χ are shown in figure 3.

Multiple-Contour Waterbag Distributions

Another waterbag distribution which was investigated numerically is one with a hole in the center, referred to as a two-contour waterbag. The only possible $F(U)$ is then one which has a constant value A for $m\epsilon_0 \leq U \leq m\epsilon$ where $m\epsilon$ is the maximum and $m\epsilon_0$ is the minimum star energy in the system and $F(U)$ is zero outside this range. The Poisson equation then takes the form

$$\frac{d^2 \varphi}{dx^2} = 8\pi G m A \sqrt{2} \left(\sqrt{\epsilon - \varphi} - \sqrt{\epsilon_0 - \varphi} \right) \quad (x < x') \quad (29)$$

and

$$\frac{d^2 \varphi}{dx^2} = 8\pi G m A \sqrt{2} \sqrt{\epsilon - \varphi} \quad (x > x') \quad (30)$$

where x' is given by $\varphi(x') = \epsilon_0$. A first integration gives the result

$$\left(\frac{d\varphi}{dx} \right)^2 = -\frac{32}{3} \sqrt{2} \pi G m A \left[(\epsilon - \varphi)^{3/2} - (\epsilon_0 - \varphi)^{3/2} + C_1 \right] \quad (x < x') \quad (31)$$

and

$$\left(\frac{d\varphi}{dx} \right)^2 = -\frac{32}{3} \sqrt{2} \pi G m A \left[(\epsilon - \varphi)^{3/2} + C_2 \right] \quad (x > x') \quad (32)$$

Using the boundary conditions $\varphi(0) = 0$, $\left(\frac{d\varphi}{dx}\right)_{x=0} = 0$, $\varphi(x_s) = \epsilon$, and $\left(\frac{d\varphi}{dx}\right)_{x=x_s} = 2\pi G N m$ yields the constants C_1 and C_2

$$C_1 = -\left(\epsilon^{3/2} - \epsilon_0^{3/2}\right) \quad (33)$$

$$C_2 = -\left(\epsilon^{3/2} - \epsilon_0^{3/2}\right) \quad (34)$$

A second integration gives the final result

$$\pm x = \left(\frac{32\sqrt{2}}{3} \pi G m A\right)^{-1/2} \int_0^\varphi \left\{ \left[\epsilon^{3/2} - (\epsilon - \zeta)^{3/2} \right] - \left[\epsilon_0^{3/2} - (\epsilon_0 - \zeta)^{3/2} \right] \right\}^{-1/2} d\zeta \quad (x < x') \quad (35)$$

and

$$\pm x = x' + \left(\frac{32\sqrt{2}}{3} \pi G m A\right)^{-1/2} \int_{\epsilon_0}^\varphi \left\{ \left[\epsilon^{3/2} - (\epsilon - \zeta)^{3/2} \right] - \epsilon_0^{3/2} \right\}^{-1/2} d\zeta \quad (x > x') \quad (36)$$

Using the dimensionless variables

$$\chi = \left(\frac{32\sqrt{2}}{3} \pi G m A\right)^{1/2} \epsilon^{-1/4} x \quad (37)$$

and

$$\Phi = \frac{\varphi}{\epsilon} \quad (38)$$

simplifies equations (35) and (36) to

$$\pm \chi = \int_0^\Phi \left\{ \left[1 - (1 - \zeta)^{3/2} \right] - \left[\nu^{3/2} - (\nu - \zeta)^{3/2} \right] \right\}^{-1/2} d\zeta \quad (\chi < \chi') \quad (39)$$

and

$$\pm \chi = \chi' + \int_\nu^\Phi \left\{ \left[1 - (1 - \zeta)^{3/2} \right] - \nu^{3/2} \right\}^{-1/2} d\zeta \quad (\chi > \chi') \quad (40)$$

where $\nu = \frac{\epsilon_0}{\epsilon}$. Figure 4 shows the normalized (dimensionless) equilibrium contours for four values of ν . The contours are obtained from the equations

$$V_n^{(1)}(x) = \sqrt{2[\nu - \Phi(x)]} \quad (41a)$$

and

$$V_n^{(2)}(x) = \sqrt{2[1 - \Phi(x)]} \quad (41b)$$

Maxwellian Distribution

For a system at thermal equilibrium the distribution function $F(U)$ has the form

$$F(U) = A \exp(-\kappa U) \quad (42)$$

Following the same method used in obtaining the solution for the waterbag model yields the equilibrium density

$$n = 2 \int_0^\infty f \, dv = 2 \int_{m\varphi}^\infty A \exp(-\kappa U) \frac{dU}{\sqrt{2m(U - m\varphi)}} = 2A \sqrt{\frac{\pi}{2m\kappa}} \exp(-\kappa m\varphi) \quad (43)$$

Equation (4) then becomes

$$\frac{d^2\varphi}{dx^2} - 8\pi Gm A \sqrt{\frac{\pi}{2m\kappa}} \exp(-\kappa m\varphi) = 0 \quad (44)$$

or

$$\frac{d^2\Phi}{dx^2} - \frac{\alpha}{2} \exp(-\Phi) = 0 \quad (45)$$

where $\Phi = \kappa m\varphi$ and $\alpha = 16\pi G\kappa m^2 A \sqrt{\frac{\pi}{2m\kappa}}$. A first integration of equation (44) gives the result

$$\left(\frac{d\Phi}{dx}\right)^2 - \alpha[1 - \exp(-\Phi)] = 0 \quad (46)$$

where the constant of integration was determined by the boundary condition $\frac{d\Phi}{dx} = 0$ at $x = 0$. A second integration gives

$$\pm x = \frac{1}{\sqrt{\alpha}} \ln \left[\frac{1 + \sqrt{1 - \exp(-\Phi)}}{1 - \sqrt{1 - \exp(-\Phi)}} \right] \quad (47)$$

Solving equation (47) for Φ gives the equation

$$\Phi(x) = -\ln \left[1 - \tanh^2 \left(\sqrt{\frac{\alpha}{4}} x \right) \right] \quad (48)$$

One of the boundary conditions to be satisfied is

$$\lim_{x \rightarrow \infty} \frac{d\Phi}{dx} = 2\pi G N m^2 \kappa \quad (49)$$

or

$$\alpha = (2\pi G N m^2 \kappa)^2 \quad (50)$$

The solution is then given by the equations

$$\varphi(x) = -\frac{2}{\kappa m} \ln \operatorname{sech}(\pi G N m^2 \kappa x) \quad (51)$$

and

$$E(x) = -2\pi G N m \tanh(\pi G N m^2 \kappa x) \quad (52)$$

and

$$n(x) = \frac{1}{2} \pi G N^2 m^2 \kappa \operatorname{sech}^2(\pi G N m^2 \kappa x) \quad (53)$$

where $1/\kappa$ is the average kinetic energy per star at any given position. This particular solution has also been considered by Camm (ref. 14).

Figure 5 shows the variation of Φ and E for the Maxwellian distribution where the values $4\pi G = 1$, $m = 1$, $\kappa = 1$, and $N = 4$ were arbitrarily chosen. In figure 6, the variation of the observed gravitational field normal to the galactic plane of the Galaxy is compared with the results obtained from equations (20) and (52). These values of $E(x)$ normal to the galactic plane were obtained by the astronomer Oort and have been tabulated by Lindblad (ref. 15). The variation of $E(x)$ for the Maxwellian distribution was found to be in good agreement with the experimentally obtained variation.

Energy Considerations

The steady-state solution for the waterbag distribution was obtained by using conservation of area in the two-dimensional phase space. For the waterbag model it was possible to obtain $F(U)$ corresponding to a given initial condition. It must therefore be determined whether energy considerations allow the relaxation from a function $f(x, v, t=0)$ of two independent variables to a function $F(U)$ of the energy only. Thus, if an equilibrium state is to be reached, the initial and final energy of the system must be equal. For the initial rectangular waterbag the kinetic energy T is given by

$$T(t=0) = \iint \frac{1}{2} m v^2 f(x, v, t=0) dx dv = \frac{Nm}{8x_0 v_0} \int_{-x_0}^{x_0} \int_{-v_0}^{v_0} v^2 dv dx = \frac{Nm}{6} v_0^2 \quad (54)$$

As before, $\pm v_0$ and $\pm x_0$ define the rectangular area of the initial distribution. By use of equation (10), the potential energy of the initial waterbag is found to be

$$P(t=0) = \frac{x_0}{4\pi G} (2\pi G N m)^2 - \frac{1}{4\pi G} \int_0^{x_0} \left(2\pi G N m \frac{x}{x_0} \right)^2 dx = \frac{2}{3} \pi G N^2 m^2 x_0 \quad (55)$$

The total initial energy W is then given by

$$W(t=0) = T(t=0) + P(t=0) = \frac{Nm}{3} \left(\frac{1}{2} v_0^2 + 2\pi G N m x_0 \right) \quad (56)$$

For a given constant value of $A = \frac{N}{4x_0 v_0}$, the minimum value that equation (56) can attain is easily found to be given by

$$W_{\min}(t=0) = \frac{Nm}{2} \left(\frac{\pi G N^2 m}{2A} \right)^{2/3} \quad (57)$$

The total energy of the equilibrium state that is defined by equation (21) is now computed. The kinetic energy is given by

$$\begin{aligned} T_{eq} &= \iint \frac{1}{2} m v^2 f \, dx \, dv = \frac{N}{x_0 v_0 \sqrt{2m}} \int_0^{x_s} \int_{m\varphi}^{m\epsilon} \sqrt{U - m\varphi} \, dU \, dx \\ &= \frac{\sqrt{2} Nm}{3x_0 v_0} \int_0^{x_s} (\epsilon - \varphi)^{3/2} dx = \frac{1}{8} Nm \left(\frac{3\pi G N^2 m}{4A} \right)^{2/3} \int_0^{\chi_s} (1 - \Phi)^{3/2} d\chi \end{aligned} \quad (58)$$

where $dv = \frac{dU}{\sqrt{2m(U - m\varphi)}}$ was used and, as before, $\Phi = \varphi/\epsilon$ and $\chi = (2\pi G N m/\epsilon)x$. By substituting equation (20) into equation (10), the potential energy for the equilibrium waterbag becomes

$$\begin{aligned} P_{eq} &= \frac{x_s}{4\pi G} (2\pi G N m)^2 - \frac{1}{4\pi G} \int_0^{x_s} \left(\frac{8\sqrt{2}\pi G N m}{3x_0 v_0} \right) \left[\epsilon^{3/2} - (\epsilon - \varphi)^{3/2} \right] dx \\ &= \frac{Nm}{4} \left(\frac{3\pi G N^2 m}{4A} \right)^{2/3} \int_0^{\chi_s} (1 - \Phi)^{3/2} d\chi \end{aligned} \quad (59)$$

The equilibrium state then has a total energy given by the expression

$$W_{eq} = T_{eq} + P_{eq} = \frac{3}{8} Nm \left(\frac{3\pi G N^2 m}{4A} \right)^{2/3} \int_0^{\chi_s} (1 - \Phi)^{3/2} d\chi \quad (60)$$

where

$$\int_0^{\chi_s} (1 - \Phi)^{3/2} d\chi \approx 0.988$$

For arbitrary x_0 and v_0 it is clear that equations (56) and (60) cannot be equal. The equilibrium energy W_{eq} depends only on the product $x_0 v_0$ whereas $W(t=0)$ is the sum of two independent quantities that are functions of the two independent variables v_0 and x_0 . The total energy as well as the area in phase space must be conserved. Thus, the only state compatible with the conservation of area in phase space and with the dynamics of the Vlasov equation does not have the same energy as the initial state. Therefore, a steady state cannot exist for an initially rectangular waterbag distribution. However, the equilibrium state has the interesting property that it is a minimum-energy

configuration. As is shown in the section on computer simulation, the system will do its best within the limitations of energy conservation to reach the equilibrium state.

The Minimum-Energy Principle

The minimum-energy property of the equilibrium waterbag distribution can be demonstrated analytically. First consider the initial rectangular waterbag distribution. Equation (57) gives the minimum initial energy for such a distribution. The ratio of this minimum initial energy to the equilibrium energy is

$$\frac{W_{\min}(t=0)}{W_{\text{eq}}} = 1.03$$

and the rectangular waterbag with the minimum energy has still more energy than does the equilibrium waterbag. The minimum-energy property can be generalized to any shape of the waterbag distribution by showing that the equilibrium state has the least possible energy.

Consider the waterbag distribution shown in figure 2. Let points along the contour be described by $V_+(x)$ and $V_-(x)$ where the plus sign indicates the upper contour and the minus sign indicates the lower contour. The equations of motion for $V_{\pm}(x)$ are

$$\frac{\partial V_{\pm}}{\partial t} + V_{\pm} \frac{\partial V_{\pm}}{\partial x} = E \quad (61)$$

For the equilibrium state $\frac{\partial V_{\pm}}{\partial t} = 0$ and equation (61) becomes

$$V_{\pm} \frac{dV_{\pm}}{dx} - E = 0 \quad (62)$$

A variational method is used to demonstrate the minimum-energy property of a one-dimensional self-gravitating system. This method has previously been applied by Hohl and Staton (ref. 25) to a plasma described by a single-contour waterbag distribution. The use of the variational method requires the energy density g in the system. Using the first integral in equation (10), the potential energy per unit length g_P is given by

$$g_P = -2mA_x V_+ \left[4\pi Gm \left(\frac{N}{2} - 2A\theta \right) \right] \quad (63)$$

where $\theta = \int_{-x_S}^x V_+(x) dx$ and $4\pi Gm \left(\frac{N}{2} - 2A\theta \right) = E$. The kinetic energy per unit length g_T is simply $\frac{A}{3} m V_+^3$. Thus, the energy density for the present problem $g(x, V_+, \theta)$ has the form

$$g = \frac{A}{3} m V_+^3 - 2mAxV_+ \left[4\pi Gm \left(\frac{N}{2} - 2A\theta \right) \right] \quad (64)$$

where A is the magnitude of f . Thus, the total energy of the system is given by

$$W = \int_{-x_S}^{x_S} g(x, V_+, \theta) dx \quad (65)$$

For the sake of simplicity the contour of the waterbag has been taken to be symmetric so that $V_+ = -V_-$. Following Courant and Hilbert (ref. 26), the extremum of equation (63) is found by the usual methods of variational calculus. The end points $\pm x_S$ of the contour are held fixed and the function $V_+(x)$ receives a variation $\alpha\eta(x)$ where α is an arbitrary constant and $\eta(x)$ is an arbitrary function which vanishes at the end points. It is then found that

$$\frac{\partial W}{\partial \alpha} = \int_{-x_S}^{x_S} \left(\frac{\partial g}{\partial V_+} \eta + \frac{\partial g}{\partial \theta} \int_{-x_S}^x \eta d\xi \right) dx = \int_{-x_S}^{x_S} \left(-\frac{d}{dx} \frac{\partial g}{\partial V_+} + \frac{\partial g}{\partial \theta} \right) \left(\int_{-x_S}^x \eta d\xi \right) dx \quad (66)$$

where

$$\int_{-x_S}^{x_S} \eta dx = 0 \quad (67)$$

Since η is an arbitrary function satisfying equation (67), the condition for obtaining an extremum is

$$\frac{d}{dx} \left(\frac{\partial g}{\partial V_+} \right) - \frac{\partial g}{\partial \theta} = 0 \quad (68)$$

If the expression for g given by equation (64) is used in equation (67), the result is

$$V_+ \frac{dV_+}{dx} - E = 0 \quad (69)$$

which is identical to equation (62) for the upper contour. Application of the Legendre criterion of the second variation of g can tell something about the extremum just calculated. For the problem under consideration

$$\frac{\partial^2 g}{\partial V_+^2} = 2mAV_+ \quad (70)$$

and, since for small perturbation about the equilibrium state V_+ is positive (or zero), the Legendre criterion shows that the extremum cannot be a maximum. Thus, the minimization of the total energy of a waterbag distribution leads to the contours satisfying the stationary Vlasov equation. The consequence of the minimum-energy property is that starting from any nonequilibrium state, energy conservation will prevent the system from reaching the steady state described by equations (21) and (25). This result was to be

expected from the analysis of DePackh (ref. 24) which shows that, for a plasma, small perturbations of the equilibrium state are not damped. Nevertheless, the interesting point is that numerical results show that the system does its best within the limitation of energy conservation to approach the equilibrium state. In general, it is found that the equilibrium state is approached very closely whenever the initial energy is not too different from the energy of the equilibrium state given by equation (60).

Generalized Minimum-Energy Property

The minimum-energy principle can be extended to arbitrary distribution functions. The waterbag model illustrated in figure 7 is used in the analysis. The contours $V_+^{(k)}(x,t)$ and $V_-^{(k)}(x,t)$ bound surfaces of constant $f = f_k$. According to equation (3) the phase fluid bounded by the contours is incompressible. In the limit of a very large number of contours the waterbag model can be used to approximate arbitrary distribution functions.

The distribution function describing a multiple-contour waterbag distribution has the form

$$f = \sum_k A_k \left[H(v - V_-^{(k)}) - H(v - V_+^{(k)}) \right] \quad (71)$$

where $H(z)$ is the Heaviside unit step function. This distribution function satisfies the Vlasov equation so that the contours are streamlines of the flow in phase space, that is

$$\frac{\partial V_{\pm}^{(k)}}{\partial t} + V_{\pm}^{(k)} \frac{\partial V_{\pm}^{(k)}}{\partial x} - E = 0 \quad (72)$$

The equilibrium contours are given by

$$V_{\pm}^{(k)} \frac{\partial V_{\pm}^{(k)}}{\partial x} - E = 0 \quad (73)$$

The force per unit mass E is obtained from the equation

$$\frac{dE}{dx} = -4\pi Gm \int f dv = -4\pi Gm \sum_k A_k (V_+^{(k)} - V_-^{(k)}) \quad (74)$$

where it is assumed that there is a total of N stars, each of mass m , in the system. To simplify the equations, symmetric contours $V_+^{(k)} = -V_-^{(k)} = v^{(k)}$ are assumed in the derivation of the minimum-energy property. The results obtained are not affected by such an assumption.

A new variable is now defined as

$$\theta^{(k)} = \int_{-x_s^{(k)}}^x v^{(k)}(\xi) d\xi \quad (75)$$

where $x_s^{(k)}$ is the end point of the contour k . In terms of $\theta^{(k)}$ the gravitational field is given by

$$E(x) = 4\pi Gm \left(\frac{N}{2} - 2 \sum_k A_k \theta^{(k)} \right) \quad (76)$$

Let g be a function such that the total energy W of the system is given by

$$W = \sum_k \int_{-x_s^{(k)}}^{x_s^{(k)}} g(x, \theta^{(k)}, v^{(k)}) dx \quad (77)$$

Taking the extremum of the integral for W , subject to the condition that

$$N = \sum_k 2A_k \theta^{(k)} \left(x_s^{(k)} \right) \quad (78)$$

is a constant, requires that the contours $v^{(k)}$ satisfy the Euler-Lagrange equations.

$$\frac{\partial g^*}{\partial \theta^{(k)}} - \frac{d}{dx} \frac{\partial g^*}{\partial v^{(k)}} = 0 \quad (79)$$

where $g^* = g + 2\lambda A_k v^{(k)}$ and λ is, as yet, an undetermined Lagrangian multiplier. Since the end points are held fixed, the condition on the total number of particles is redundant and $\lambda = 0$. If the end points $x_s^{(k)}$ are not held fixed in the variational process, additional equations will appear which will not change the main results given.

For a multiple waterbag the total kinetic energy per unit length is

$$\sum_k g_T = \sum_k \frac{m}{3} A_k v^{(k)3} \quad (80)$$

From equation (10) the potential energy per unit length is

$$\sum_k g_P = -2m \sum_k x A_k v^{(k)} \left[4\pi Gm \left(\frac{N}{2} - 2 \sum_k A_k \theta^{(k)} \right) \right] \quad (81)$$

Therefore, the expression for g is

$$g = \frac{1}{3} m A_k v^{(k)3} - 2m x A_k v^{(k)} \left[4\pi Gm \left(\frac{N}{2} - 2 \sum_k A_k \theta^{(k)} \right) \right] \quad (82)$$

The Euler-Lagrange equations then become

$$-2mA_k \left[v^{(k)} \frac{dv^{(k)}}{dx} - 4\pi Gm \left(\frac{N}{2} - 2 \sum_k A_k \theta^{(k)} \right) \right] = 0 \quad (83)$$

or

$$v^{(k)} \frac{dv^{(k)}}{dx} - E = 0 \quad (84)$$

Equations (84) are the equations for the equilibrium contours satisfying the Vlasov equation.

If equations (84) are to represent a minimum-energy configuration, then the Legendre criterion of the second variation of g must be satisfied. Following Courant and Hilbert (ref. 26), the Legendre criterion for the case of several unknown functions $\theta^{(k)}$ is that the quadratic form whose coefficient matrix has the elements

$$a_{ij} = \frac{\partial^2 g}{\partial v^{(i)} \partial v^{(j)}} \quad (85)$$

must not be negative. For the present problem, only the diagonal elements of equation (85) are nonzero and are given by

$$a_{kk} = 2mA_k v^{(k)} \quad (86)$$

Since $2mv^{(k)}$ is never negative, the Legendre criterion requires that

$$A_k > 0 \quad (87)$$

From the definition of f given by equation (71) it can be seen that equation (87) is equivalent to stating that the distribution function must always decrease in going outward from the center of the system where $f = f_1$ must be the largest. If equation (87) is satisfied, the system is a minimum-energy configuration and is always stable. However, if $A_k > 0$ is not satisfied for all k , the system is not a minimum-energy configuration. If the Legendre criterion is not satisfied, the system may be unstable since two or more contours can now be deformed while keeping the total energy of the system constant. In a subsequent section the results of a numerical experiment are presented which show how two-contour systems with $A_1 = -A_2$ become unstable.

COMPUTER SIMULATION OF STELLAR SYSTEMS

The simplest system of stars that can be considered is the one-dimensional system in which the stars are stratified into plane parallel layers and all parameters vary only

in one direction. The nonrelativistic motion of stars in one dimension is simple enough so that the motion of large numbers of stars can be followed on an electronic computer.

Initial distributions of the waterbag type were used extensively in the numerical experiments since they allow a comparison with the results obtained in the preceding sections. Two types of initial waterbag distributions have to be considered separately. The first type is a "fat" waterbag for which the dimension of the system is near D and the total energy is near the energy of the equilibrium distribution. The system then quickly approaches the equilibrium state with the exception of the arms in phase space which develop to accommodate the excess energy. The second type of initial distribution is a "thin" waterbag which has a total energy much larger than the energy of the equilibrium distribution. For this second type the system cannot even come near its equilibrium state and an instability develops which causes the system to break up into small clusters.

Description of the One-Dimensional Model

The one-dimensional model consists of a system of N stars which are represented by mass sheets. These sheets are of infinite extent along the Y - and Z -axes and the sheets are constrained to move along the X -axis. The equations of motion of all the N stars are solved simultaneously by computing the gravitational field at the position of each star and then integrating the equations of motion for each star over a small time interval Δt and repeating the process. When two sheets meet they are allowed to pass freely through each other.

The evolution of the system of stars is studied by using various nonequilibrium initial distributions as input to the computer and then following the time development of the system on the computer.

The equation of motion for the i th sheet with a mass m per unit area is given by the expression

$$\frac{d^2 x_i(t)}{dt^2} = E(x_i, t) \quad (88)$$

where x_i is the position of the i th sheet and $E(x, t)$ is obtained from

$$-\frac{\partial E(x, t)}{\partial x} = 4\pi G\rho(x, t) = 4\pi Gm \sum_{j=1}^N \delta[x - x_j(t)] \quad (89)$$

The expression for the gravitational field is then

$$E(x, t) = 2\pi Gm \sum_{j=1}^N \text{sgn}[x - x_j(t)] \quad (90)$$

where

$$\begin{aligned}\text{sgn}(z) &= -1 & (z > 0) \\ &= 0 & (z = 0) \\ &= 1 & (z < 0)\end{aligned}$$

Figure 8 illustrates the variation of the gravitational field for an eight-sheet system. In the actual numerical calculations the field was computed by first ordering the mass sheets according to their coordinate $x_j^{(k)}$ so that

$$x^{(k)} \leq x^{(k+1)} \quad (91)$$

The gravitational field is then given by

$$E(x_j^{(k)}) = 4\pi Gm \left(\frac{N}{2} - k + \frac{1}{2} \right) \quad (92)$$

and the summation indicated in equation (90) does not have to be performed at every time step and for each star. The sorting routine used in ordering the stars is very fast and takes advantage of the fact that advancing the motion of the stars for a small time interval will not get the stars too far out of order.

The motion of the mass sheets can also be computed by a more exact method. That is, the times at which neighboring pairs of sheets cross are computed and the shortest of these crossing times is used to recompute the new positions and velocities for the sheets affected. The time for the next crossing is then found and the process is repeated. The accelerations are constant until two sheets cross. This very accurate program has been used by Lecar (ref. 2) to study certain "invariants" of the system. The exact program is also used in the present study to investigate thermalization for systems with small numbers (up to 40) of stars. However, the exact program takes a large amount of machine time and is not suitable for investigating the motion of large numbers of sheets.

The electronic data processing system was used to calculate the self-consistent motion of systems containing several thousand stars. The position and velocity of each sheet are computed at successive times $t_1, t_2, t_3, \dots, t_j$. For each time step $\Delta t = t_{n+1} - t_n$ the new positions and velocities of the sheets are computed from the equations

$$x_i(t_{n+1}) = x_i(t_n) + \frac{dx_i(t_n)}{dt} \Delta t + \frac{1}{2} \frac{d^2 x_i(t_n)}{dt^2} (\Delta t)^2 \quad (93)$$

and

$$\frac{dx_i(t_{n+1})}{dt} = \frac{dx_i(t_n)}{dt} + \frac{d^2 x_i(t_n)}{dt^2} \Delta t + \frac{1}{2} \frac{d^3 x_i(t_n)}{dt^3} (\Delta t)^2 \quad (94)$$

where

$$\frac{d^2 x_i(t_n)}{dt^2} = 2\pi G m \sum_{j=1}^N H[x_i(t_n) - x_j(t_n)] \quad (95)$$

and

$$\frac{d^3 x_i(t_n)}{dt^3} = \frac{1}{\Delta t} \left[\frac{d^2 x_i(t_n)}{dt^2} - \frac{d^2 x_i(t_{n-1})}{dt^2} \right] \quad (96)$$

Introduction of the term $d^3 x_i/dt^3$ allows use of a larger time interval Δt in the computations while keeping the error very small. The accuracy of the computer program was checked by comparing the results for various values of Δt and also by checking the reversibility of the motion. For example, the error in the computed total energy of the star system was less than 0.005 percent for the systems investigated. Similarly, the total momentum of the system remained constant to within 0.0005 percent. If n is the average density of stars and D is the Debye length or dimension of the system, then the numerical experiments using the model described are very nearly exact for $nD \gg 1$ and actually simulate the solution of the nonlinear Vlasov equations.

The potential energy for a system of N stars, each of mass m per unit area, is given by the equation

$$P = \frac{1}{8\pi G} \left[(2\pi G N m)^2 (x_N - x_1) - \sum_{j=2}^N E_j^2(x) (x_j - x_{j-1}) \right] \quad (97)$$

where $E_j(x)$ is defined by equation (90) so that for each j , $x_{j-1} < x < x_j$. This definition of the potential energy is such that if all stars are at the same point, then the potential energy of the system is zero. The kinetic energy of the system is given by the usual expression

$$T = \frac{1}{2} m \sum_{j=1}^N v_j^2 \quad (98)$$

The total energy U_j of a star is of interest and is given by

$$U_j = \frac{1}{2} m v_j^2 + m \varphi_j \quad (99)$$

The gravitational potential φ_j is obtained after first ordering the mass sheets according to their increasing x -coordinates as indicated by equation (91). Thus, $\varphi_j^{(1)}$ indicates the gravitational potential of the sheet labeled j (which is the first sheet). Dropping the subscript j results in

$$\varphi\left(\frac{N}{2}+1\right) = \varphi\left(\frac{N}{2}\right) = \pi Gm \left(x\left(\frac{N}{2}+1\right) - x\left(\frac{N}{2}\right) \right) \quad (100)$$

and

$$\varphi^{(k)} = \varphi\left(\frac{N}{2}\right) + 4\pi Gm \sum_{i=k}^{\frac{N}{2}-1} \left(\frac{N}{2} + \frac{1}{2} - i \right) \left(x^{(i+1)} - x^{(i)} \right) \quad \left(k < \frac{N}{2} \right) \quad (101)$$

and

$$\varphi^{(k)} = \varphi\left(\frac{N}{2}\right) + 4\pi Gm \sum_{i=\frac{N}{2}+2}^k \left(i - \frac{1}{2} - \frac{N}{2} \right) \left(x^{(i)} - x^{(i-1)} \right) \quad \left(k > \frac{N}{2} \right) \quad (102)$$

where N is an even integer. Also, φ was chosen equal to zero at the midpoint of the system which divides it into two equal masses.

The virial theorem can also be applied to a discrete system in equilibrium. Equation (6) then takes the form

$$0 = \sum_{k=1}^N m \left(\frac{dx^{(k)}}{dt} \right)^2 + \sum_{k=1}^N m x^{(k)} \frac{d^2 x^{(k)}}{dt^2} = 2T + \sum_{k=1}^N m x^{(k)} \frac{d^2 x^{(k)}}{dt^2} \quad (103)$$

where $\frac{d^2}{dt^2} \left[\frac{1}{2} m \sum x^{(k)} \right] = 0$ and $m^{(k)} = m$ for all k . Use of the expression

$$m \frac{d^2 x^{(k)}}{dt^2} = 4\pi Gm^2 \left(\frac{N}{2} - k + \frac{1}{2} \right) \quad (104)$$

yields

$$\begin{aligned} \sum_{k=1}^N m x^{(k)} \frac{d^2 x^{(k)}}{dt^2} &= 2\pi Gm^2 \left[(N-1)x^{(1)} + (N-3)x^{(2)} + (N-5)x^{(3)} + \dots \right. \\ &\quad \left. + (N-2n+1)x^{(n)} + \dots - (N-3)x^{(N-1)} - (N-1)x^{(N)} \right] \end{aligned} \quad (105)$$

If symmetry of the system is assumed such that $x^{\left(\frac{N}{2}-2\right)} = x^{\left(\frac{N}{2}+2+1\right)}$, equation (105) can be written in the form

$$\sum_{k=1}^N m x^{(k)} \frac{d^2 x^{(k)}}{dt^2} = -4\pi G m^2 \left[x^{\left(\frac{N}{2}+1\right)} + 3x^{\left(\frac{N}{2}+2\right)} + 5x^{\left(\frac{N}{2}+3\right)} + \dots + (N-3)x^{(N-1)} + (N-1)x^{(N)} \right] \quad (106)$$

The potential energy of the system is given by

$$\begin{aligned} P &= 4\pi G m^2 \left(\frac{N}{2}\right)^2 x^{(N)} - \sum_{k=\frac{N}{2}+1}^N \left(k - \frac{N}{2} - 1\right)^2 (x^{(k)} - x^{(k-1)}) \\ &= 4\pi G m^2 \left[x^{\left(\frac{N}{2}+1\right)} + 3x^{\left(\frac{N}{2}+2\right)} + 5x^{\left(\frac{N}{2}+3\right)} + \dots + (N-3)x^{(N-1)} + (N-1)x^{(N)} \right] \end{aligned} \quad (107)$$

Comparison of equation (107) and equation (106) shows that

$$\sum_{k=1}^N m x^{(k)} \frac{d^2 x^{(k)}}{dt^2} = -P \quad (108)$$

and therefore

$$2T = P \quad (109)$$

as was shown before for a continuous system.

Initial Distributions Near Equilibrium

Since the computer simply solves the equations of motion of the stars in the system, the one-dimensional sheet model includes individual or star-star interactions as well as the interaction of the stars with the smoothed potential of the system. The graininess or collisional effects are affected by going to the "fluid limit" as implied by the Vlasov equation.

The effects of graininess on the time development of a system can be determined by varying the number of sheets while keeping the total mass of the system constant. The effects of graininess must be checked to determine whether the model is adequately described by the Vlasov equation. Figure 9 shows the time development of two equivalent systems with the same initial distribution but with different graininess. The curves indicate the variation in time of the kinetic energy for an initially rectangular waterbag distribution. The initial conditions are obtained by using a random number generator to give a nearly uniform distribution over a rectangular region in phase space. For all the

numerical calculations the gravitational constant was normalized such that $4\pi G = 1$. Also, all time scales are normalized to $\tau_{c,0} = \tau_c(t=0)$. The initial ratio of kinetic to potential energy for both curves in figure 9 is 2, whereas the equilibrium value is 0.5. The upper curve is for a system of 1000 stars with $nD \approx 1000$ and $m = 2$. The lower curve is for a system of 2000 stars with $nD \approx 2000$ and $m = 1$. The oscillations of the kinetic energy are identical for the two systems, an indication that the graininess effects do not affect the development of the system.

Comparison of the curves in figure 9 shows that after only a few periods nonlinear damping or phase mixing has almost eliminated the oscillations in the kinetic energy and the kinetic energy remains near the equilibrium value. These results indicate that the Vlasov equation correctly describes the system.

To determine when the effects of graininess become important, the evolution of several equivalent systems with varying numbers of stars is compared. Figure 10 shows the variation of the kinetic energy for equivalent systems which contain from 20 to 500 stars. For the system with 500 stars the behavior is still very similar to that shown in figure 9. The time behavior of the energy distribution function and the density for equivalent systems which contain more than 500 stars is also very similar. As can be seen in figure 10, when the number of stars of the system becomes 200 or less the time behavior of the kinetic energy differs markedly from that of figure 9. Also, the time development of the energy distribution function and of the density is different for the systems shown in figure 10. In general, it was found that oscillations in the various parameters of the system persisted much longer when the number of stars of the system was less than 500.

Figure 11 shows the time development of the density of the waterbag distribution for a system of 2000 stars with a mass m per unit area equal to one. The ratio of initial energy to equilibrium energy $\left(\frac{W(t=0)}{W_{eq}}\right)$ for this system is 1.33 and the initial ratio of kinetic to potential energy is 2. The corresponding variation of the kinetic energy is shown by the lower curve of figure 9. The dashed curve in figure 11 is the theoretical equilibrium density as obtained from equation (25). After only a few periods $2\pi\tau_{c,0}$, the "experimental" density is close to the calculated value. The time development of the energy distribution function $F(U)$ for the same system is shown in figure 12, where $F(U)$ represents the relative number of sheets in an energy interval ΔU . The dashed line shown in figure 12 represents the theoretical distribution. Again, after only about six periods the experimental distribution closely approximates the theoretical distribution. Thus, even for values of 1.33 for the ratio of initial to equilibrium energy the system approaches its nonstationary equilibrium state closely in a time of the order of $2\pi\tau_{c,0}$. The best way to see the approach to equilibrium is to take a sequence of photographs showing the time development of the system in phase space. Figure 13 shows

such a sequence for the system of 2000 stars. Each star is represented by a small circle. While approaching the nonstationary equilibrium state indicated by the area inside the oval at time $t = 33.0\tau_{C,0}$ in figure 13, the system rotates in phase space with a frequency near $1/2\pi\tau_C$. An interesting feature of the time development shown in figure 13 is the development of "spiral arms" in phase space. Such arms were found to develop in all systems having an initial energy larger than the equilibrium energy. The relatively few particles in the long arms shown in figure 13 are required to accommodate the excess energy, and they correspond to the high-energy bump shown in figure 12 at time $t = 38\tau_{C,0}$. The arms develop because the period of oscillation of the sheets increases with energy. Figure 14 shows the period as a function of energy for the equilibrium state.

The calculations just described for the 2000-sheet system with an initial waterbag distribution were also performed for an equivalent 1000-sheet system. The variation of the kinetic energy for this system is given by the upper curve in figure 9. The variation of the density with time is shown in figure 15 and is found to be very similar to that of the 2000-sheet system (fig. 11). The corresponding time development of the energy distribution function shown in figure 16 is also very similar to that of the 2000-sheet system (fig. 12).

The results of Hénon (ref. 3) show that the oscillations for a system of spherically concentric mass shells are damped more rapidly than those for the one-dimensional system shown in figure 9. The reason for this is that the period of oscillation of a spherical shell increases much more rapidly with increasing energy than it does for a mass sheet in the one-dimensional system. Therefore, the effectiveness of phase-mixing, which depends on the change in period with changing energy, is different for the two models.

In the equilibrium state the gravitational potential is time independent and the trajectories of individual stars form fixed closed contours in phase space as shown in figure 17. Figure 18 shows the actual trajectories for five mass sheets for the time-dependent system shown in figure 13. The phase-space trajectories shown in figure 18 are typical for systems which are initially near the equilibrium state. Initially, while the system is approaching the equilibrium configuration the orbits are very much perturbed; this causes the redistribution of the orbits required to approach equilibrium. After only about two orbits the trajectories are nearly the same as the theoretical orbits.

The time behavior described so far is characteristic of the waterbag model whenever the initial energy given by equation (56) is near the equilibrium energy given by equation (60). Since the system approaches the equilibrium configuration within the limits of energy conservation, it appears that the steady state given by equation (21) has some significance. The stability of the steady state has been checked by use of an initial distribution which satisfies equation (21). Even after many periods $2\pi\tau_C$, the system is found

to remain in the equilibrium state. The effect of a perturbation of the equilibrium state has also been checked. Figure 19 shows the time development of a local sinusoidal perturbation of the equilibrium state. Because the outermost stars are now outside the main system they have a longer period and cause the development of arms. After this small perturbation the nonstationary equilibrium state can never be completely reached.

A system with an initially constant density between x_0 and $-x_0$ and with a Maxwellian velocity distribution has a time development similar to that for the waterbag distribution. For example, if the initial ratio of kinetic to potential energy is of the order of the equilibrium value, then the system shows a time behavior very similar to that shown in figure 13. However, the arms in phase space develop more rapidly because some of the high-velocity mass sheets are now able to stay outside the main system longer and therefore have a longer period. For example, figure 20 shows the variation of the kinetic energy of such a system with an initially Maxwellian velocity distribution. The initial ratio of kinetic to potential energy is 2. As shown in figure 20, the kinetic energy of the system quickly approaches its equilibrium value. The corresponding time development of the density and energy distribution function is shown in figure 21. The dashed curves are those obtained from equation (53) and from the relation $F(U) = A \exp(-\kappa U)$. The experimental density approaches its theoretical value closely whereas the energy distribution again develops a high-energy bump. Figure 22 shows the time development of the system in phase space. With the exception of the more rapid development of the spiral arms the time development in phase space is close to that shown in figure 13 for the waterbag model. Thus, the results obtained with the waterbag distribution do indicate the general behavior of one-dimensional self-gravitating systems.

Initial Distributions Far From Equilibrium

If the energy of the initial rectangular waterbag distribution is much larger than the equilibrium energy given by equation (60), the system is unstable and will break up into smaller clusters. Figure 23 shows the time development of the kinetic energy for a waterbag distribution. The system contains 1000 stars and the ratio of initial to equilibrium energy is 6 whereas the ratio of initial kinetic to potential energy is 32. Figure 23 shows that the oscillations in the kinetic energy are damped only very slowly with time. The time development of the density for the same system is shown in figure 24. From the density plots it can be seen that the system quickly breaks up into three clusters which later combine into two clusters. Similar information is obtained from the time development of the velocity distribution function shown in figure 25. There are large fluctuations in time of the energy distribution function of the system as shown in figure 26. Again, the time development of the system can best be observed by viewing it in phase space. Figure 27 shows the time development for the system of 1000 stars in phase space. The breakup into three clusters is clearly demonstrated. The instability which

develops and causes the system to break up into smaller clusters is a manifestation of the Jeans instability (pp. 345-347 of ref. 27). After a long time the system shown in figure 27 condenses into two clusters with a halo of high-energy stars. In figure 28 the position of every 20th star for this system is plotted as a function of time. After only one complete oscillation the bunching of the stars into four distinct regions is clearly visible.

The initial development of the instability depends on the initial fluctuation of the star density in phase space. To illustrate the effects of initial fluctuation of the phase-space density the calculations for the unstable system of 1000 stars have been repeated by using a different random number sequence to obtain the initial distribution. The results are shown in figures 29 to 32. Figures 30 to 32 show that the system now breaks up into four clusters. However, after a long time the system in phase space appears very similar to the previous case in that only two clusters remain with a halo of high-energy stars.

Changing the graininess of the system does not affect the behavior just discussed. To show this, the calculations were again repeated for an equivalent system with 3000 stars. The results are shown in figures 33 to 35. The system appears to break up into three clusters but it quickly condenses into two clusters by effectively winding itself into two spirals. The Vlasov character of the system is clearly demonstrated by the continuity of the spiral arms shown in figure 35.

Distributions with large initial ratios of kinetic to potential energy and which have a constant density between x_0 and $-x_0$ and a Maxwellian velocity distribution are also unstable and will break up into smaller clusters. However, the breakup now does not occur as readily as for the waterbag distribution.

Initially "Cold" Systems

Considered next is an initial distribution in which the particles initially are placed a unit distance apart and have zero velocity. Each star is then attracted toward the center of the system with a constant acceleration. In the absence of any perturbation the crossings will not take place until the stars reach the center of the system. All the stars will reach the center simultaneously and cross at the same instant. After this time the force on a particular star changes sign and the system begins to expand until it reaches its original size with zero kinetic energy and the process is repeated. The results of the calculations for a 1000-star system are shown in figures 36 and 37. Figure 36 shows the variation of the kinetic energy with time. The curve is very similar to that shown in figure 29 except that now there is no damping of the oscillation. If the calculation were extended for a longer time, the error in the numerical solution would eventually cause stars to get out of order and the oscillations would be damped. The variation of the density with time is shown in figure 37. As all particles approach the center of the system simultaneously, the density at that point increases without limit. The system has the

interesting property that during the expanding phase the velocity of recession of the stars as viewed from any particular star increases linearly with distance in either direction.

Another initially "cold" system investigated is the two-stream case. The particles are initially uniformly spaced along x with half the particles at velocity v_0 and the other half at velocity $-v_0$. The variation of the kinetic energy for such a system with 1000 stars is shown in figure 38. After a slight initial rise the oscillations of the kinetic energy show a strong damping. The time development in phase space for this system is shown in figure 39. The two streams wind around each other and in this manner attempt to reach some sort of equilibrium state. Figure 40 shows the evolution in phase space of a system which is very similar to that shown in figure 39 except that the initial positions of the mass sheets were random. It can be seen that the local condensations for this system are much more pronounced.

In the last two systems considered, the relaxation which occurs is of a violent nature and it appears that such systems are suitable to check the theory of violent relaxation as given by Lynden-Bell (ref. 28). For the simple case of a single-contour waterbag the averaged distribution function $\langle f \rangle$ is given by (ref. 28)

$$\langle f \rangle = A \frac{\exp[-\beta(U - \mu)]}{1 + \exp[-\beta(U - \mu)]}$$

where U is the total energy of a star and β and μ are two constants determined by conservation of energy and mass. This distribution is formally identical to the Fermi-Dirac distribution. To determine whether a system approaches the distribution proposed by Lynden-Bell, the phase plane is divided into a number of cells and the number of particles in each cell is found. This process is repeated for different times and the average of a number of such samplings gives $\langle f \rangle$. Figure 41 shows the results for the system shown in figure 39. However, $\langle f \rangle$ was determined after the system had been advanced to $t = 250\tau_{c,0}$. According to the Lynden-Bell distribution a plot of $\ln \frac{\langle f \rangle}{A - \langle f \rangle}$ as a function of U should give a linear relationship since

$$-\beta(U - \mu) = \ln \frac{\langle f \rangle}{A - \langle f \rangle}$$

These results are partially confirmed in figure 6 where the points corresponding to about 75 percent of the total mass lie near the dashed line. Similar results have been obtained by Hénon (ref. 29) who used a model with concentric spherical shells to simulate stellar systems.

In almost all cases considered so far, the system tried to approach a steady state and the dimensions of the system are then of the order of a Jeans or Debye length. This

result is also found if the dimensions of a globular cluster or even a galaxy are considered. Thus, if this simple Newtonian picture is extended to a larger scale, it could be speculated that the present radius of, say, the universe is

$$R \sim D = v_T \tau_c \sim \frac{v_T}{\sqrt{G\rho}} \quad (110)$$

If a spherical geometry and uniform mass density are assumed, R can be written as

$$R \sim \frac{v_T}{\sqrt{GM/R^3}} \quad (111)$$

or

$$\frac{GM}{Rv_T^2} \sim 1 \quad (112)$$

where M is the total mass in the universe. For v_T near the velocity of light c equation (112) becomes the well-known relation

$$\frac{GM}{Rc^2} \sim 1 \quad (113)$$

often used (refs. 30 and 31) to define the radius of the universe. Note that as soon as the average density of a self-gravitating system is known, its characteristic frequency can be computed. For a typical globular cluster τ_c is of the order of 3×10^6 years; for a galaxy τ_c is of the order of 10^8 years. Assuming that the average density in the neighborhood of the Galaxy represents that of the universe, the characteristic period for the universe is found to be of the order of 8×10^{10} years. The characteristic period for the universe is close to the period of oscillation generally quoted in the oscillating-universe theories.

Unstable Stationary States

In a previous section it was shown that if a stationary distribution function always decreases in going outward from the center of the system, the stationary state is a minimum-energy state and is stable. However, if this condition is not satisfied, deformations of the waterbag contours are possible and there is a possibility that the system is unstable. The interchange instability which destroys the stationary state has been numerically investigated for two-contour systems with $A_1 = -A_2$ (refer to fig. 4). The results are shown in figures 42 and 43. Figure 42 illustrates the interchange instability for a system of 2000 stars with ν , the ratio of the minimum to the maximum star energy of the stationary state, equal to 0.4. At the initial time the contours satisfy equations (41a) and (41b). The equilibrium contours are quickly distorted while the heavier

outer waterbag tries to displace the inner bag. Figure 43 shows the time development of an unstable 2000-star system for $\nu = 0.25$. The growth of the instability is now much slower because the central waterbag or hole is smaller.

Thermalization Effects In a One-Dimensional Stellar System

In a one-dimensional system crossings will always take place so that the system can be expected to approach a Maxwellian distribution. An exact double-precision computer program was used to investigate thermalization effects for low numbers of stars. The exact program is one in which the shortest crossing time for a mass sheet is determined and the system is then advanced by that time and the process is repeated. This model, of course, differs from the model used for the results presented so far in that the system was always advanced for a constant time interval Δt , irrespective of the number of crossings during this time interval. The exact program is very accurate. For example, after time-reversing the numerical integration of a typical system investigated, it was found that the initial conditions were reproduced accurately to 12 digits.

Lecar (ref. 2) has investigated the exact one-dimensional motion of low numbers of stars. He found that no thermalization occurs to order $nD\tau_c$ where $nD \approx N$. In the present study of thermalization effects a low number of mass sheets was chosen so that the system can be followed for a long period of time. In order to obtain meaningful results, time averages of the systems are investigated. The constant time interval used in the averaging process is taken to be smaller than the average crossing time for sheets in the system. The time averages are taken over times of the order $n^2 D^2 \tau_c$. It should be noted that the investigation of thermalization effects is still in progress and only some of the initial numerical results are presented here.

For all of the systems investigated, it was found that the time-averaged potential and kinetic energies satisfied the virial theorem; that is, $\frac{\langle T \rangle}{\langle P \rangle} = 0.5$ with an accuracy of at least three digits. The $\langle \rangle$ signify time-averaged quantities. As discussed by Ford (ref. 32), the Poincaré recurrence time and the general behavior of the system are dependent on the initial conditions. For example, special initial conditions can be chosen so that the time behavior of the system is very nearly periodic. However, for the results presented the initial conditions were arbitrarily chosen.

Figure 44 shows the time-averaged velocity distribution and density for a three-particle system. The solid line for the velocity distribution corresponds to a Maxwellian distribution and is obtained by integrating $A \exp(-\kappa U)$ over x ; that is,

$$f(v) = \frac{N}{2} \sqrt{\frac{2m\kappa}{\pi}} \exp\left(-\frac{1}{2} m\kappa v^2\right) \quad (114)$$

The solid line for the density is given by equation (53). The value of κ is obtained from

$$\kappa = \frac{3N}{2\langle T \rangle + 2\langle P \rangle} = \frac{N}{2\langle T \rangle} \quad (115)$$

The circles in figure 44 represent the time-averaged numerical results. The experimental velocity distribution is near the Maxwellian distribution. However, the variation of the density indicates that there is some near-periodic behavior of the system. Such near-periodic behavior is likely to occur for very low numbers of stars.

For example, for a three-particle system, equation (88) can be integrated with the result

$$x_1(t) = x_1(t=0) + v_1(t=0)t + 4\pi Gm \int_0^t \int_0^\xi \left\{ \text{sgn}[x_1(t) - x_2(t)] + \text{sgn}[x_1(t) - x_3(t)] \right\} dt d\xi \quad (116a)$$

$$x_2(t) = x_2(t=0) + v_2(t=0)t + 4\pi Gm \int_0^t \int_0^\xi \left\{ \text{sgn}[x_2(t) - x_1(t)] + \text{sgn}[x_2(t) - x_3(t)] \right\} dt d\xi \quad (116b)$$

$$x_3(t) = x_3(t=0) + v_3(t=0)t + 4\pi Gm \int_0^t \int_0^\xi \left\{ \text{sgn}[x_3(t) - x_1(t)] + \text{sgn}[x_3(t) - x_2(t)] \right\} dt d\xi \quad (116c)$$

If a coordinate system is chosen such that

$$x_1(t=0) + x_2(t=0) + x_3(t=0) = 0 \quad (117a)$$

and

$$v_1(t=0) + v_2(t=0) + v_3(t=0) = 0 \quad (117b)$$

then

$$x_1(t) + x_2(t) + x_3(t) = 0 \quad (118)$$

Thus, whenever the coordinate x_2 equals the coordinate x_3 , a straight line

$$x_1 = 2x_3 = 2x_2 \quad (119)$$

is obtained and a near-periodic behavior of the system is to be expected. Figure 45 shows the results for a four-particle system. Again, the variation of the time-averaged velocity distribution and density indicates that there is near-oscillatory behavior of the system. This near-oscillatory behavior is also observed in plots of the kinetic-energy correlation function

$$C(\tau) = \langle [T(t) - \langle T \rangle][T(t+\tau) - \langle T \rangle] \rangle \quad (120)$$

and also by plotting directly the kinetic energy of the system as a function of time. Figure 46 shows the energy correlation function as a function of τ for a six-particle system. The figure shows that the energy correlation decays only very slowly with τ , an indication of near-oscillatory behavior. The fluctuations of the kinetic energy of the systems investigated are very violent and show no decrease with time. Even though these fluctuations show no decrease with time, the computer results show that a steady distribution can be reached while the fluctuations in the kinetic energy remain extremely violent. The time-averaged velocity distribution and density for the six-particle system are shown in figure 47. The experimental points are near the Maxwellian distribution for both curves. Figure 48 shows that for a 10-particle system the experimental velocity distribution and density points reproduce the theoretical Maxwellian curves.

The results presented so far were obtained by time averaging the system over times of the order of $N^2\tau_c$, and they indicate that the time-averaged distribution is very nearly Maxwellian. However, to show relaxation to a Maxwellian distribution, a system should be prepared which is initially non-Maxwellian and then the relaxation to a Maxwellian distribution observed. This procedure was followed and the results for a 40-particle system are shown in figure 49. The solid line in the upper plot corresponds to a Maxwellian velocity distribution. The circles represent the initial velocity distribution of the system obtained by time averaging over $5N\tau_c$. After the system was advanced in time for $2N^2$ characteristic periods, it was found that the experimental velocity distribution was still nearly the same as the initial distribution. Similar results are obtained for the density shown in the lower plot of figure 49. These results would indicate that no relaxation to a Maxwellian distribution occurs to order $N^2\tau_c$, but to be conclusive the calculations should be extended to $5N^2$ or $10N^2$ characteristic periods. The calculations were terminated after $2N^2$ periods because of computer time limitations. Figure 50 shows the time variation of the kinetic energy for the 40-particle system. The corresponding energy correlation function is shown in figure 51. The correlation of the kinetic energy appears to be very persistent and fluctuations seem to be superimposed on fluctuations. For large τ the results resemble an amplitude modulated wave. The two cases shown in figure 51 were obtained by averaging over N^2 and $2N^2$ characteristic periods. It can be seen that if the average is taken over a smaller time interval, then modulation of the basic frequency for large τ is much more pronounced whereas for small τ the results do not change. The results presented in figure 51 indicate that for small τ there exists Landau damping but some smaller correlation persists for a long time.

It is also of interest to determine whether the fluctuation of the kinetic energy of the one-dimensional system is due to thermal fluctuations. This has been done by plotting the relative fluctuation of the kinetic energy

$$\mu = \frac{\sqrt{C(0)}}{\langle T \rangle} \quad (121)$$

as a function of the total number of particles in a system N . The results are shown in figure 52. The solid line corresponds to $\mu = 1/\sqrt{N}$ and as can be seen, most of the experimental points are near the solid line. Thus the magnitude of the fluctuations of the kinetic energy is of the same order as would be expected from thermal fluctuations. The same result has been obtained by M. Hénon with his model of concentric spherical mass shells.

The rate at which the system will achieve equipartition of energy among stars of different mass has also been investigated for systems containing sheets of mass m and of mass $4m$. It was found to be convenient to present the results by means of the quantities

$$\left. \begin{aligned} \epsilon_1 &= (\langle T \rangle)^{-1} \int_0^\tau T_1 dt \\ \epsilon_2 &= (\langle T \rangle)^{-1} \int_0^\tau T_2 dt \end{aligned} \right\} \quad (122)$$

where T_1 is the total kinetic energy of the heavy stars and T_2 is the total kinetic energy of the light stars. The upper plot in figure 53 shows the results for a 10-particle system containing 5 heavy and 5 light stars. The time-averaged kinetic energies for the heavy and light stars approach each other. This result indicates that equipartition of energy occurs. Similar results are shown in the lower plot in figure 53 for a system containing 5 heavy and 15 light stars. The time-averaged kinetic energies of the heavy and light stars are now in the ratio 5/15, another indication that equipartition of energy occurs to order $N^2\tau_c$.

CONCLUDING REMARKS

The equilibrium properties of one-dimensional self-gravitating systems are investigated analytically. One-dimensional computer models are used to perform experiments tracing the evolution of stellar systems.

For the one-dimensional stellar system it was shown that for an initial distribution of the waterbag type with a given initial area in phase space the equilibrium state is a minimum-energy configuration. Numerical experiments with large numbers of particles illustrate these results. Thus, starting from any nonequilibrium state, the stationary

state described by the time-independent Vlasov equation can never be completely reached because the excess initial energy causes spiral arms to develop in phase space. These arms are required to accommodate the excess energy, and they wind around the main system and become longer and thinner as time progresses. After a sufficiently long time it becomes increasingly more difficult to detect changes in the distribution function since successive turns of the arms approach each other. It may then be possible to obtain an average distribution function by averaging over the gravitational potential. Such an analysis has been performed by Lynden-Bell (Monthly Notices of the Royal Astronomical Society, vol. 136, no. 1, 1967). Lynden-Bell suggests that the encounterless relaxation of an unsteady system will lead to an equilibrium related to Fermi-Dirac statistics. The results of the present investigation of encounterless relaxation with a one-dimensional model appear to confirm the Lynden-Bell theory. Systems with an initial waterbag distribution near equilibrium were found to approach a Fermi-Dirac distribution closely with the exception of a high-energy concentration of particles. For initial distributions far from equilibrium the system approaches a Maxwellian distribution as predicted by the Lynden-Bell theory. This result should not be too surprising since relaxing conditions which lead to the distribution given by Lynden-Bell are expected to persist only over regions where the system is dynamically unstable. Computer calculations show that for initial distributions other than the waterbag type the results are nevertheless very similar to those for the waterbag distribution. An extension of the minimum-energy property showed that all one-dimensional stationary distributions that are always decreasing in going outward from the center of the system are stable. Numerical experiments were performed for two systems which did not satisfy this criterion and these two systems were found to be unstable.

The waterbag model is found to have the interesting property that for initial energies near the equilibrium energy the system approaches its equilibrium configuration very closely. For initial energies far from the equilibrium energy the system is unstable and breaks up into smaller clusters.

The one-dimensional model is also of interest as an approximation to the distribution of velocity and mass normal to the galactic plane of a greatly flattened galactic system. For the two distributions investigated in this study the theoretical gravitational field $E(x)$ normal to the galactic plane was compared with the results deduced by Oort from observations. The variation of $E(x)$ for the Maxwellian distribution was found to be in good agreement with the experimentally obtained variation. The difference for small values of the position coordinate x is probably due to the central core of the galaxy. As expected, for the waterbag distribution the force $E(x)$ differs markedly from the experimentally obtained variation for large x .

From the results obtained in the study of thermalization effects in a one-dimensional model for a stellar system, relaxation to a Maxwellian distribution appears to take place to times of the order of $N^2\tau_c$ where N is the total number of particles in the system and τ_c is the characteristic period. These results were obtained by taking a time average for systems containing small numbers of stars. It was also found that equipartition of energy among sheets of different mass occurs to order $N^2\tau_c$.

Langley Research Center,

National Aeronautics and Space Administration,

Langley Station, Hampton, Va., March 25, 1968,

129-02-01-01-23.

REFERENCES

1. Pasta, John; and Ulam, S.: Heuristic Studies in Problems of Mathematical Physics on High Speed Computing Machines. LA-1557, Los Alamos Sci. Lab., Univ. of California, June 29, 1953.
2. Lecar, Myron: The Validity of the Vlasov Equation for a One-Dimensional Self-Gravitating Gas. *Instabilité Gravitationnelle et Formation des Étoiles, des Galaxies et de Leurs Structures Caractéristiques*, Inst. Astrophys. (Belgique), 1967, pp. 227-237.
3. Hénon, M.: Initial Collapse and Dynamical Mixing of a Spherical Cluster. *Instabilité Gravitationnelle et Formation des Étoiles, des Galaxies et de Leurs Structures Caractéristiques*, Inst. Astrophys. (Belgique), 1967, pp. 243-248.
4. Hockney, R. W.: Gravitational Experiments With a Cylindrical Galaxy. *Symposium on Computer Simulation of Plasma and Many-Body Problems*, NASA SP-153, 1967, pp. 337-347.
5. Hohl, Frank: One- and Two-Dimensional Models to Study the Evolution of Stellar Systems. *Symposium on Computer Simulation of Plasma and Many-Body Problems*, NASA SP-153, 1967, pp. 323-336.
6. Lindblad, P. O.: Gravitational Resonance Effects in the Central Layer of a Galaxy. *The Distribution and Motion of Interstellar Matter in Galaxies*, L. Woltjer, ed., W. A. Benjamin, Inc., 1962, pp. 222-233.
7. Von Hoerner, Sebastian: Die numerische Integration des n-Körper-Problems für Sternhaufen, I. *Z. Astrophys.*, Bd. 50, Heft 3, 1960, pp. 184-214.
8. Von Hoerner, Sebastian: Die numerische Integration des n-Körper-Problems für Sternhaufen, II. *Z. Astrophys.*, Bd. 57, Heft 2, 1963, pp. 47-82.
9. Aarseth, S. J.: Dynamical Evolution of Clusters of Galaxies, I. *Mon. Notic. Roy. Astron. Soc.*, vol. 126, no. 3, 1963, pp. 223-255.
10. Miller, R. H.: Irreversibility in Small Stellar Dynamical Systems. *Astrophys. J.*, vol. 140, no. 1, July 1, 1964, pp. 250-256.
11. Michie, Richard W.: The Dynamics of Star Clusters. *Annu. Rev. Astron. Astrophys.*, vol. 2, Leo Goldberg, ed., Annu. Rev., Inc., 1964, pp. 49-72.
12. Woolley, R. v. d. R.: Motions of Stars of Type A Perpendicular to the Galactic Plane. *Mon. Notic. Roy. Astron. Soc.*, vol. 117, no. 2, 1957, pp. 198-211.
13. Oort, J. H.: Note on the Distribution of Luminosities of K and M Giants. *Bull. Astron. Inst. Neth.*, vol. VI, no. 239, Aug. 17, 1932, pp. 289-294.

14. Camm, G. L.: Self-Gravitating Star Systems. Mon. Notic. Roy. Astron. Soc., vol. 110, no. 5, 1950, pp. 305-324.
15. Lindblad, Bertil: Galactic Dynamics. Encycl. Phys., vol. LIII, Astrophysics IV: Stellar Systems, S. Flügge, ed., Springer-Verlag (Berlin), 1959, pp. 21-99.
16. Woolley, Richard: Motions of the Nearby Stars. Galactic Structure, Adriaan Blaauw and Maarten Schmidt, eds., Univ. of Chicago Press, c.1965, pp. 85-110.
17. Oort, J. H.: Stellar Dynamics. Galactic Structure, Adriaan Blaauw and Maarten Schmidt, eds., Univ. of Chicago Press, c.1965, pp. 455-511.
18. Prendergast, Kevin H.: One Dimensional Self-Gravitating Star Systems. Astron. J., vol. 59, no. 1219, Aug. 1954, pp. 260-262.
19. Chandrasekhar, S.: Principles of Stellar Dynamics. Enlarged ed., Dover Publ., Inc., 1960.
20. Eldridge, O.; and Feix, M.: Fokker-Planck Coefficients for a One-Dimensional Plasma. Phys. Fluids (Res. Notes), vol. 5, no. 10, Oct. 1962, pp. 1307-1308.
21. Camm, G. L.: Self-Gravitating Star Systems. II. Mon. Notic. Roy. Astron. Soc., vol. 112, no. 3, 1952, pp. 155-176.
22. Kurth, Rudolf: Introduction to the Mechanics of Stellar Systems. Pergamon Press, 1957.
23. Serrin, J.: Mathematical Principles of Classical Fluid Mechanics. Encycl. Phys., vol. VIII, pt. 1, Fluid Mechanics I, S. Flügge, ed., Springer-Verlag (Berlin), 1959, pp. 125-263.
24. DePackh, D. C.: The Water-Bag Model of a Sheet Electron Beam. J. Electron. Contr., First ser., vol. XIII, no. 5, Nov. 1962, pp. 417-424.
25. Hohl, Frank; and Staton, Leo D.: Dynamics of a One-Dimensional Plasma Sheath. NASA TN D-4651, 1968.
26. Courant, R.; and Hilbert, D.: Methods of Mathematical Physics. Vol. I. Interscience Publ., Inc. (New York), c.1953.
27. Jeans, James H.: Astronomy and Cosmogony. Dover Publ., Inc., c.1961.
28. Lynden-Bell, D.: Statistical Mechanics of Violent Relaxation in Stellar Systems. Mon. Notic. Roy. Astron. Soc., vol. 136, no. 1, 1967, pp. 101-121.
29. Hénon, Michel: Collective Motions in a Spherical Star Cluster. Symposium on Computer Simulation of Plasmas and Many-Body Problems, NASA SP-153, 1967, pp. 349-364.

30. Dicke, R. H.: Dirac's Cosmology and Mach's Principle. *Nature (Letters to Ed.)*, vol. 192, no. 4801, Nov. 4, 1961, pp. 440-441.
31. Whitrow, G. J.: *The Structure and Evolution of the Universe*. Harper & Row, Publ., c.1959.
32. Ford, Joseph: Approach of One-Dimensional Systems to Equilibrium. *Phys. Rev., Second Ser.*, vol. 112, no. 5, Dec. 1, 1958, pp. 1445-1451.

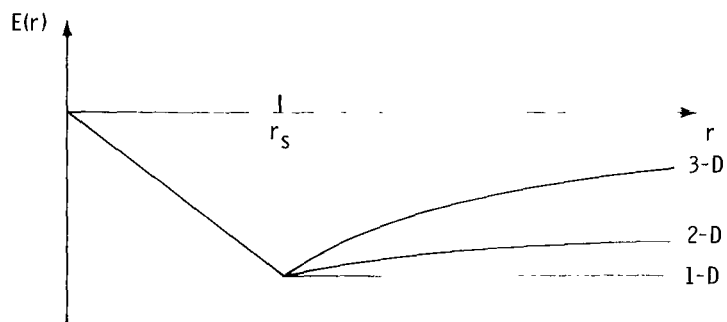


Figure 1.- Comparison of gravitational field for constant-density systems in one, two, and three dimensions.

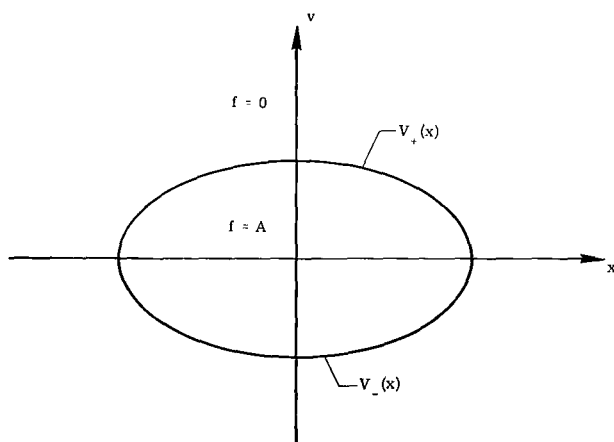


Figure 2.- Waterbag distribution.

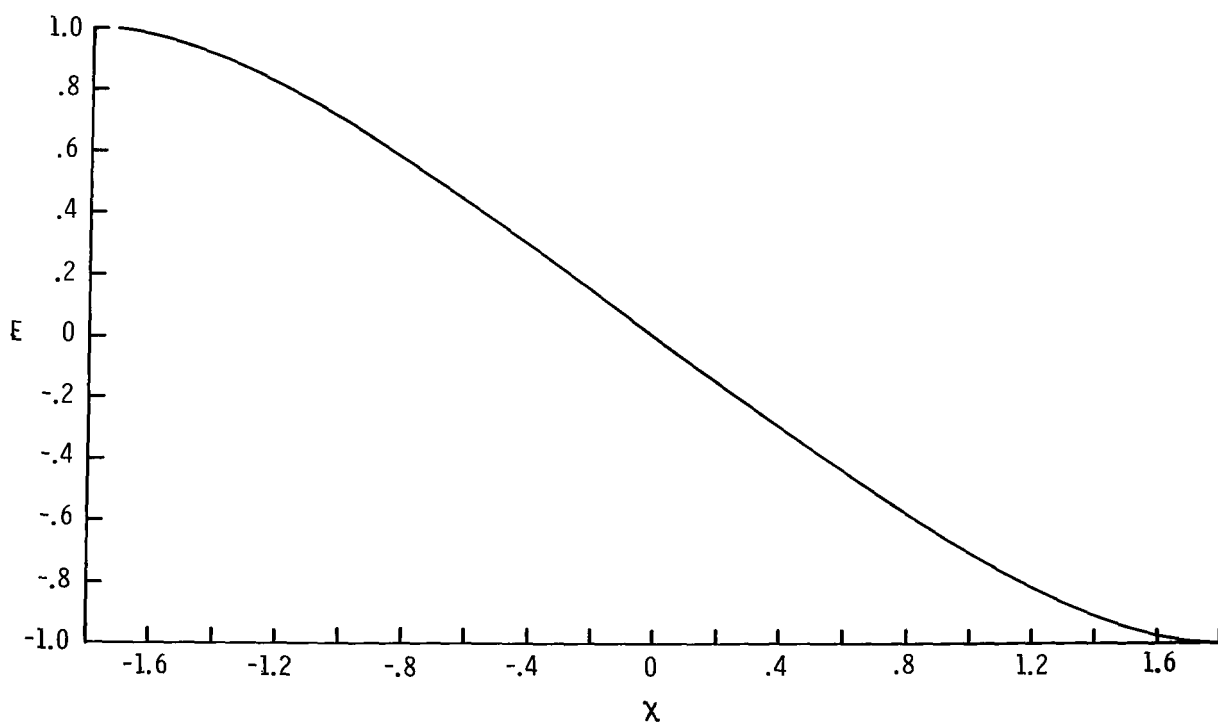
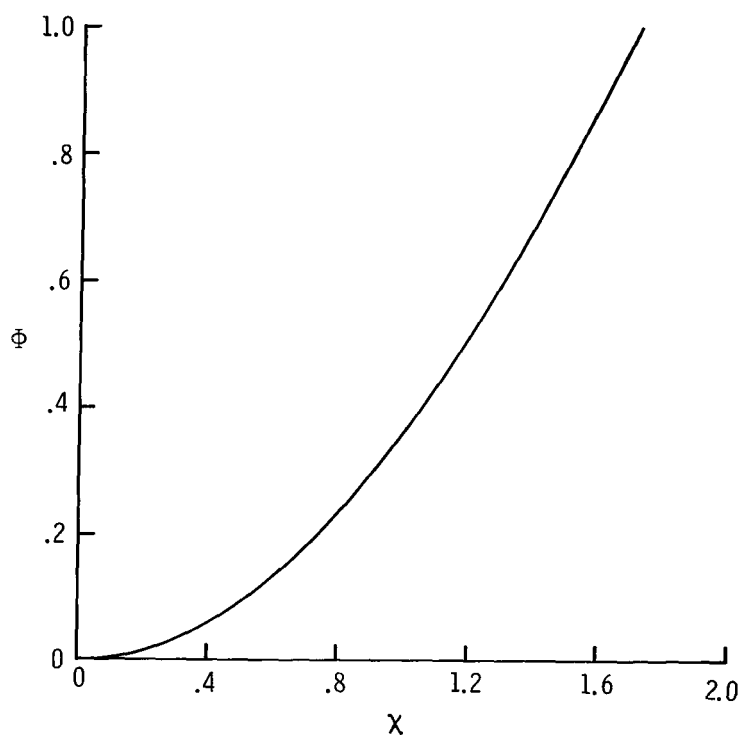


Figure 3.- Dimensionless gravitational potential and dimensionless gravitational field for equilibrium waterbag.

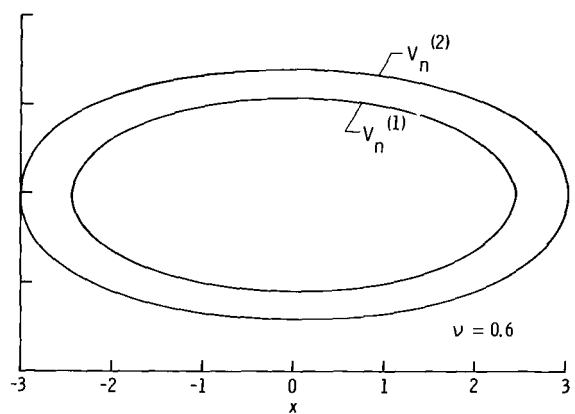
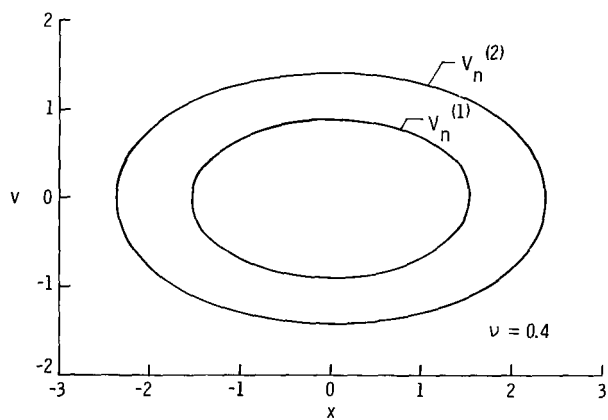
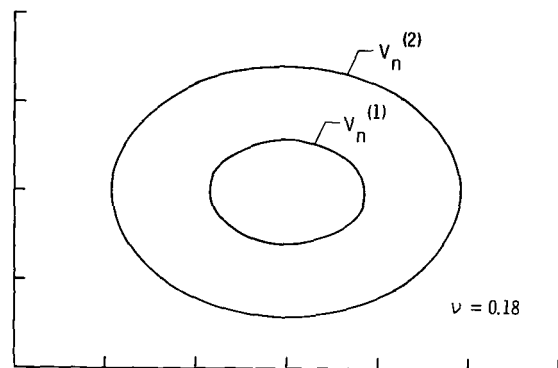
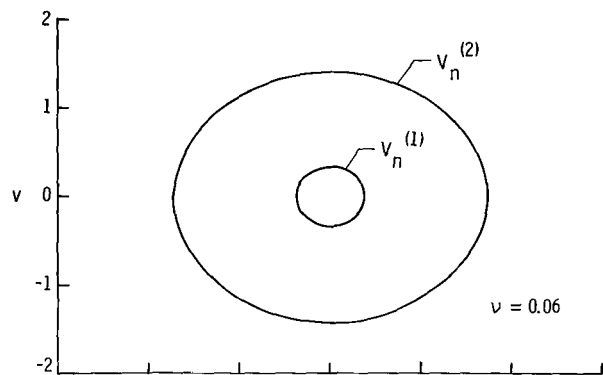


Figure 4.- Equilibrium contours for two-contour waterbag distributions.

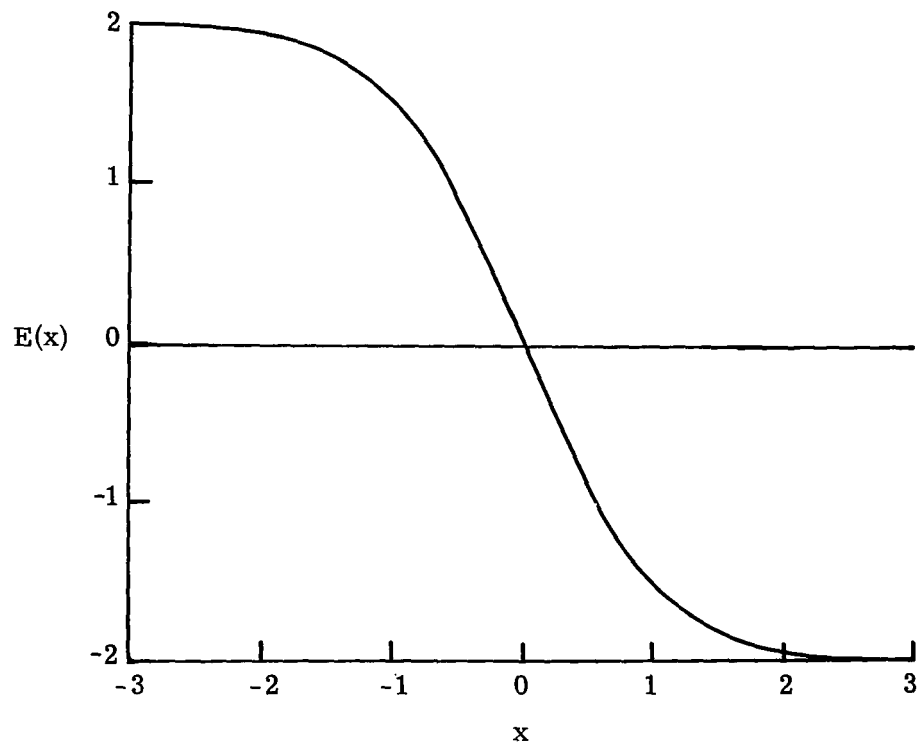
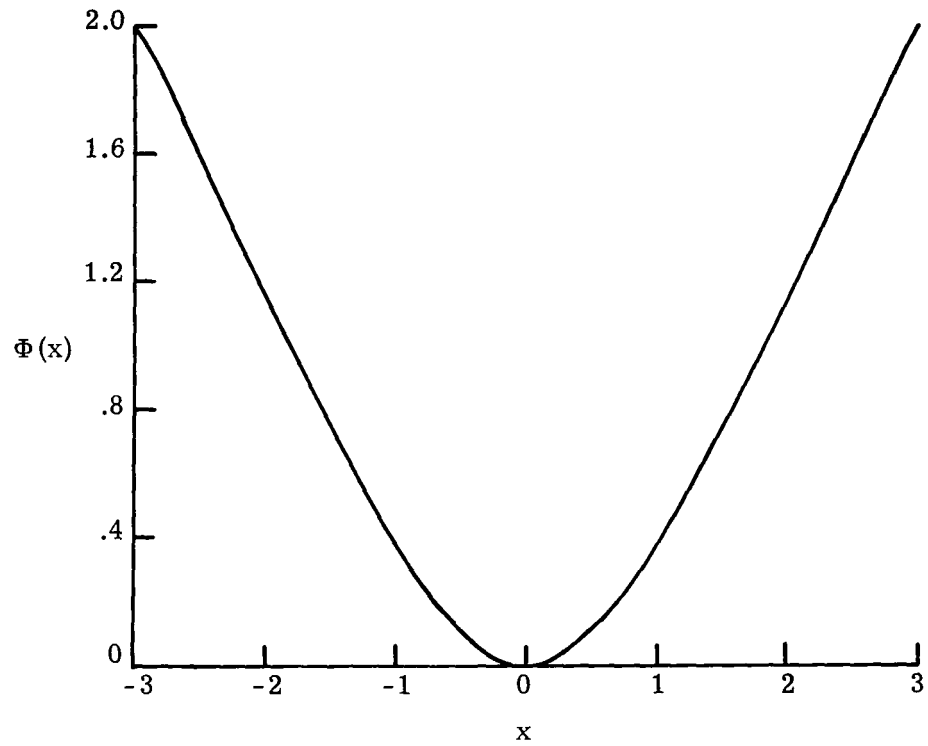


Figure 5.- Dimensionless gravitational potential and dimensionless gravitational field for Maxwellian distribution.

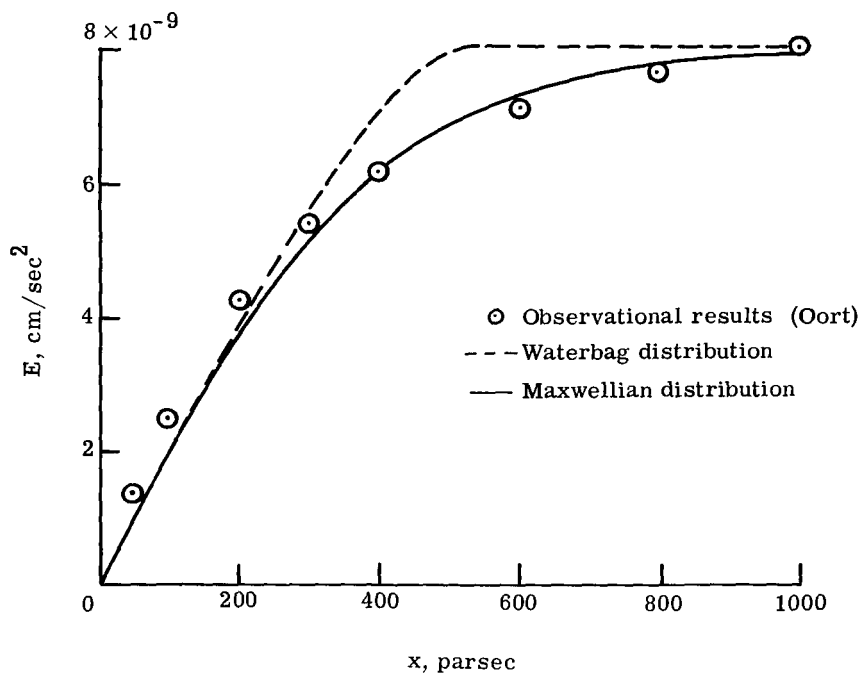


Figure 6.- Variation of gravitational force normal to galactic plane.

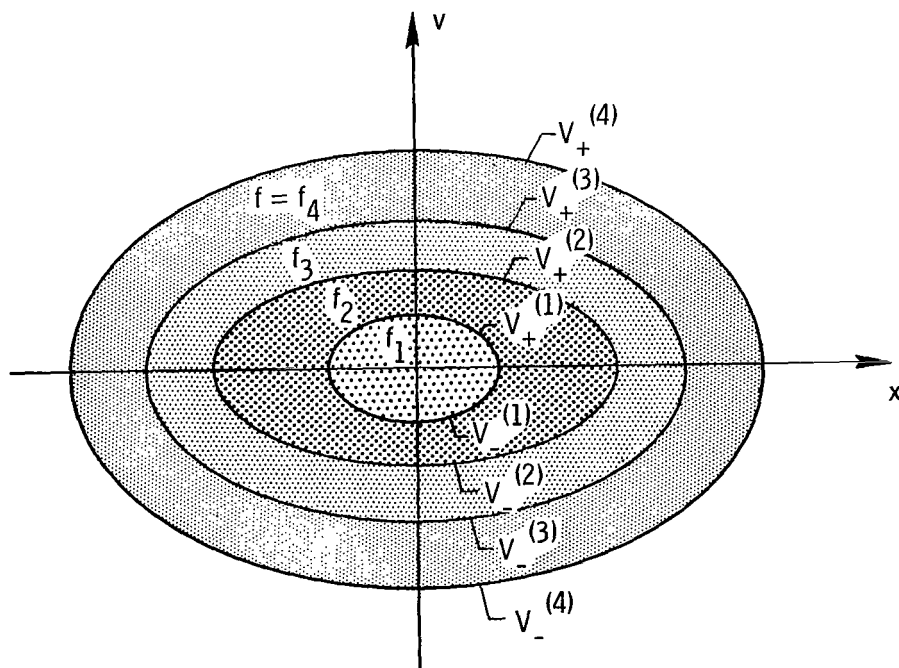


Figure 7.- Illustration of multiple-contour waterbag distribution.

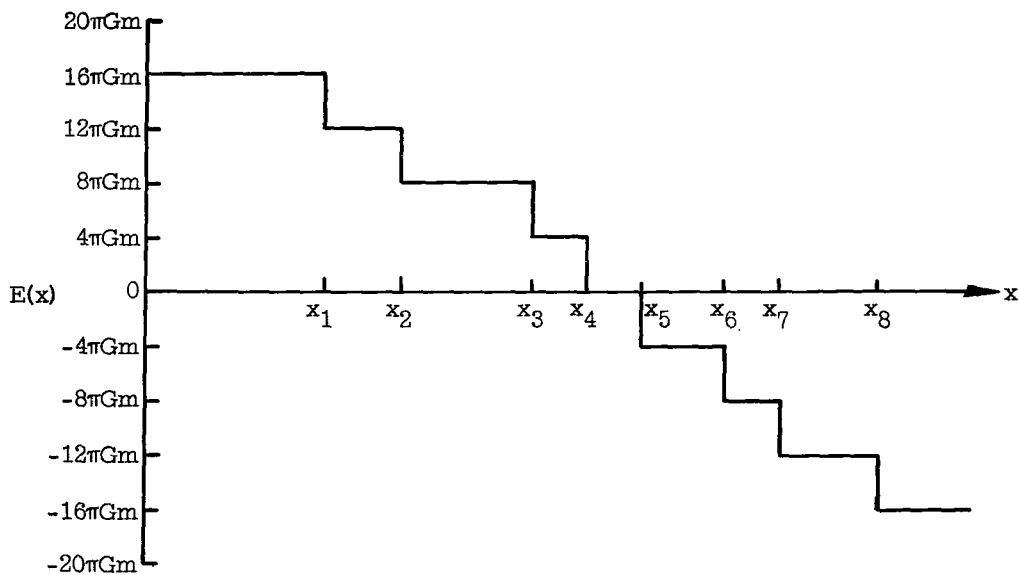


Figure 8.- Variation of gravitational field for eight-sheet system.

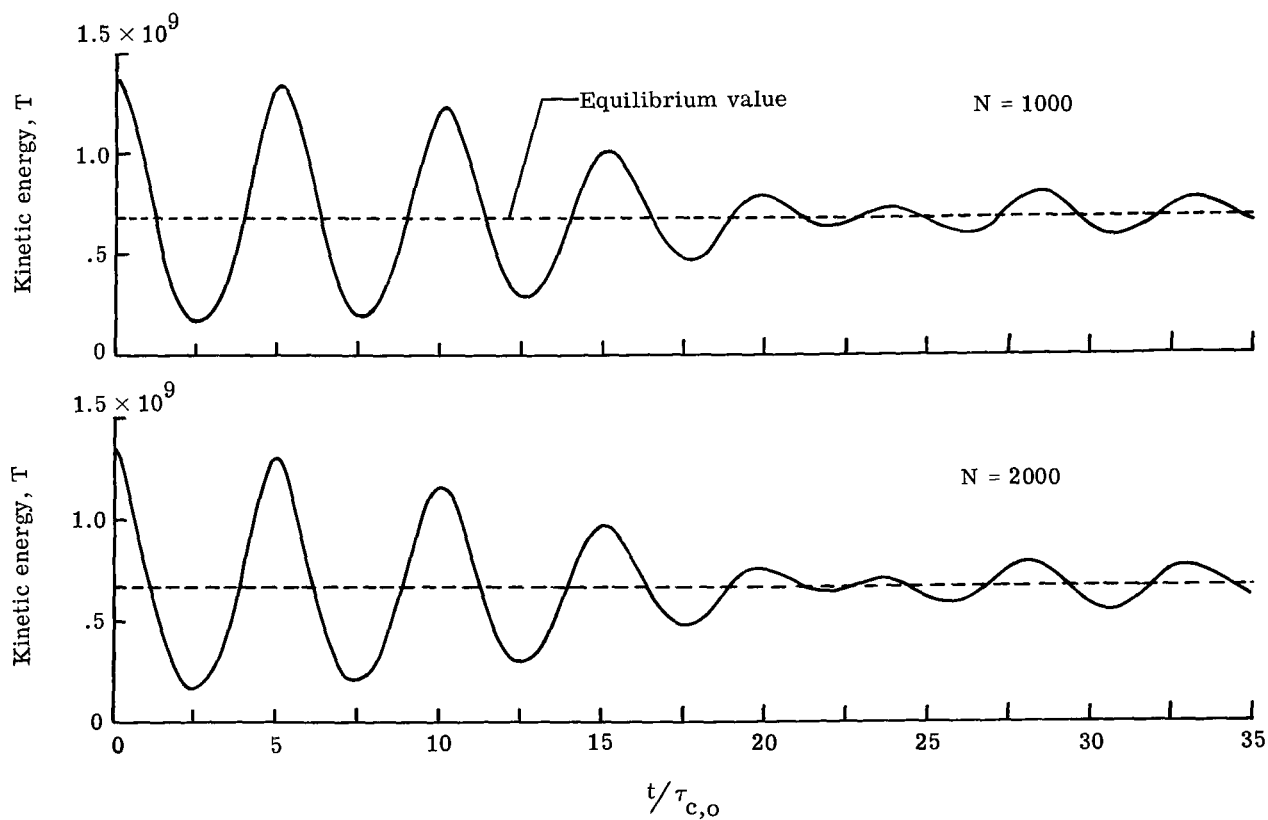


Figure 9.- Time development of kinetic energy for two equivalent systems with different graininess.

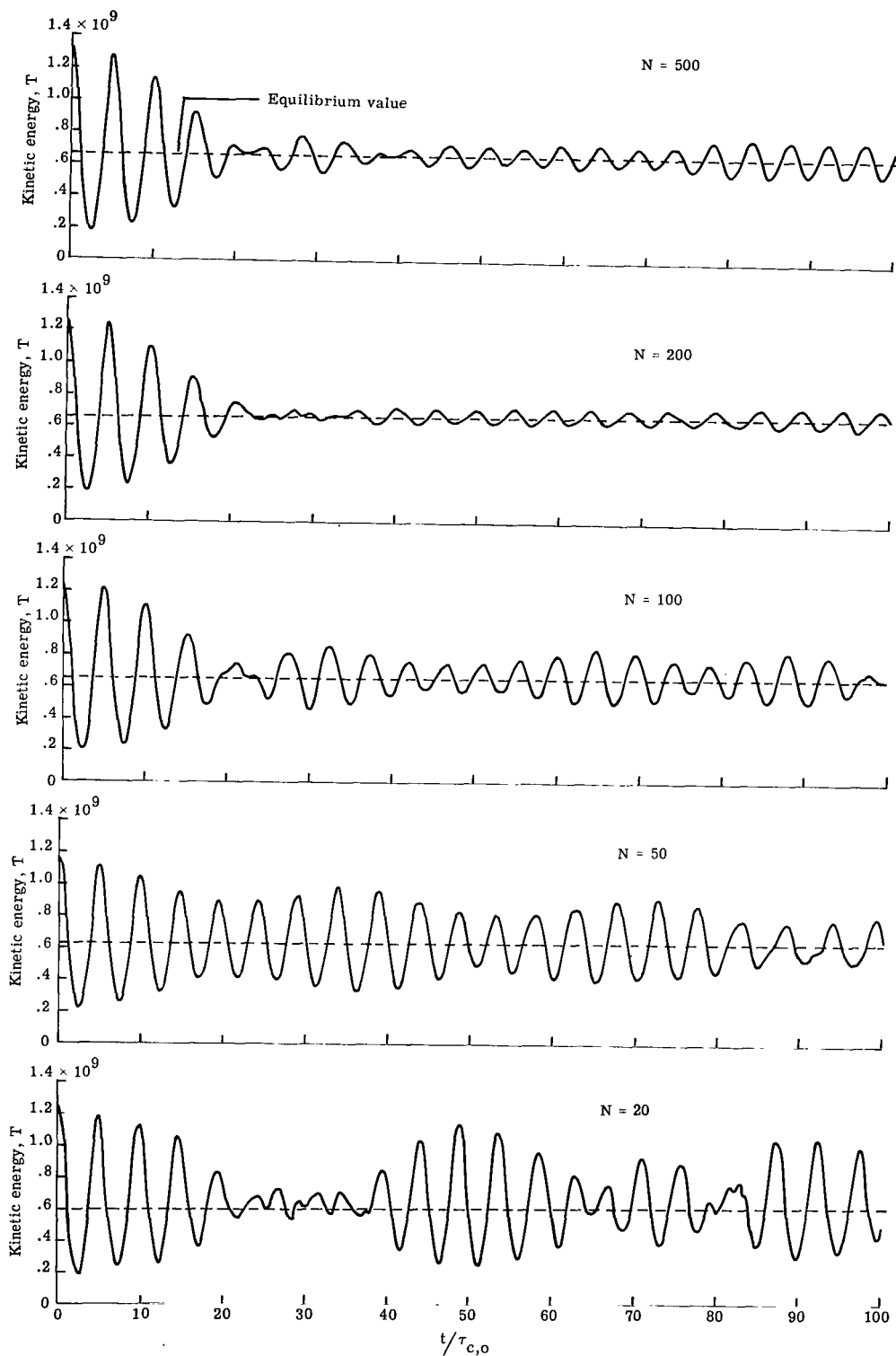


Figure 10.- Comparison of time development of kinetic energy for several equivalent systems with number of stars per system varying from 20 to 500.

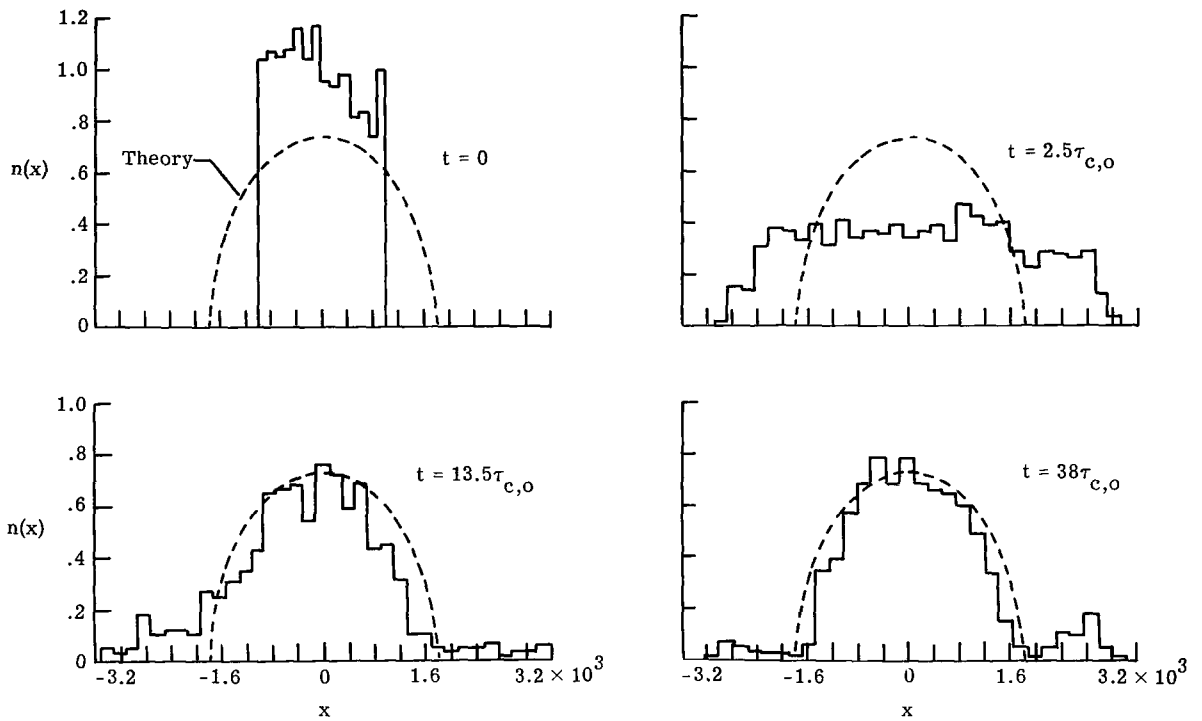


Figure 11.- Time development of density for waterbag distribution near equilibrium with $N = 2000$.

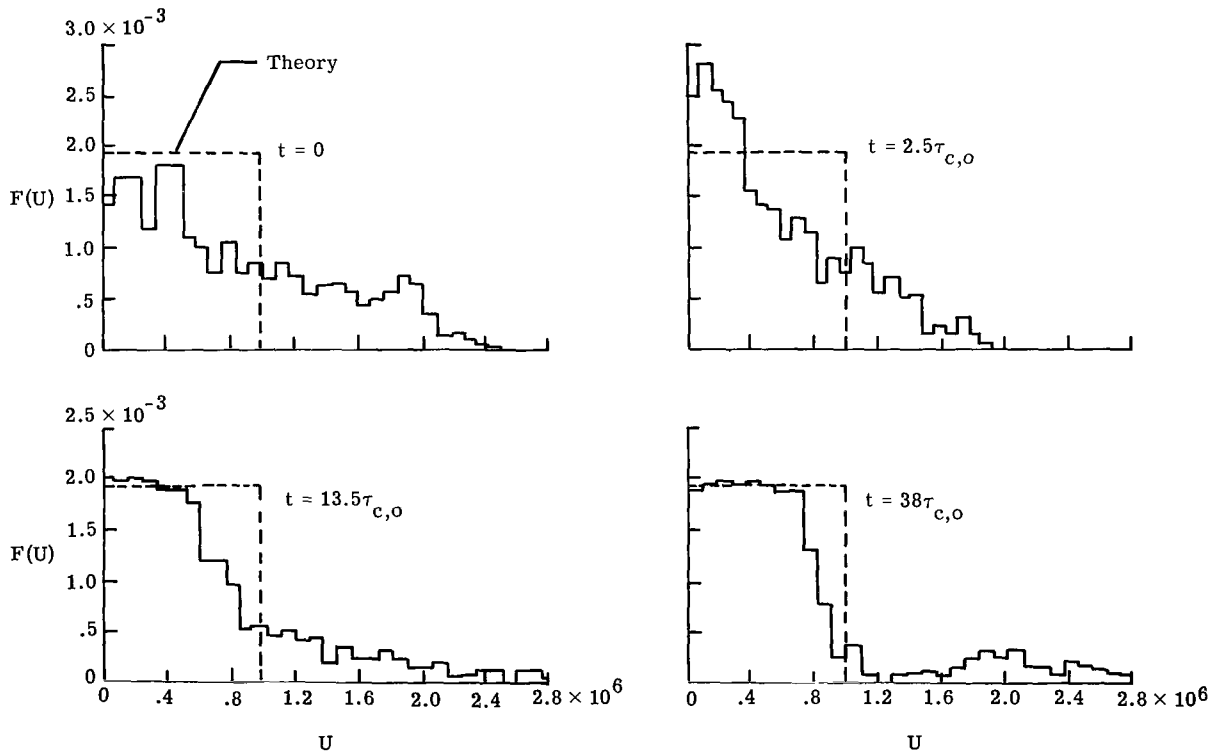


Figure 12.- Time development of energy distribution function for initial waterbag distribution near equilibrium with $N = 2000$.

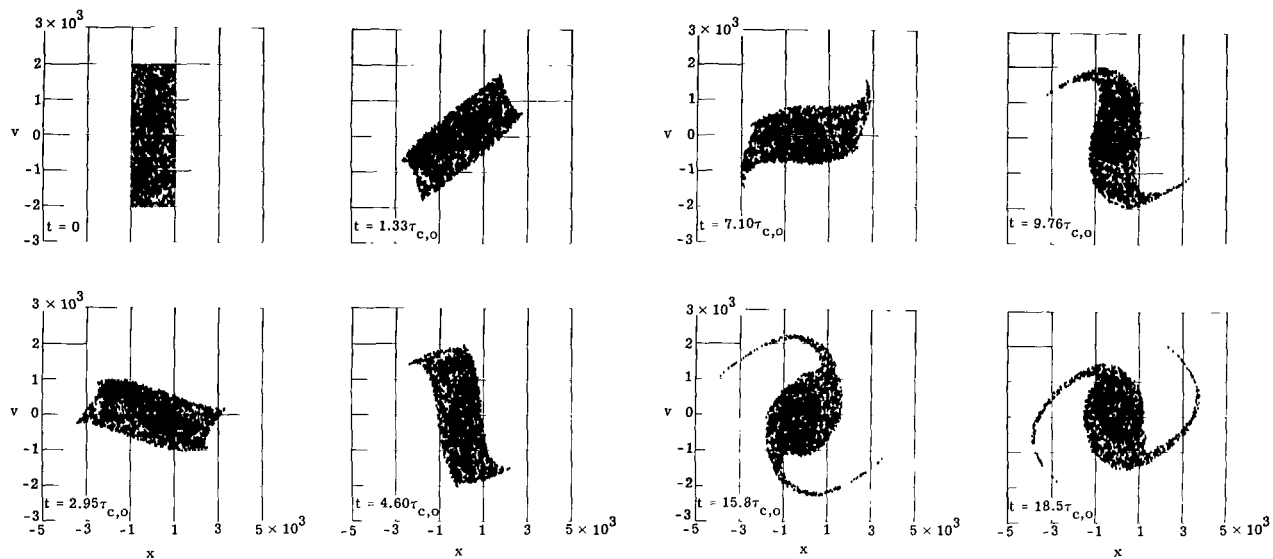


Figure 13.- Approach to equilibrium in phase space for system of 2000 mass sheets with ratio of initial to equilibrium energy equal to 1.33.

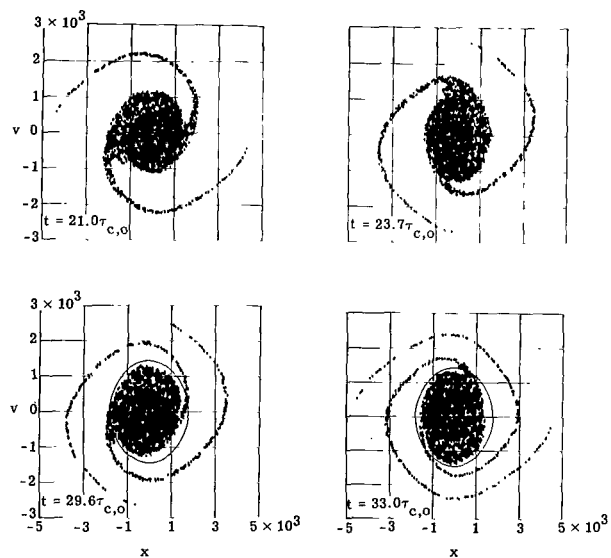


Figure 13.- Concluded.

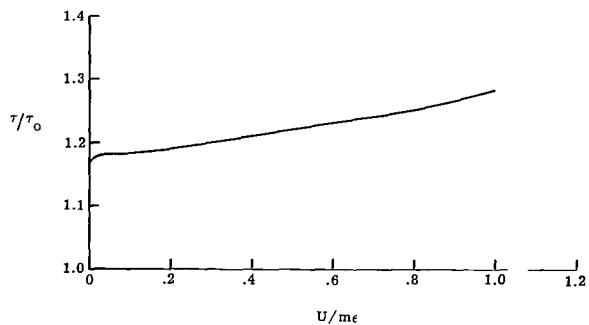


Figure 14.- Variation of period of oscillation of mass sheets with energy for equilibrium waterbag model. Time τ_0 has been arbitrarily chosen.

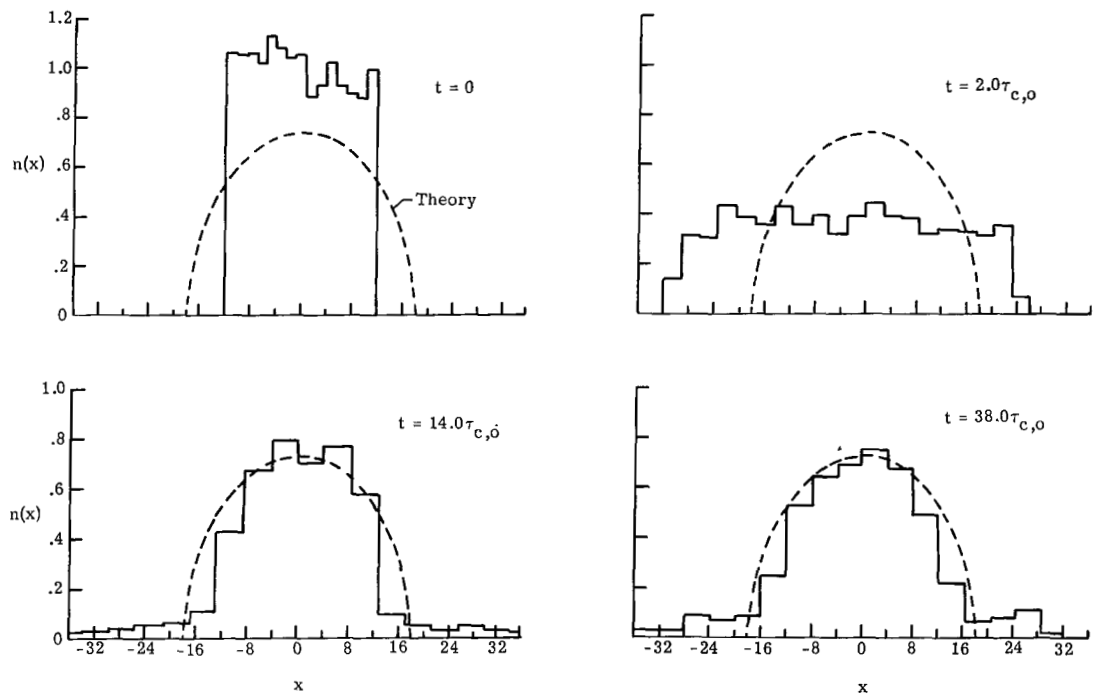


Figure 15.- Time development of density for waterbag distribution near equilibrium with $N = 1000$.

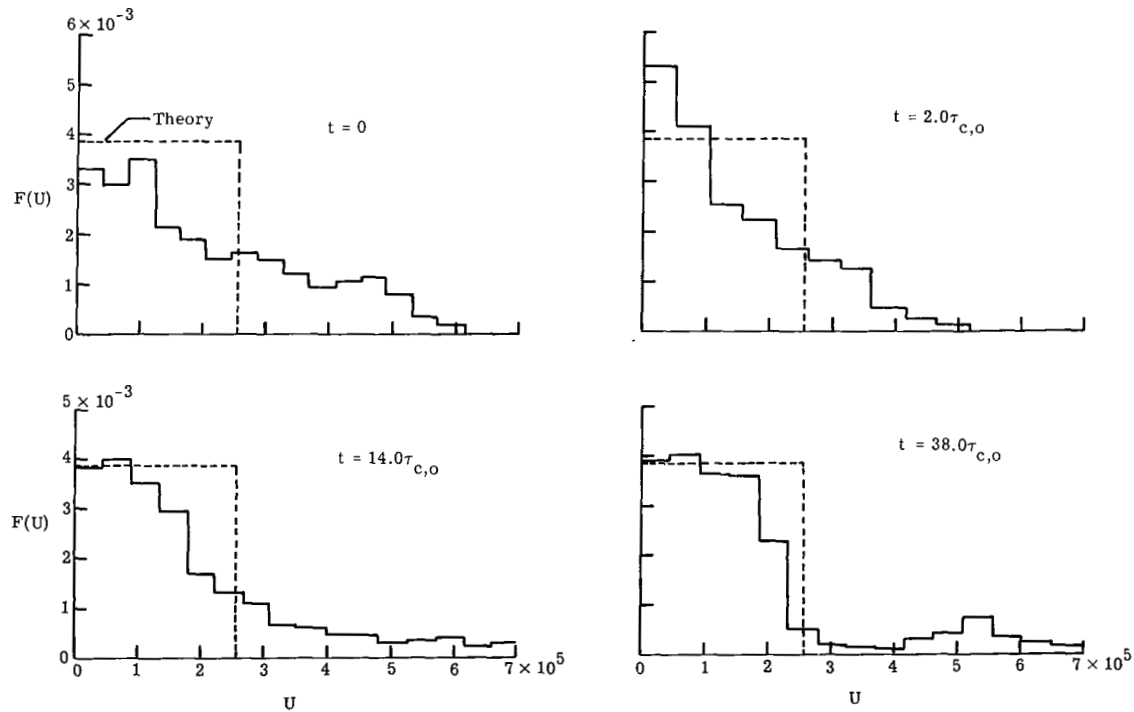


Figure 16.- Time development of energy distribution function for waterbag distribution near equilibrium with $N = 1000$.

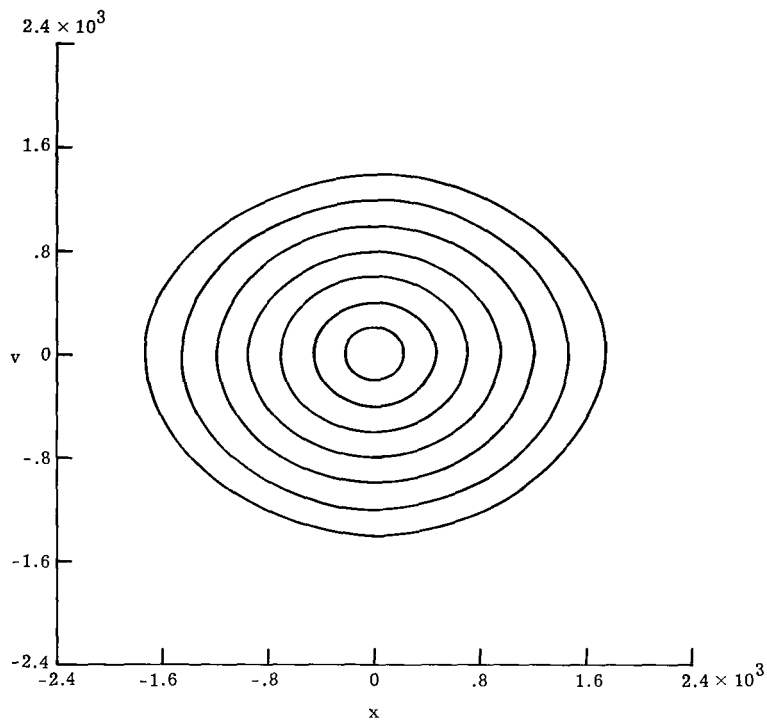


Figure 17.- Theoretical equilibrium trajectories in phase space for waterbag model.

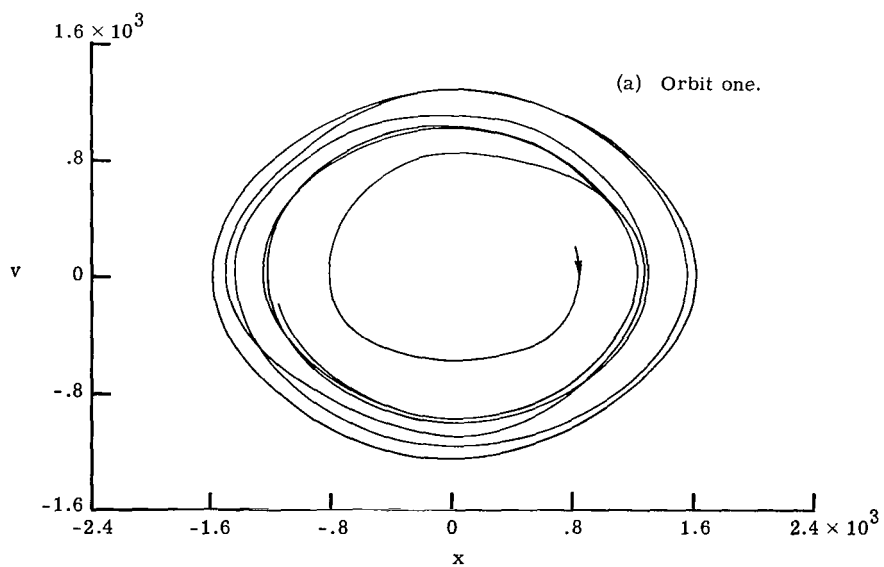


Figure 18.- Actual phase-space trajectories for five mass sheets for waterbag distribution near equilibrium.

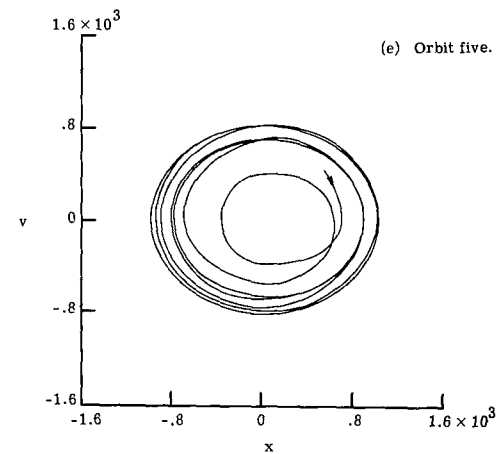
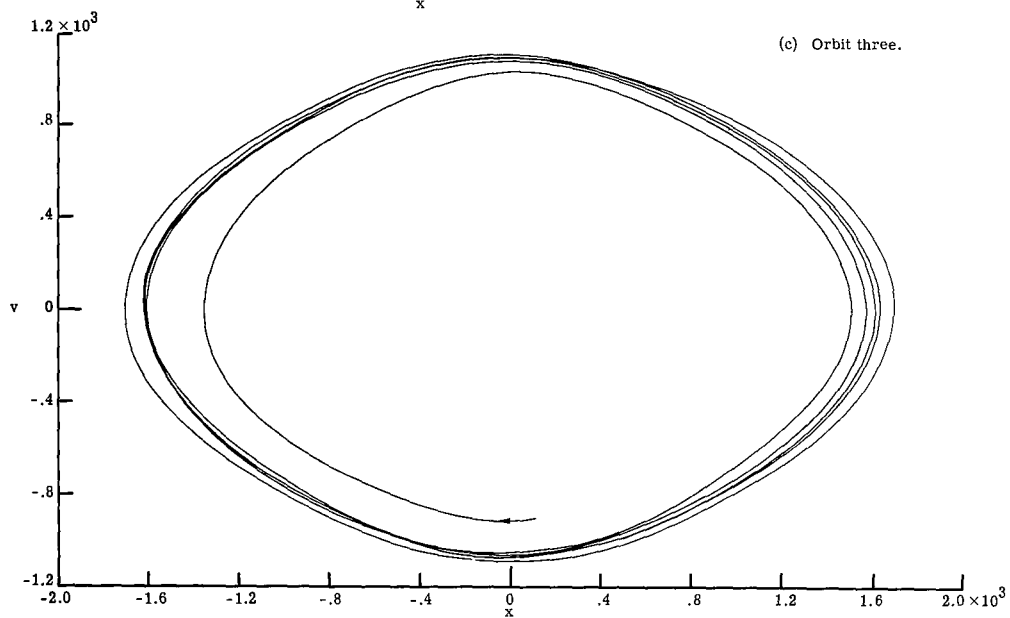
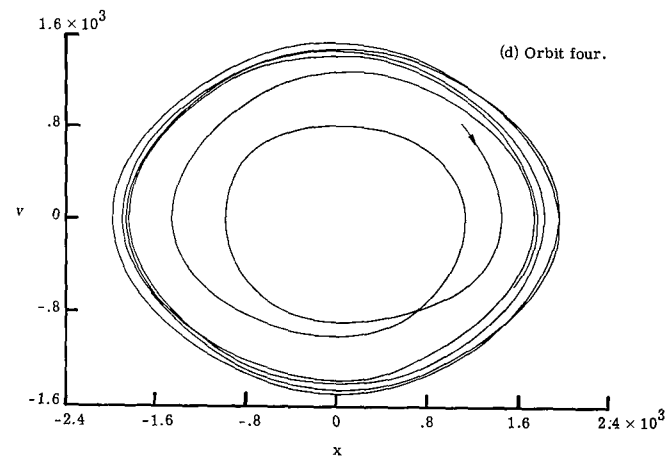
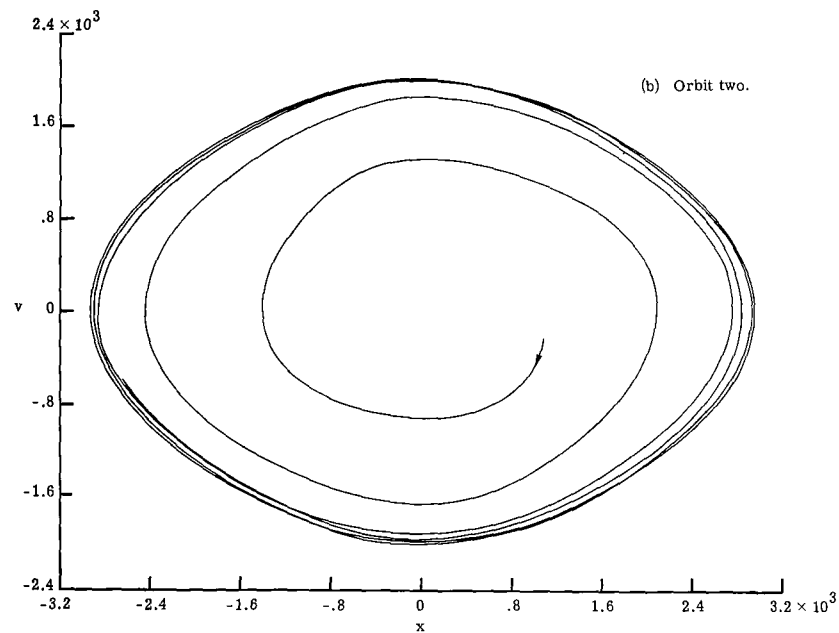


Figure 18.- Concluded.

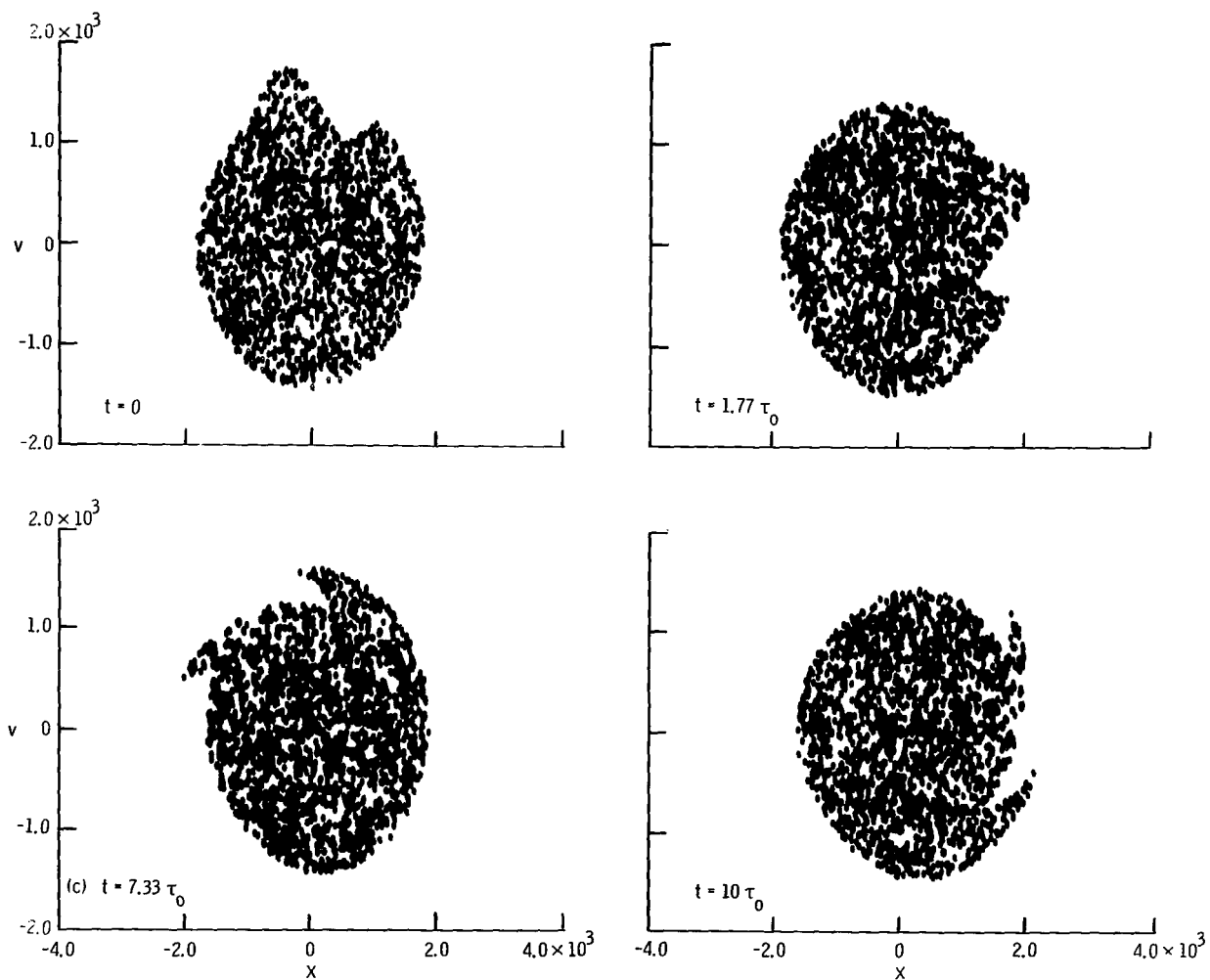


Figure 19.- Time development of local sinusoidal perturbation of equilibrium state. Time τ_0 is same as that used in figure 14.

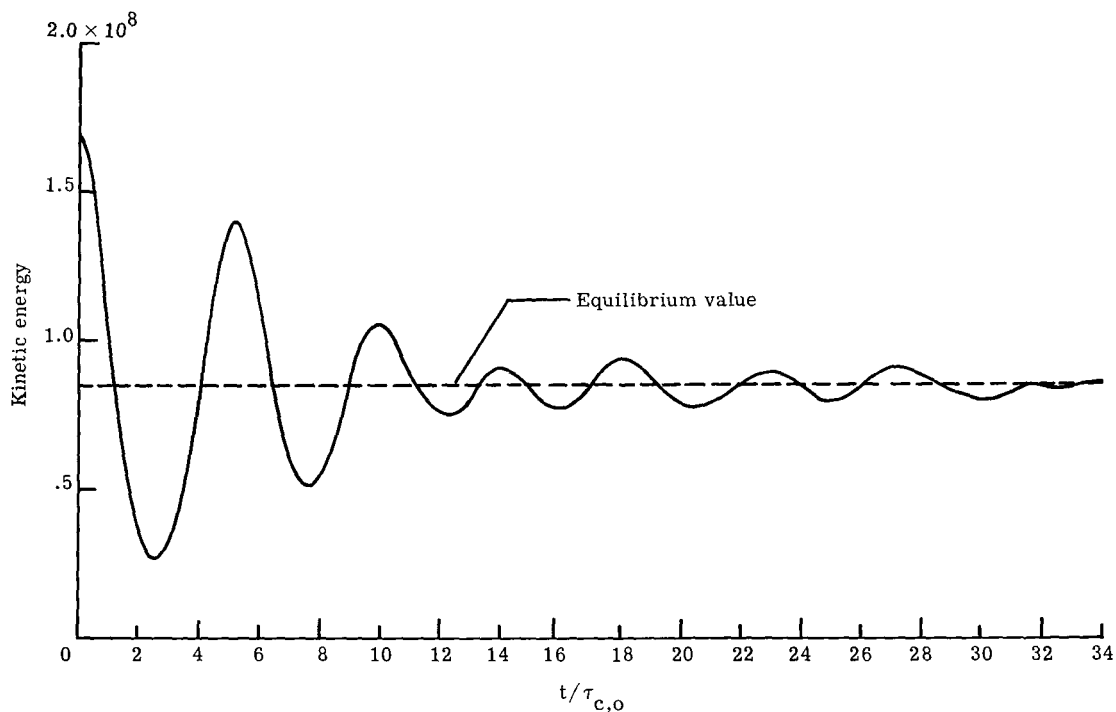


Figure 20.- Time development of kinetic energy for system near equilibrium with initially Maxwellian velocity distribution.

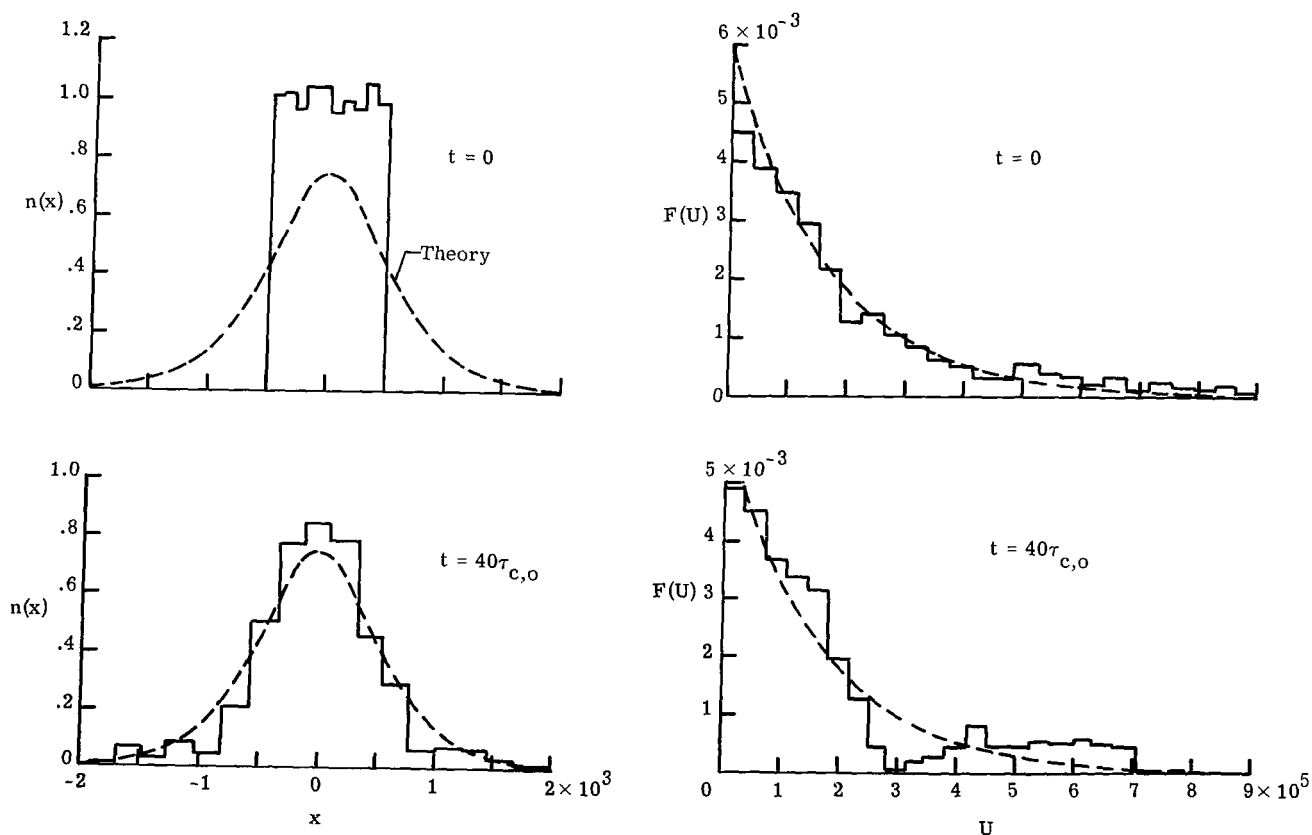


Figure 21.- Time development of density and energy distribution function for system near equilibrium with initially Maxwellian velocity distribution.

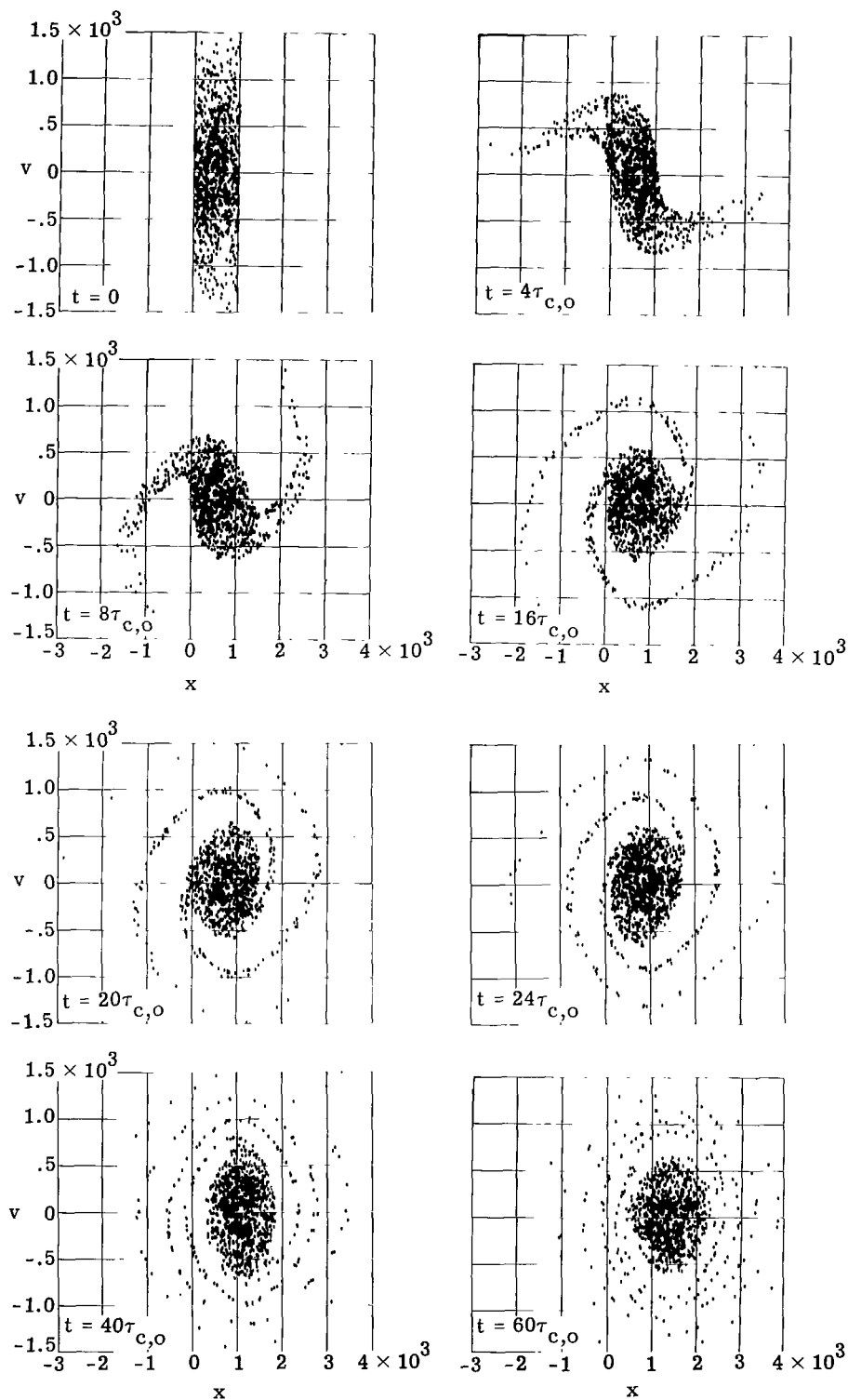


Figure 22.- Time development in phase space for system of 1000 mass sheets near equilibrium with initially Maxwellian velocity distribution.

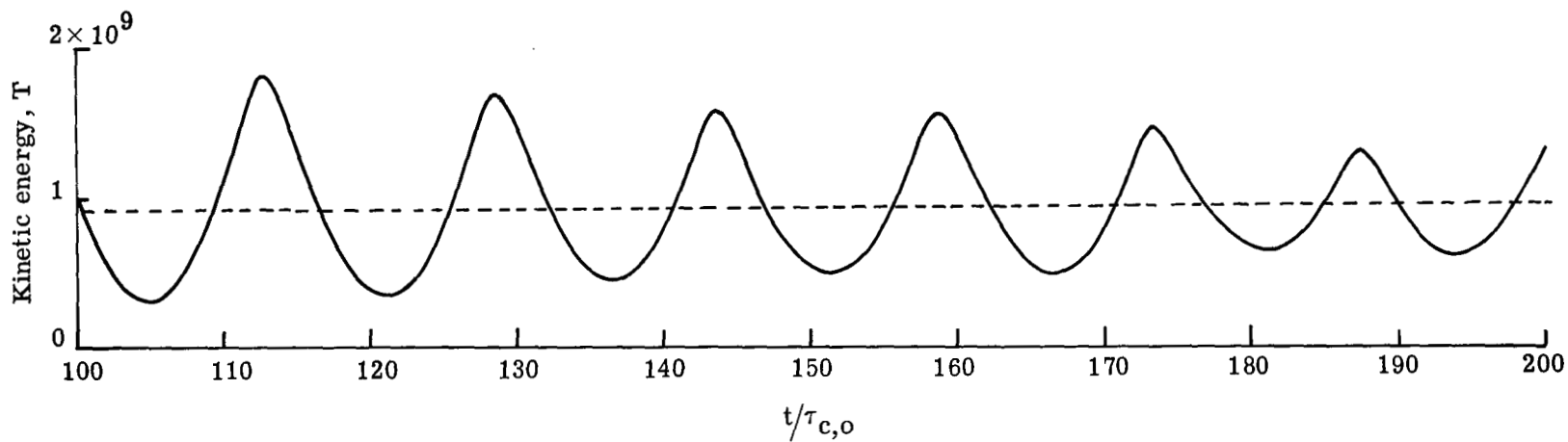
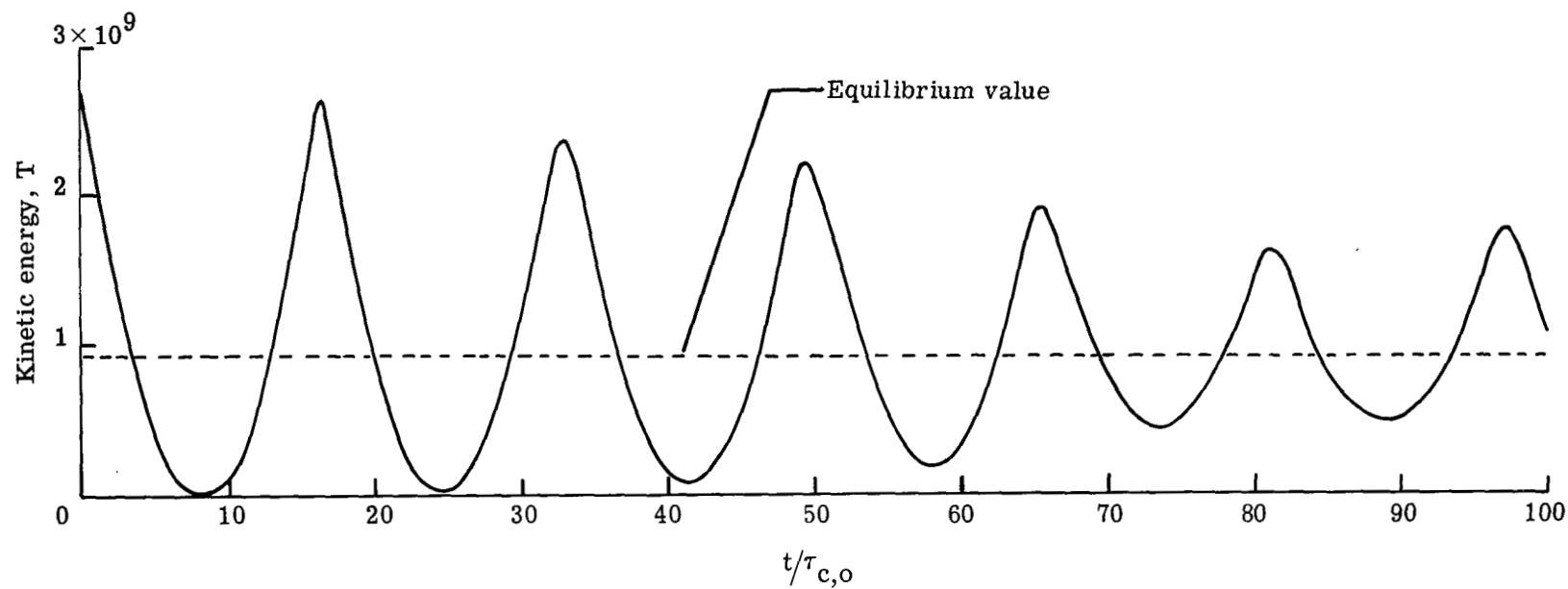


Figure 23.- Time development of kinetic energy for system of 1000 stars far from equilibrium.

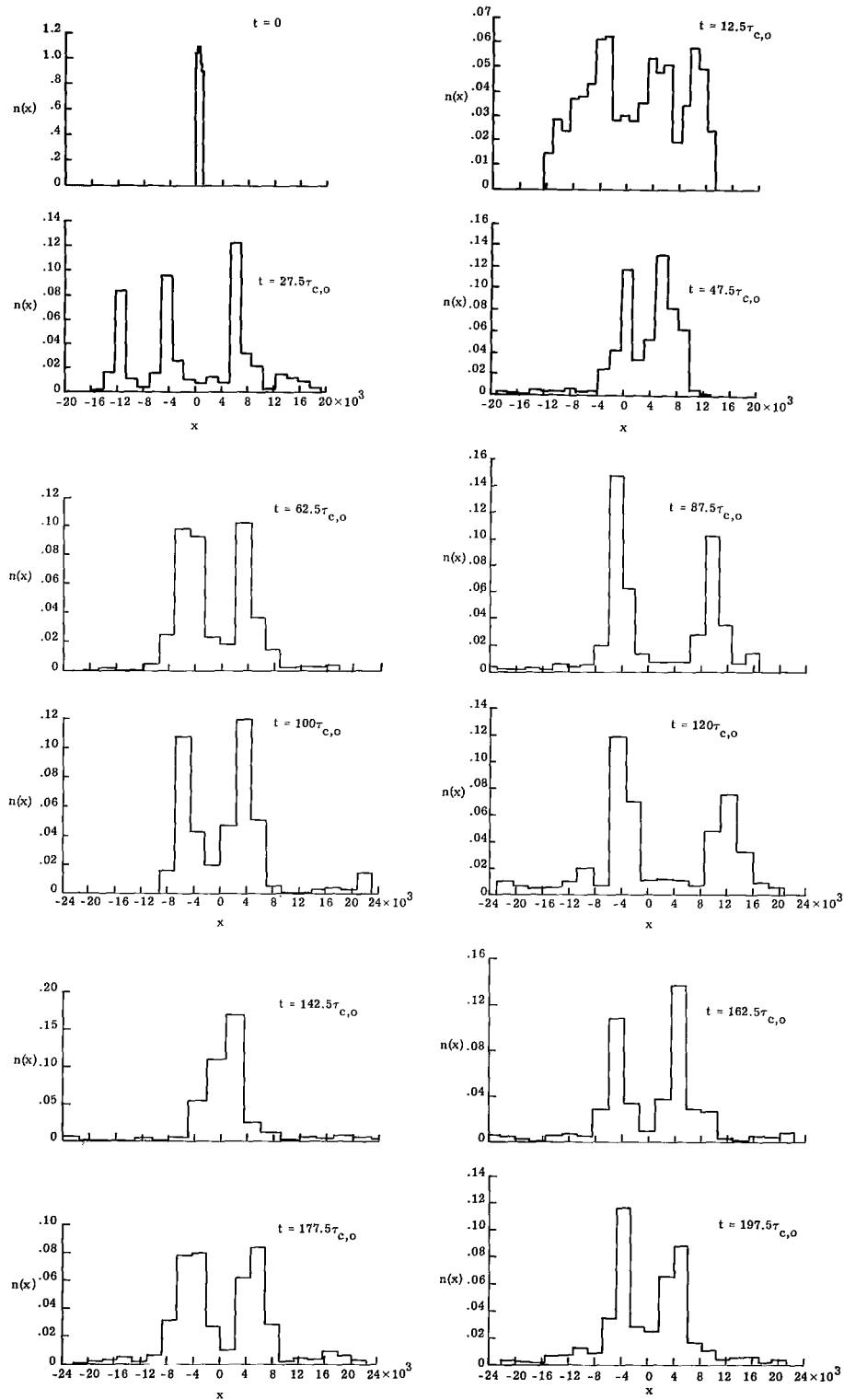


Figure 24.- Time development of density for system of 1000 stars far from equilibrium.

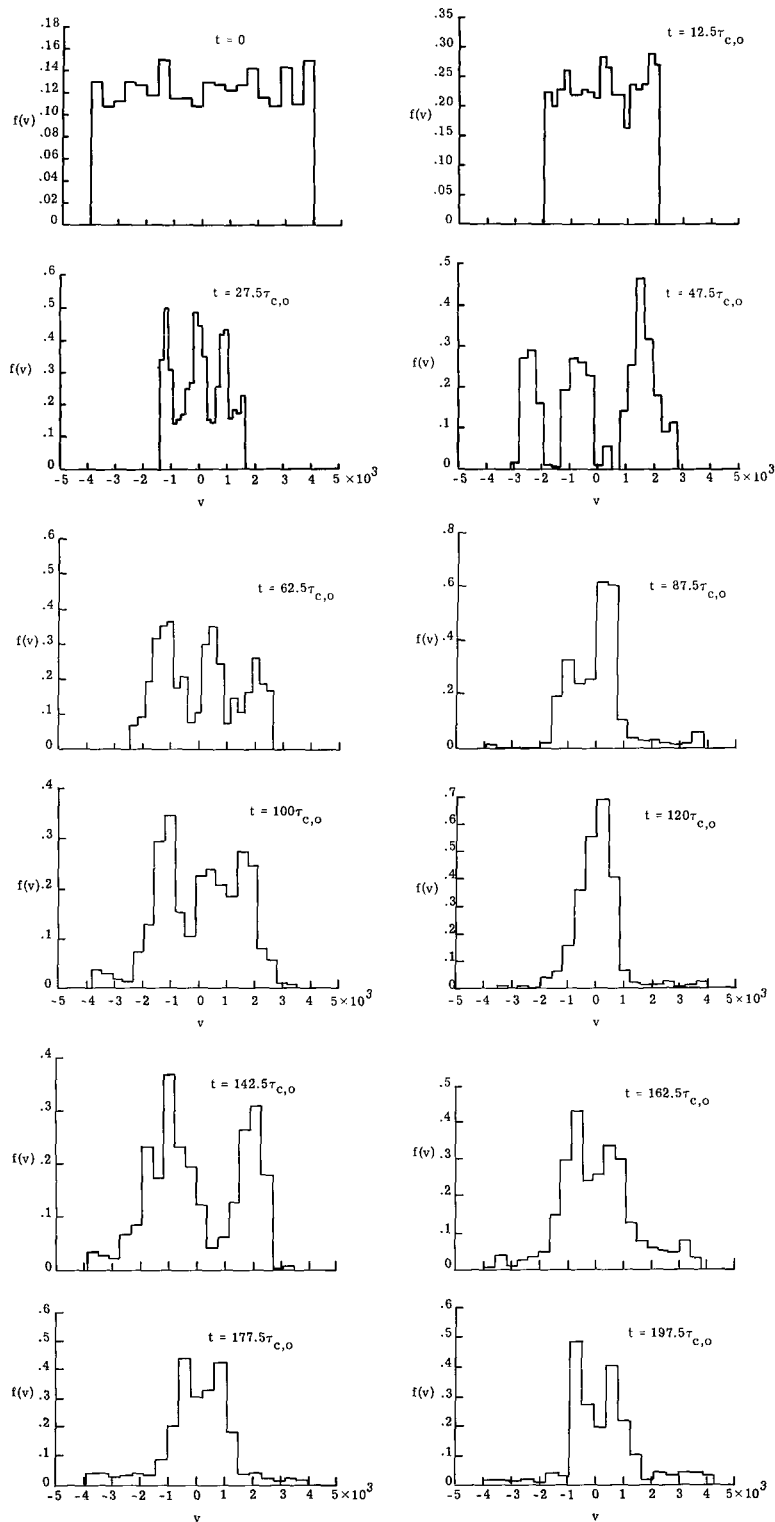


Figure 25.- Time development of velocity distribution function for system of 1000 stars far from equilibrium.

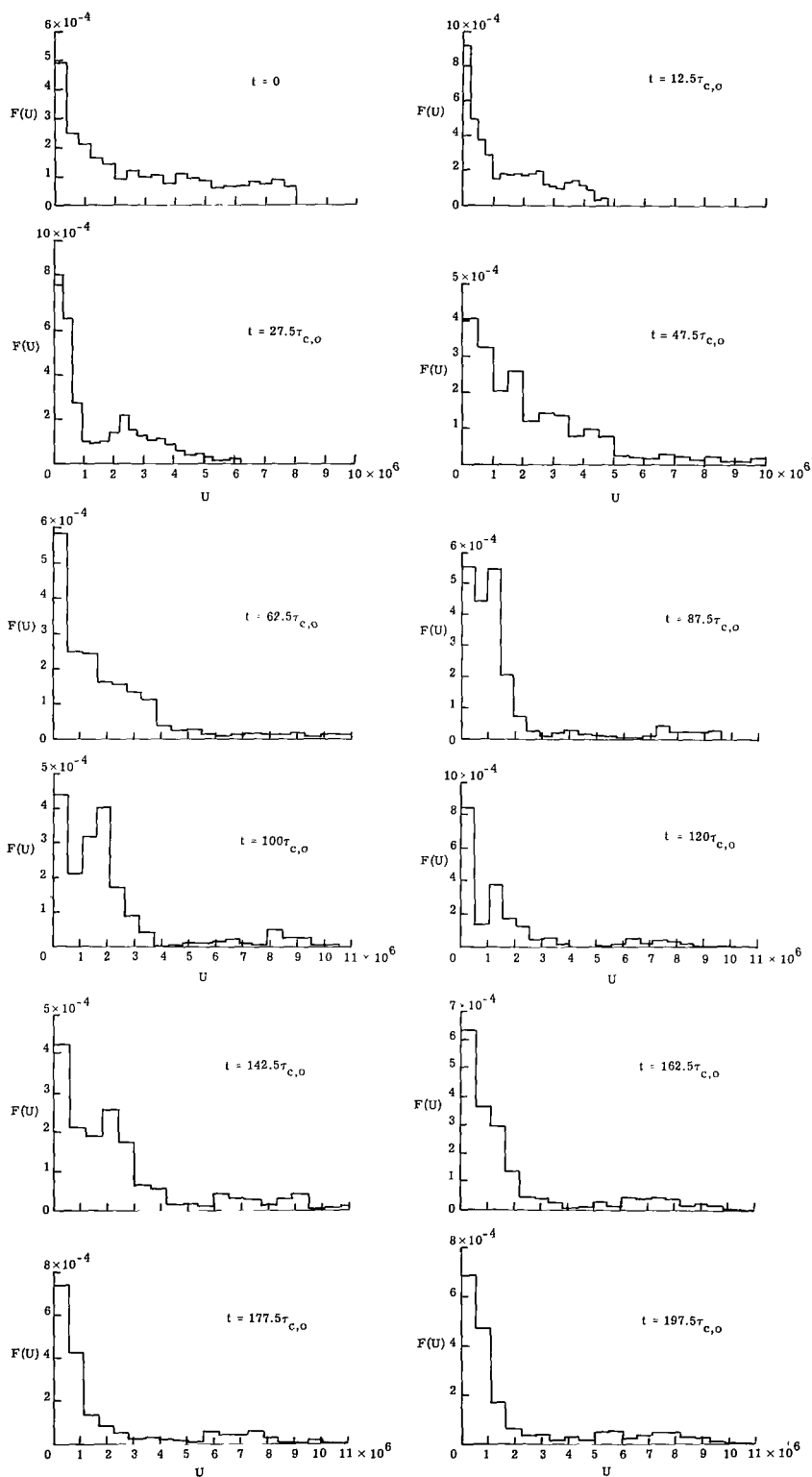


Figure 26.- Time development of energy distribution function for system of 1000 stars far from equilibrium.

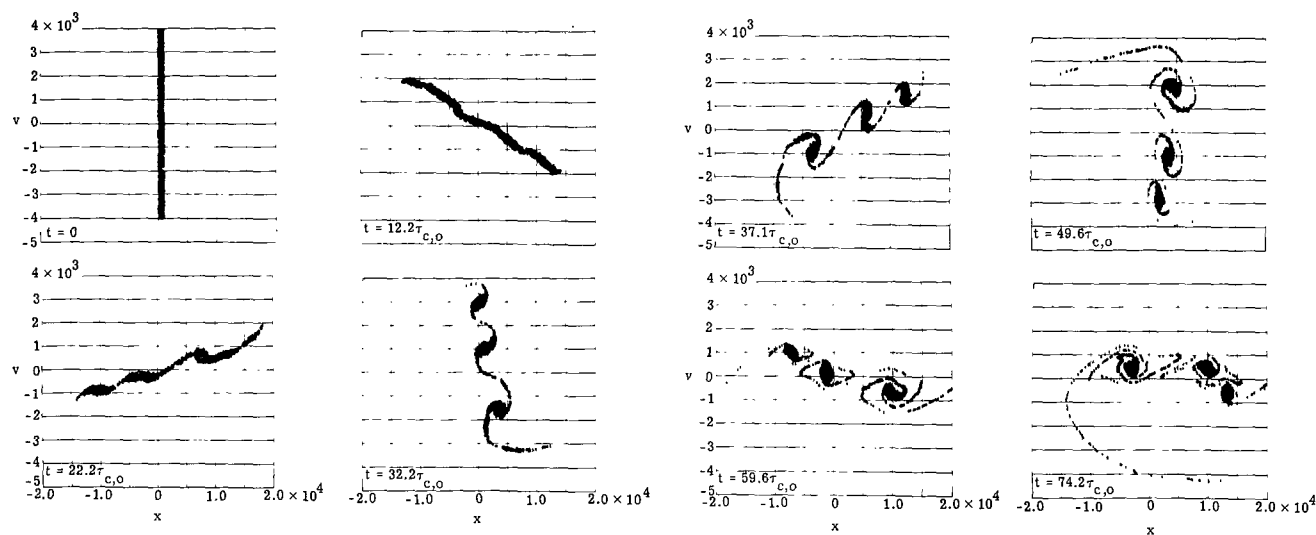


Figure 27.- Time development in phase space for system of 1000 stars far from equilibrium.

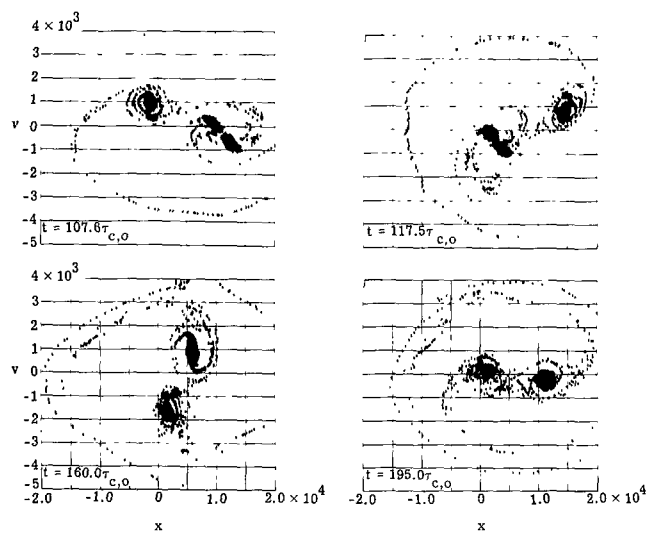


Figure 27.- Concluded.

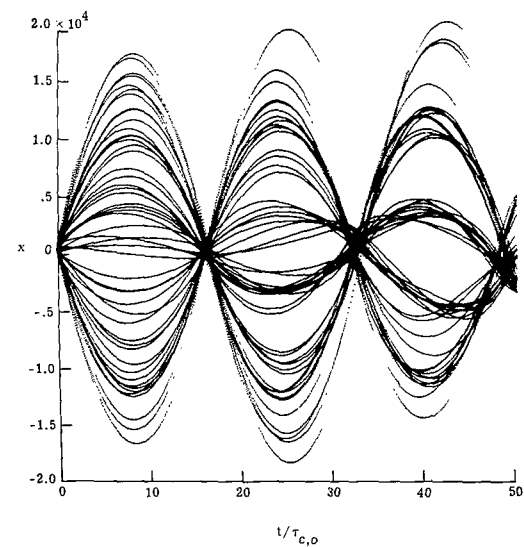


Figure 28.- Position as function of time for every 20th star for system shown in figure 27.

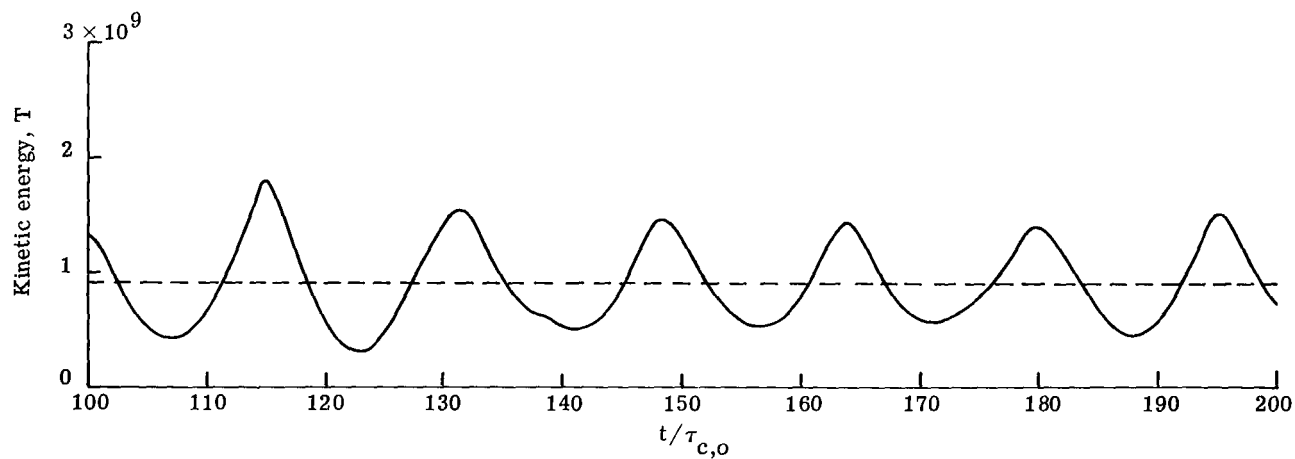
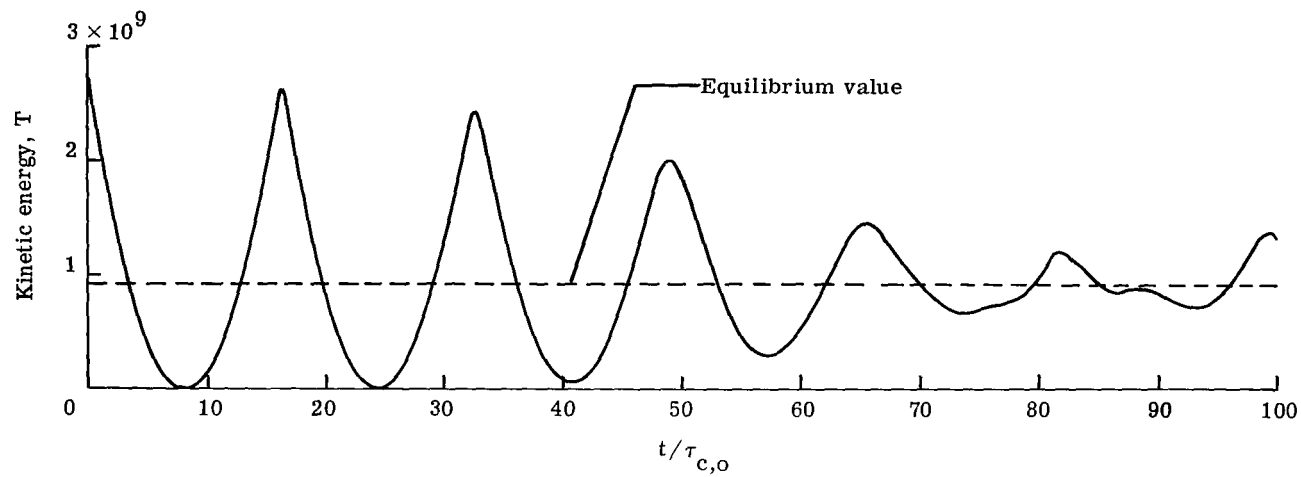


Figure 29.- Time development of kinetic energy for unstable system of 1000 stars.

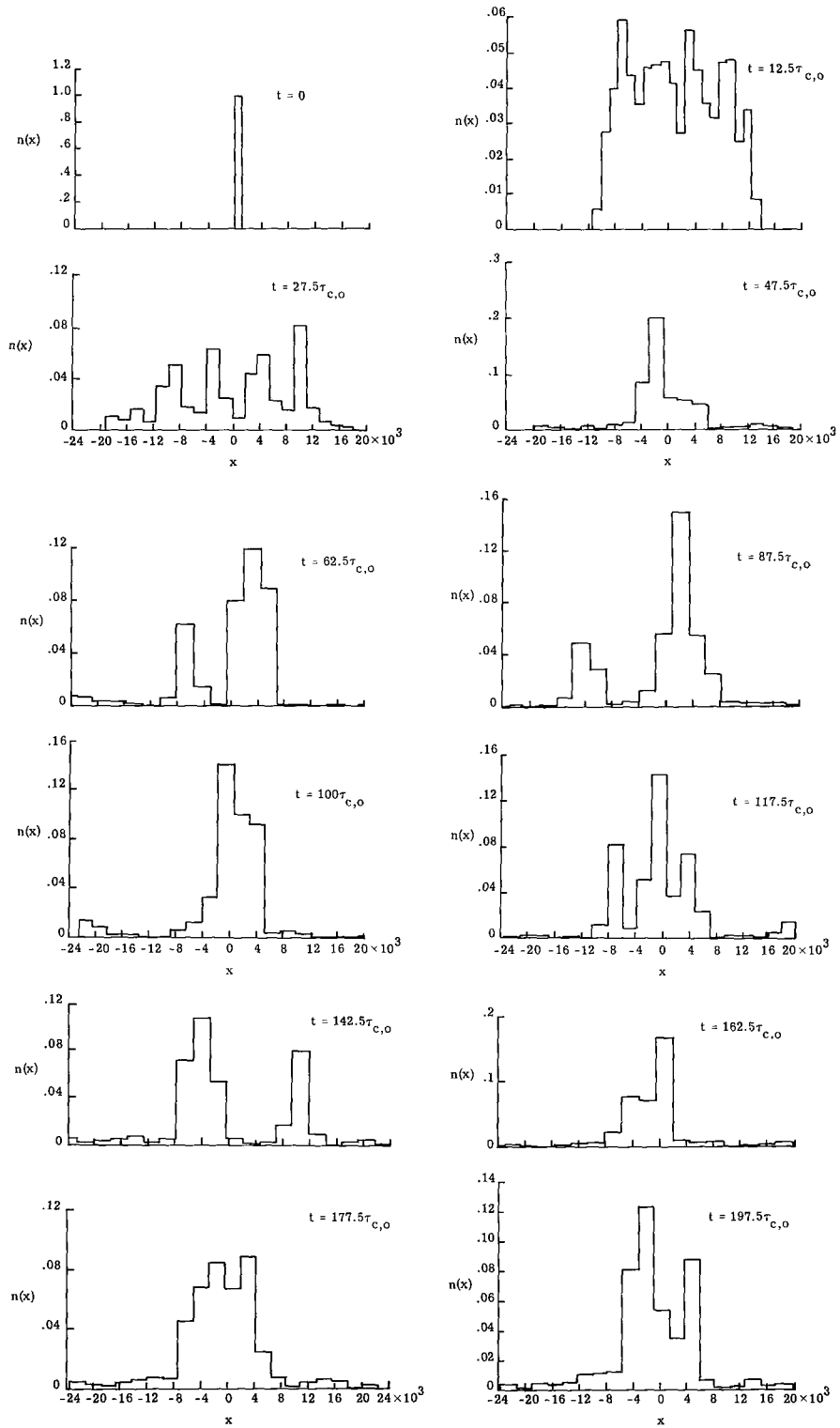


Figure 30.- Time development of density for unstable system.

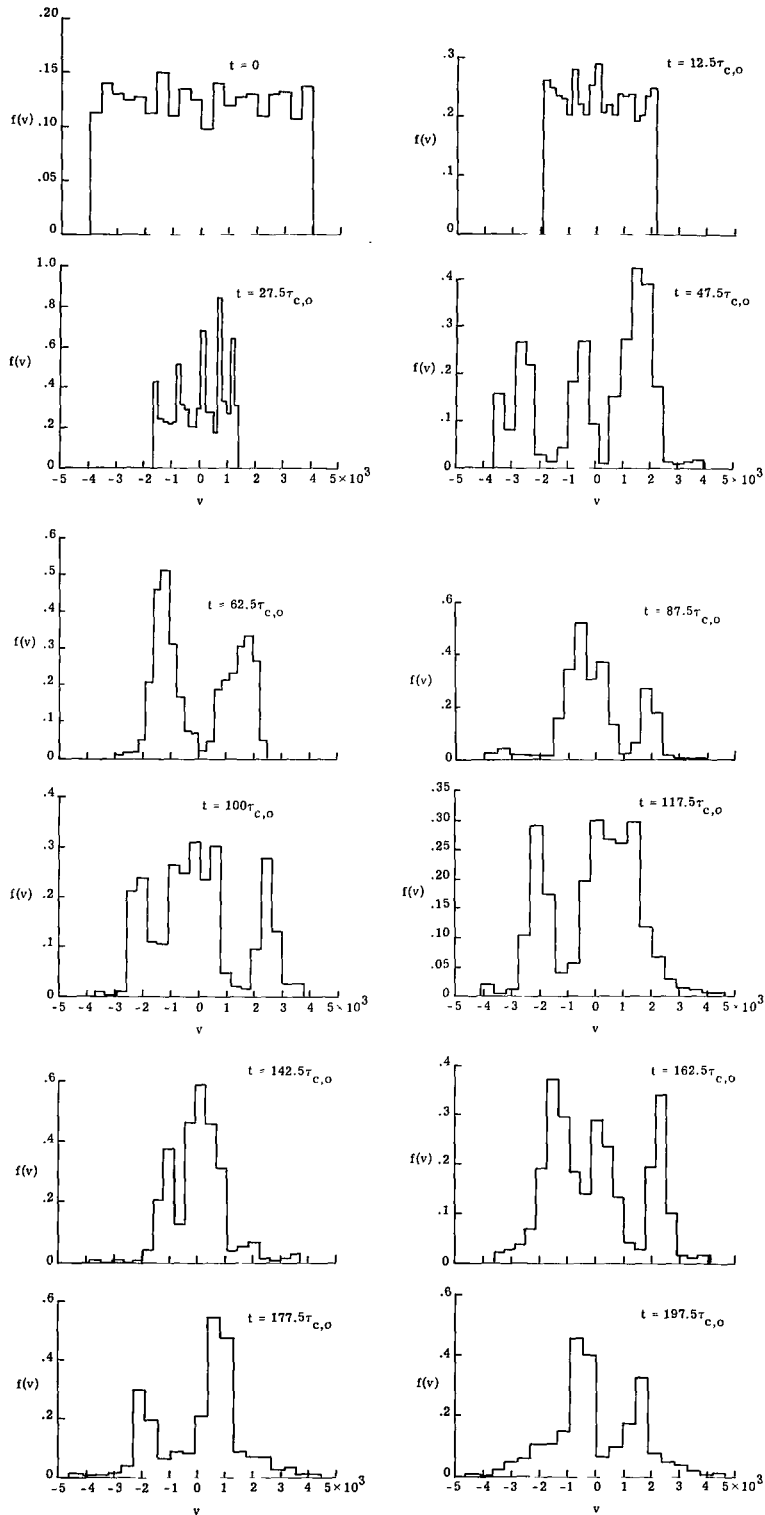


Figure 31.- Time development of velocity distribution for unstable system.

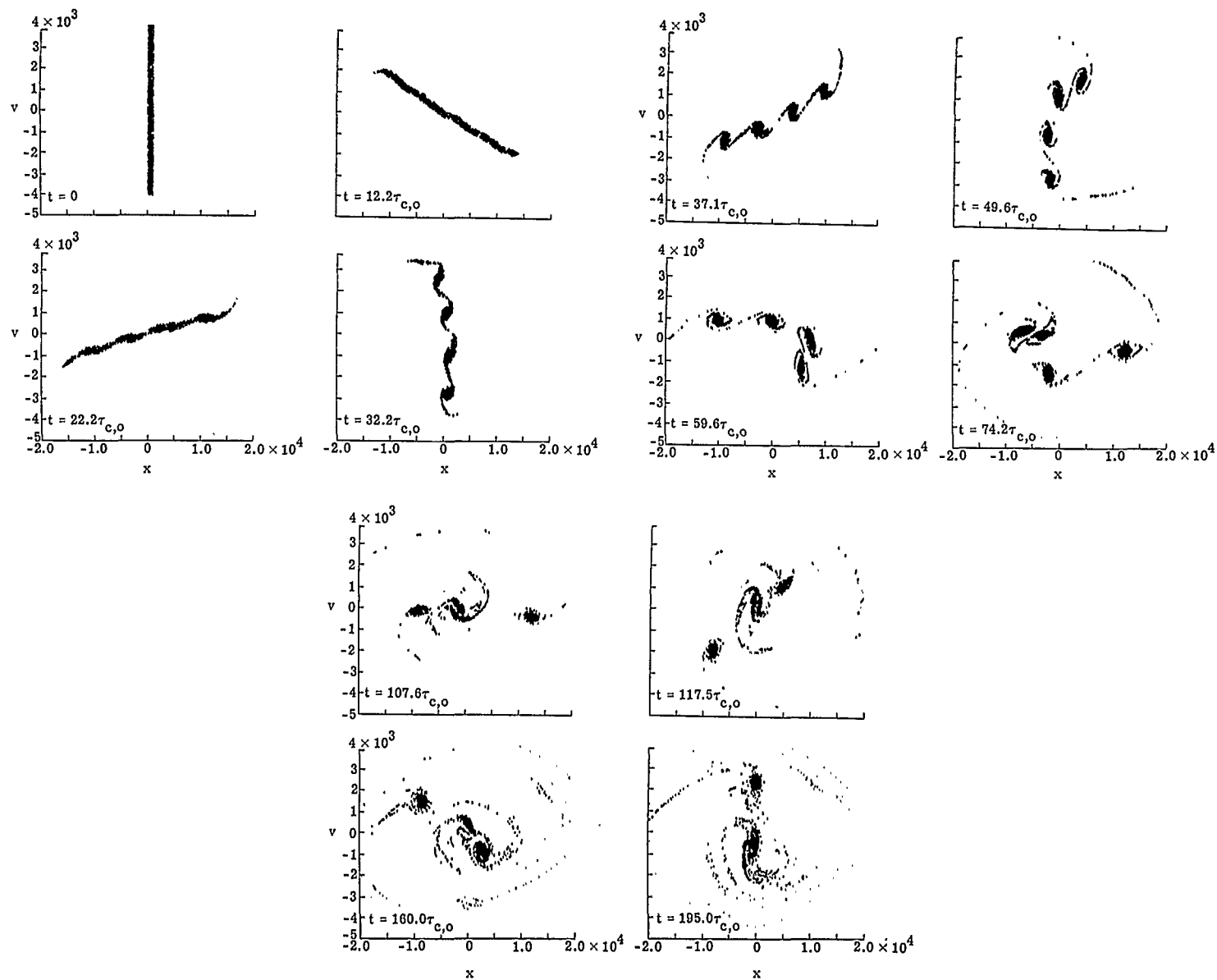


Figure 32.- Time development in phase space of unstable system.

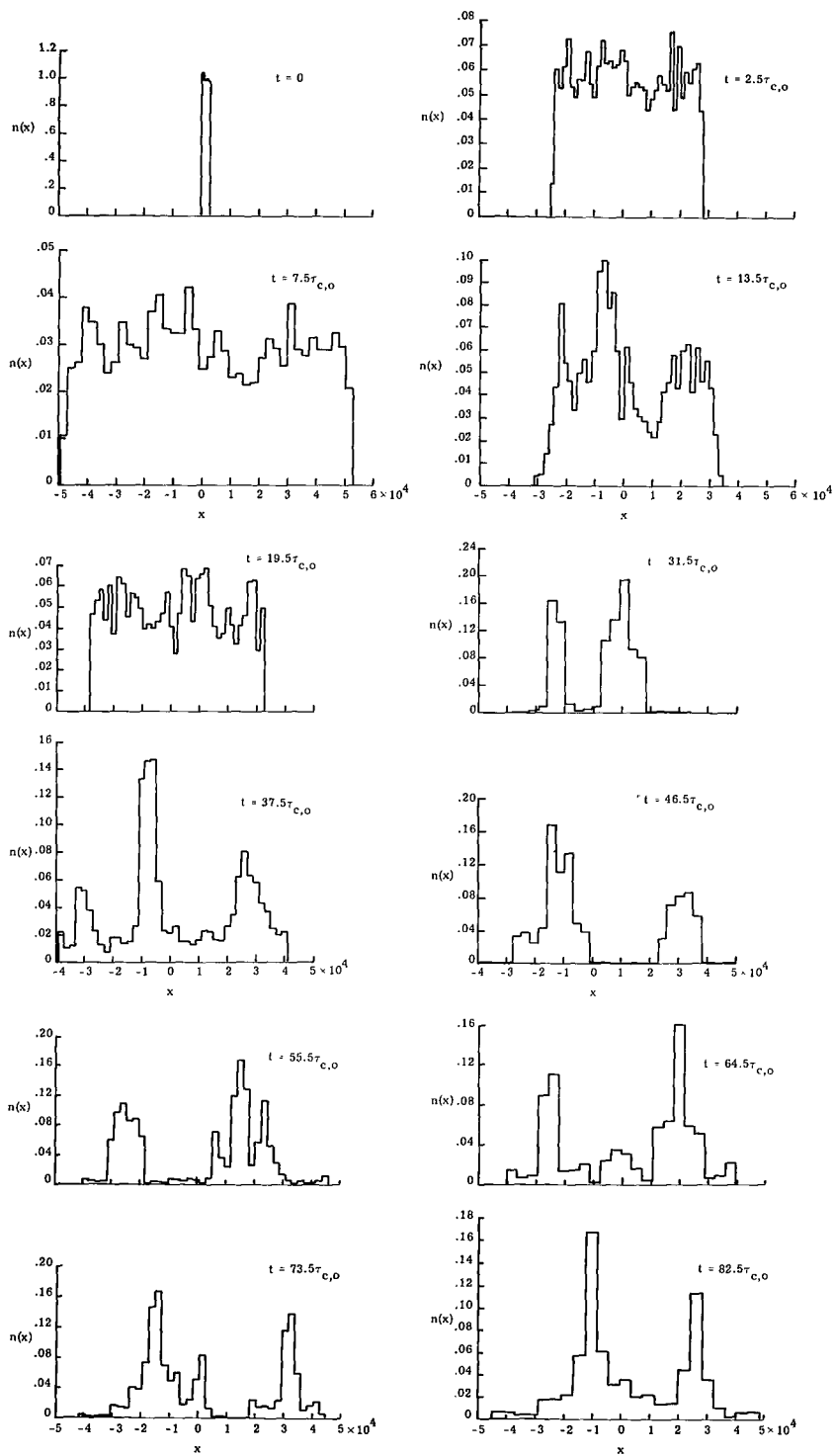


Figure 33.- Time development of density for unstable system with $N = 3000$.

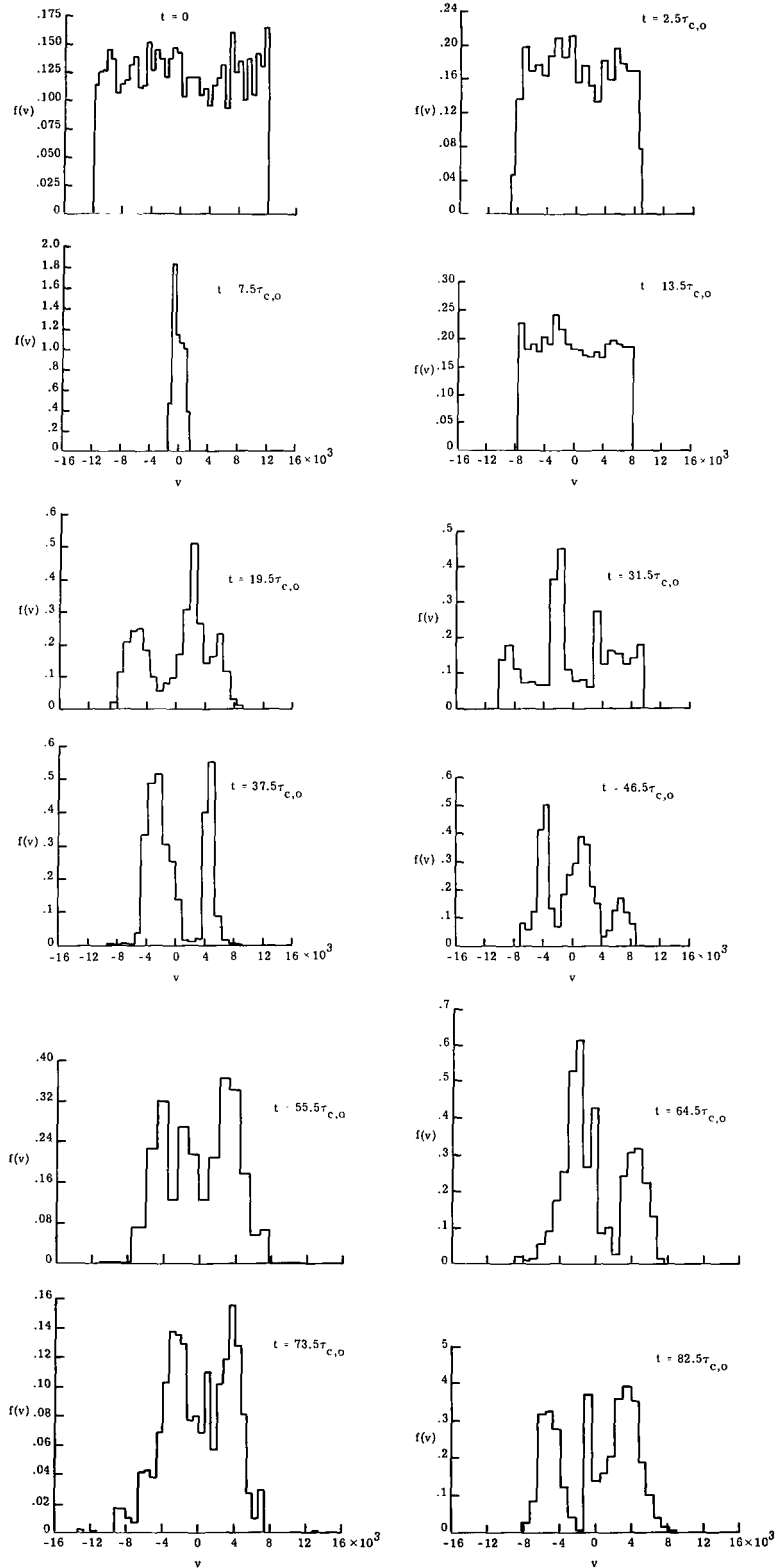


Figure 34.- Time development of velocity distribution function for unstable system with $N = 3000$.

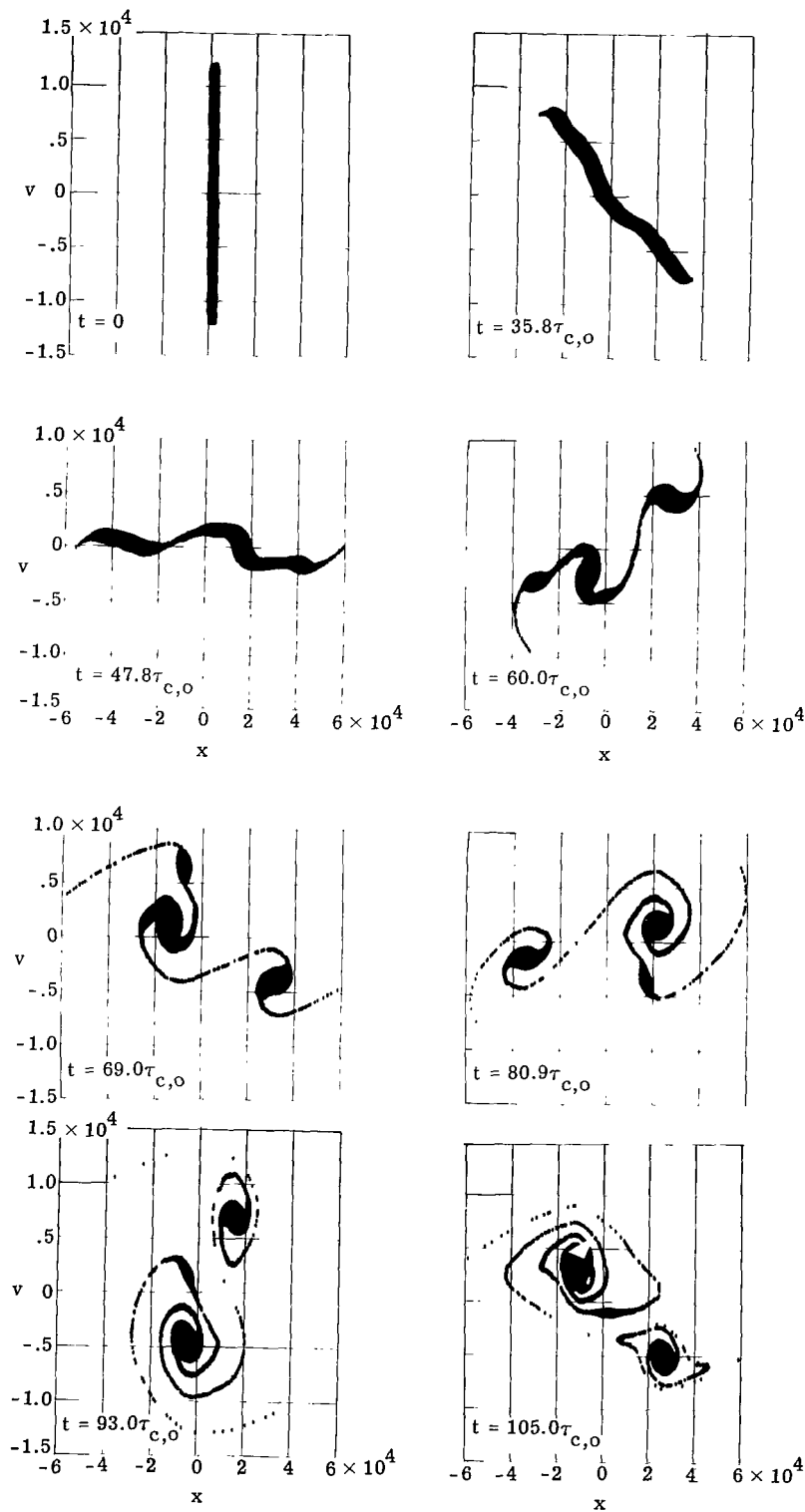


Figure 35.- Time development in phase space for unstable system with $N = 3000$.

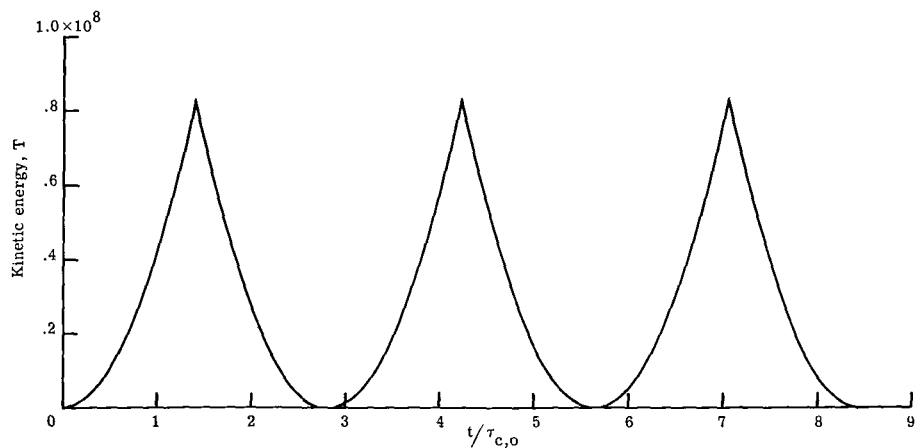


Figure 36.- Time development of kinetic energy for "cold" system.

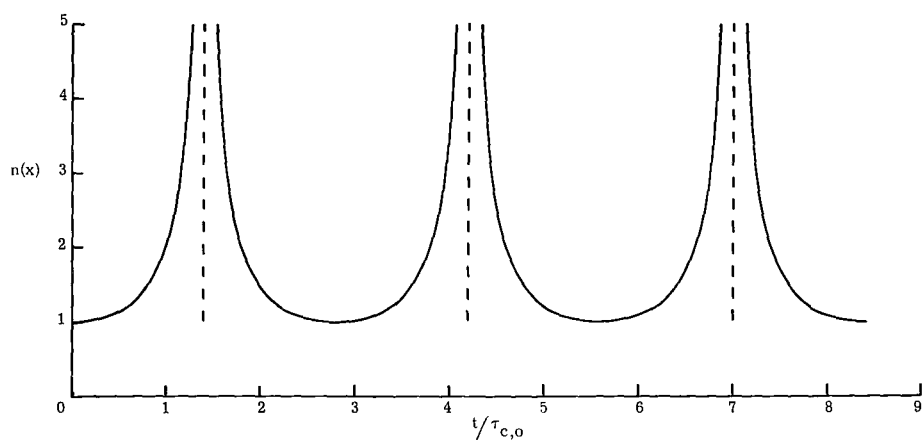


Figure 37.- Time development of density for "cold" system.

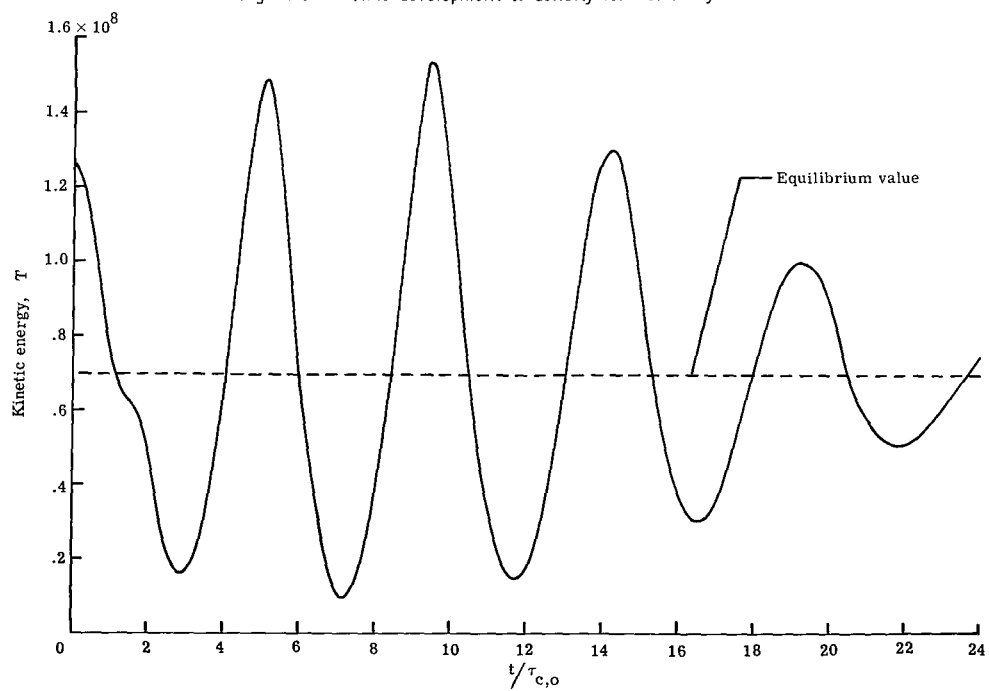


Figure 38.- Time development of kinetic energy for initial two-stream distribution.

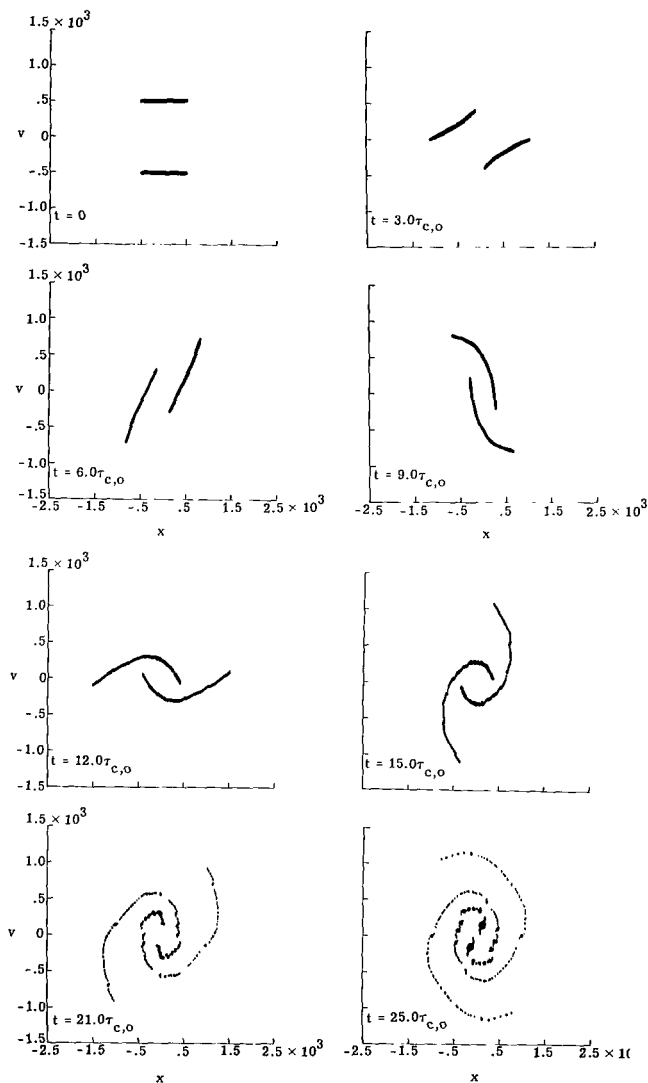


Figure 39.- Time development of system of 1000 stars with initial two-stream distribution.

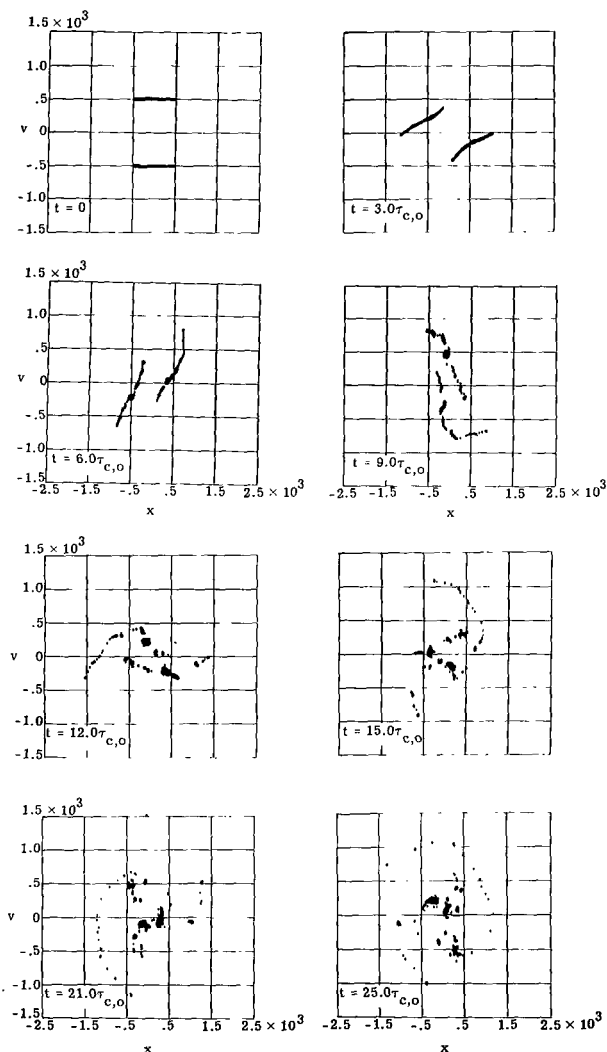


Figure 40.- Time development of system of 1000 stars with initial random two-stream distribution.

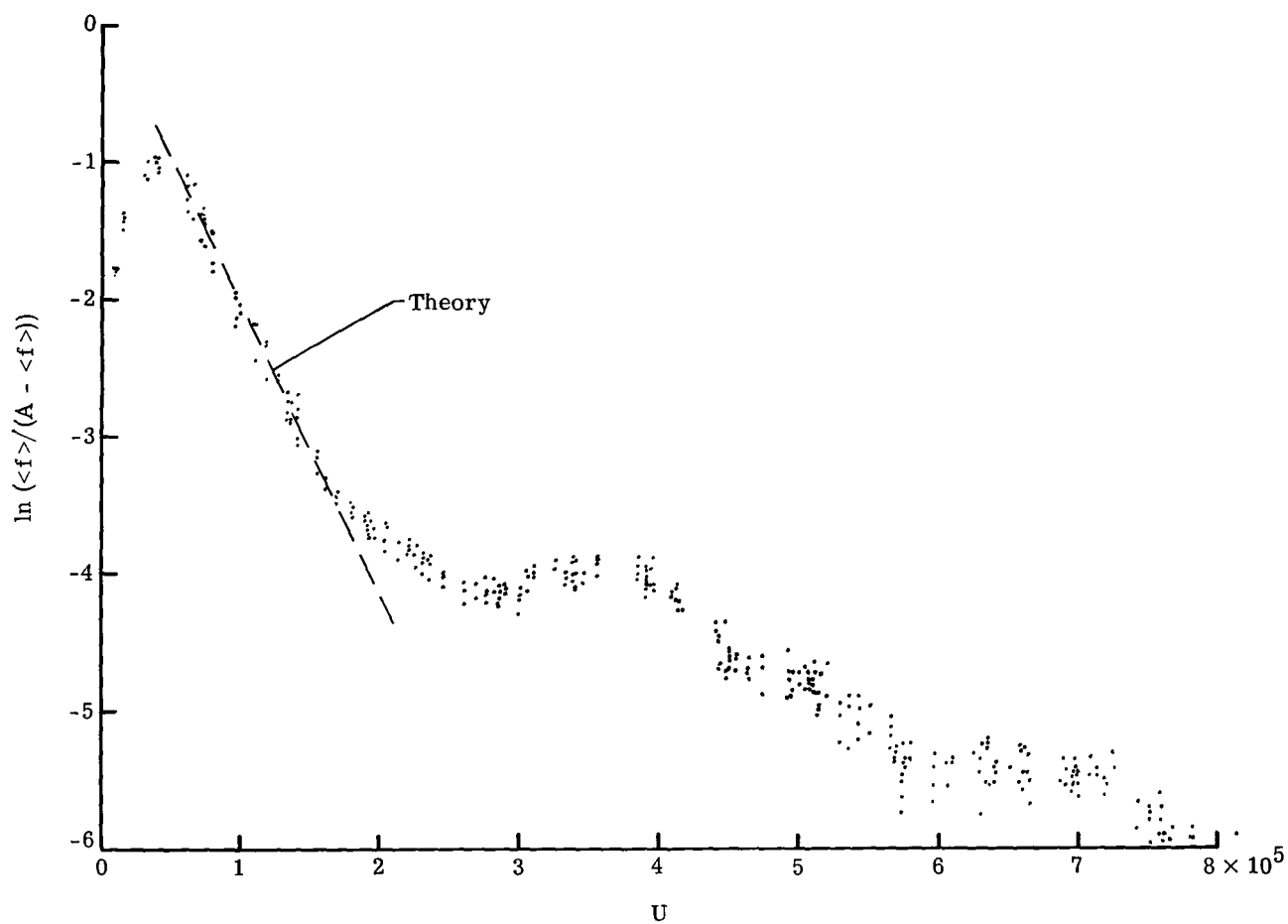


Figure 41.- Plot of $\ln(\langle f \rangle / (A - \langle f \rangle))$ as function of energy
for system shown in figure 39.

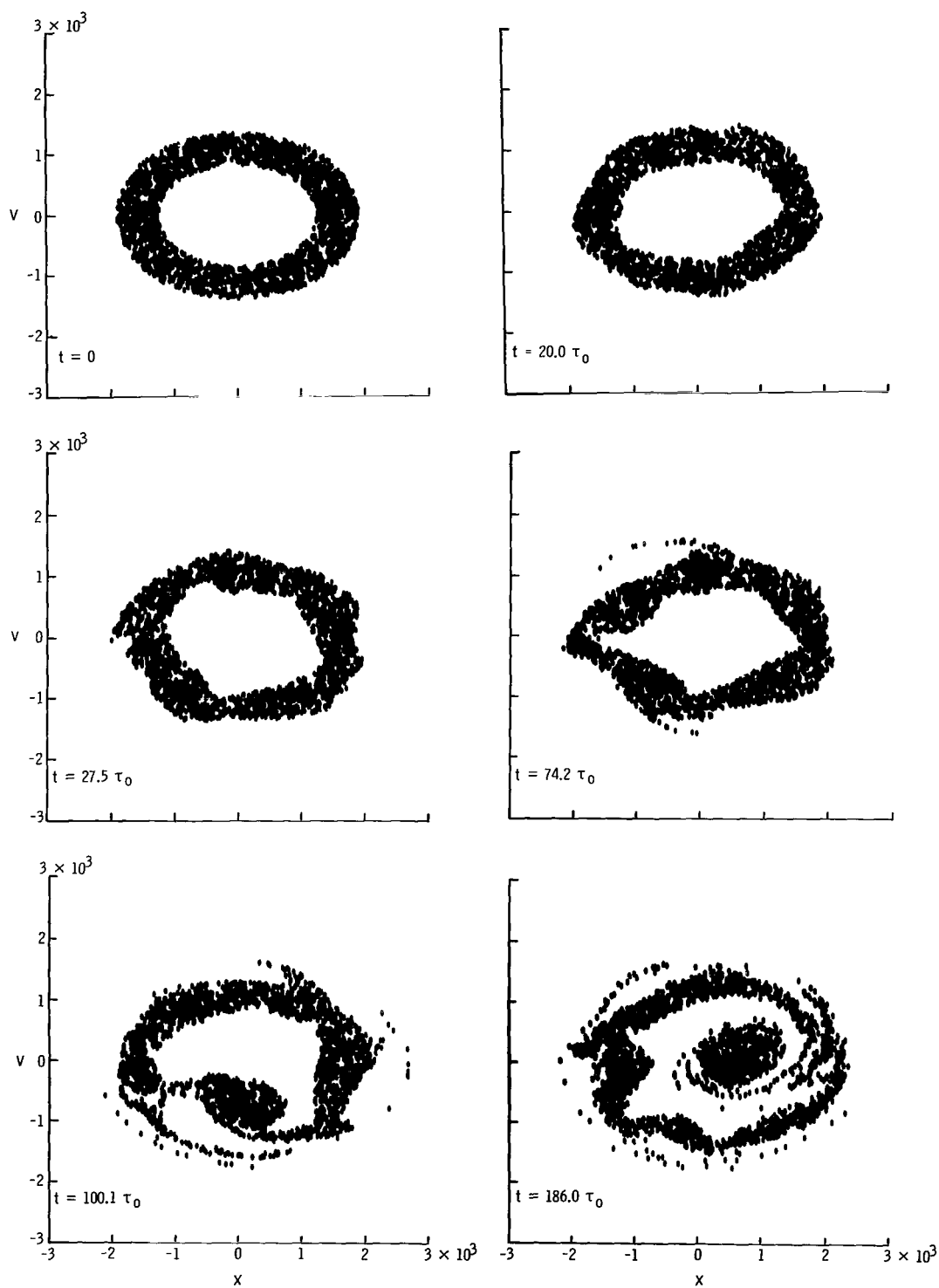


Figure 42.- Illustration of time development of unstable two-contour system with $\nu = 0.4$.

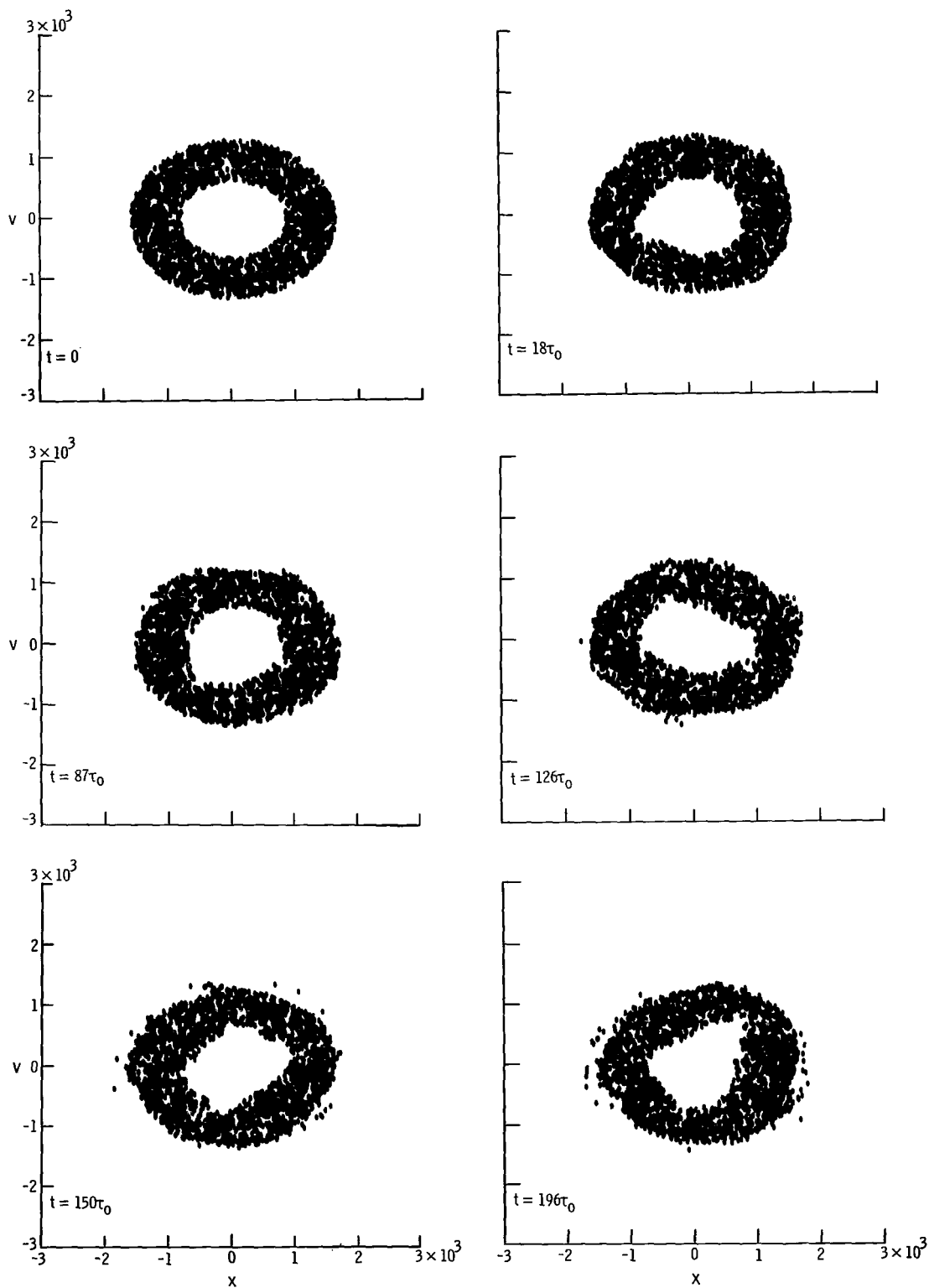


Figure 43.- Illustration of time development of unstable two-contour system with $\nu = 0.25$.

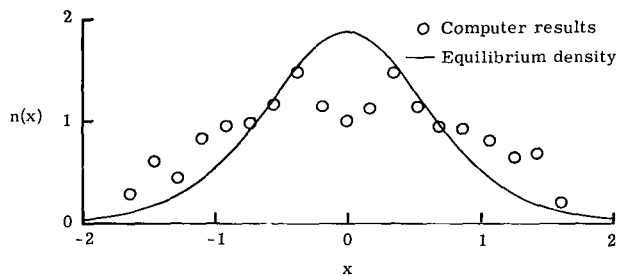
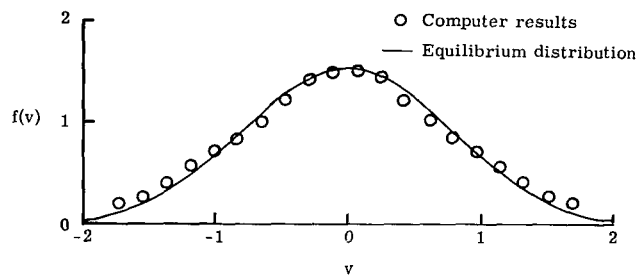


Figure 44.- Time-averaged velocity distribution and density for three-particle system.

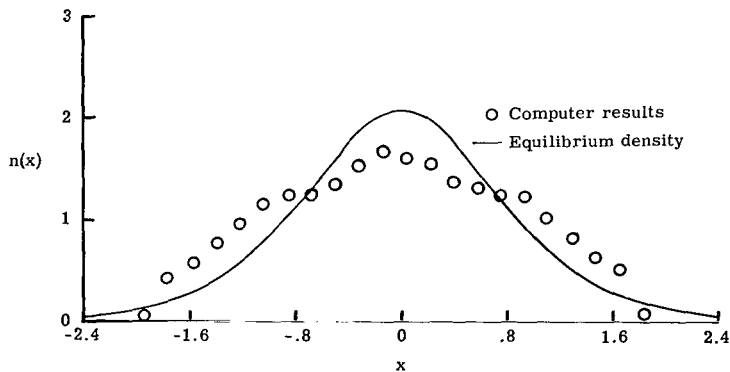
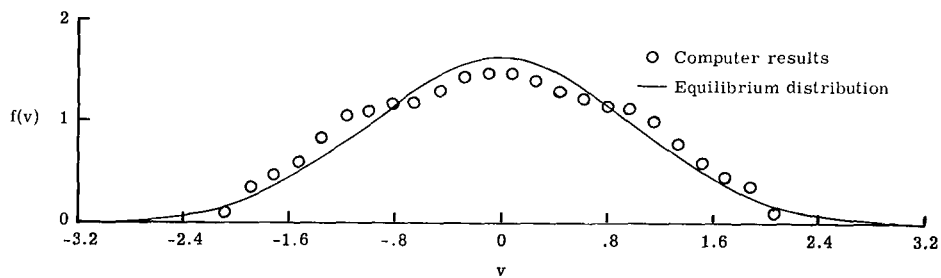


Figure 45.- Time-averaged velocity distribution and density for four-particle system.

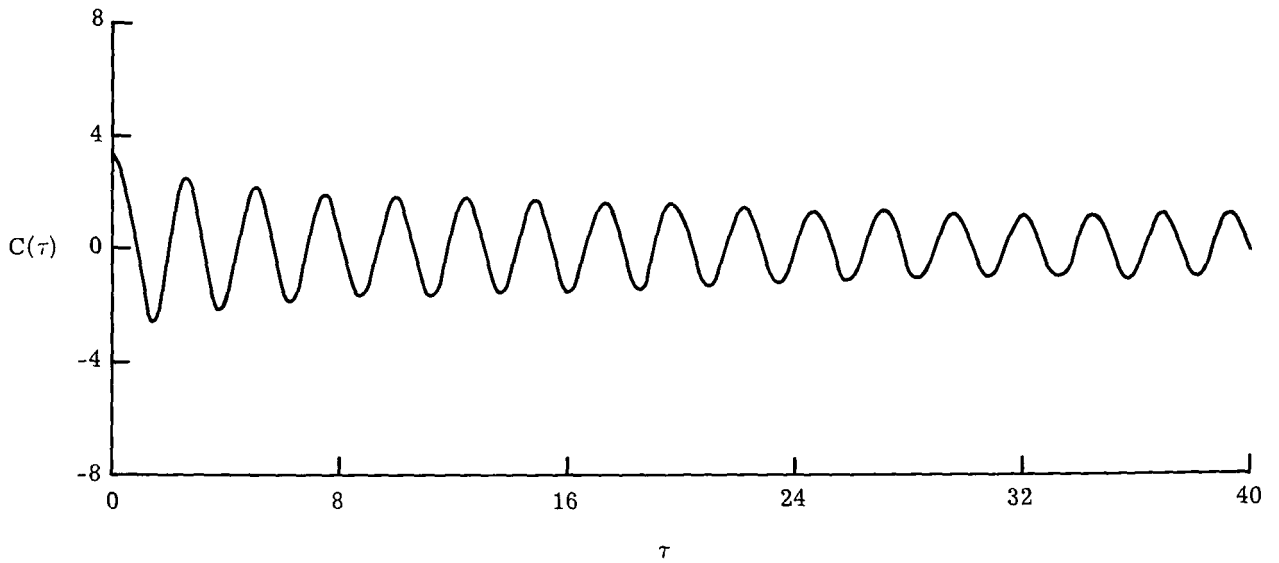


Figure 46.- Energy correlation function for six-particle system averaged over $20N^2$ periods.

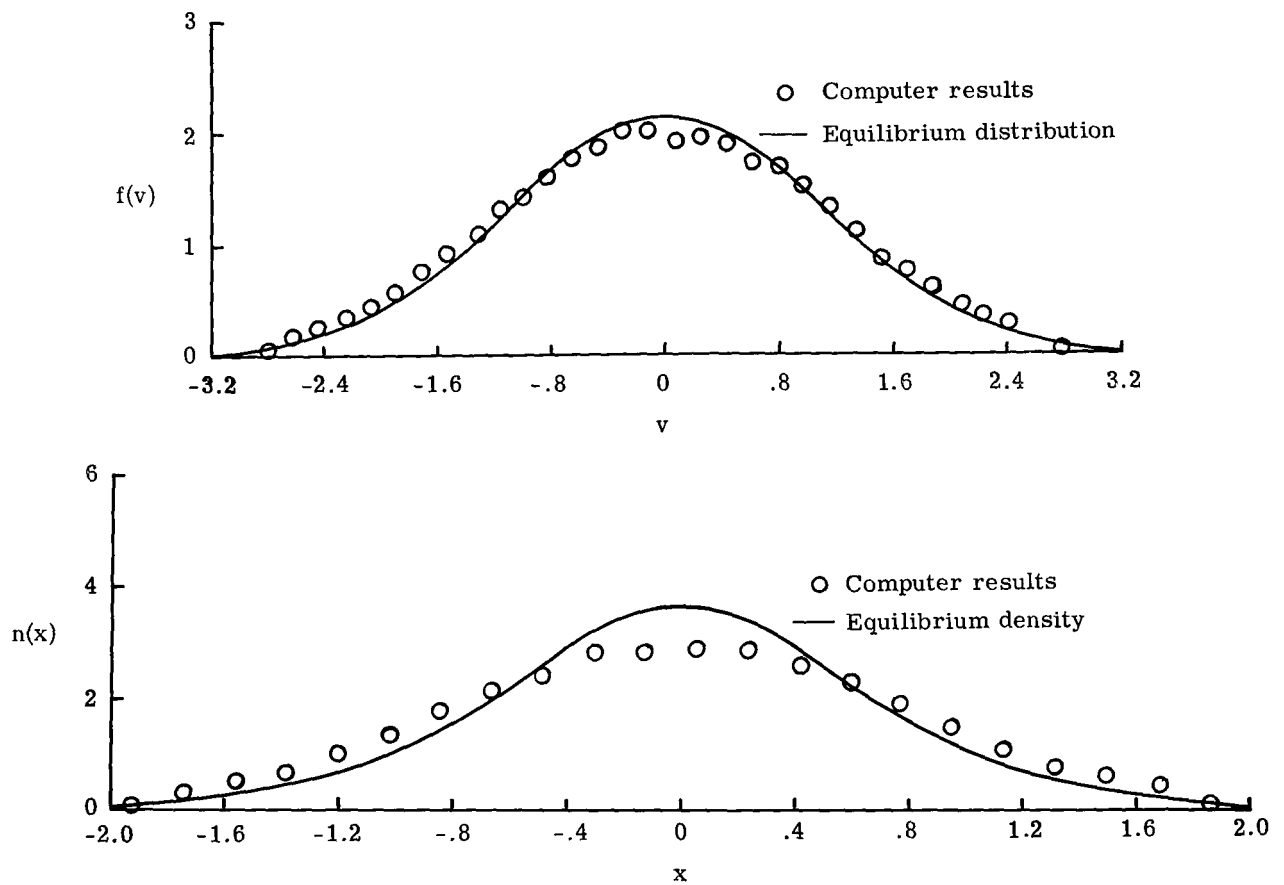


Figure 47.- Time-averaged velocity distribution and density for six-particle system.

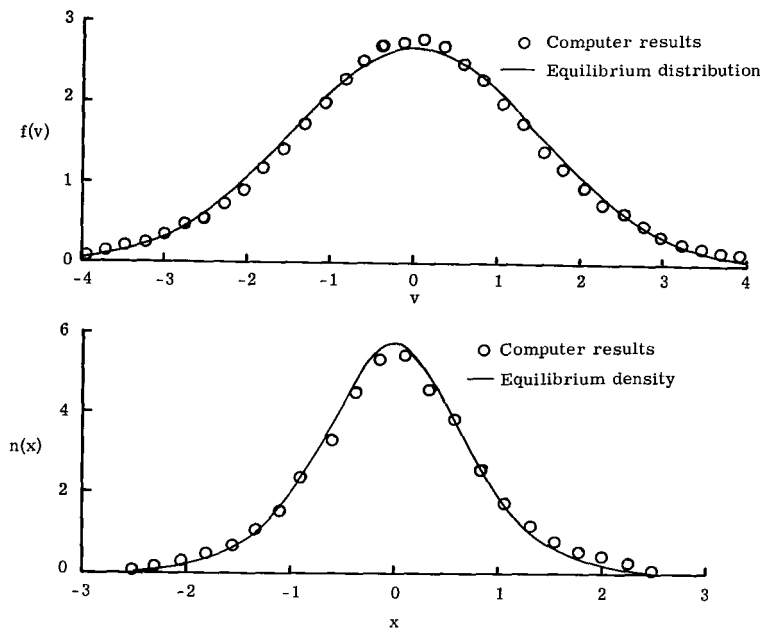


Figure 48.- Time-averaged velocity distribution and density for 10-particle system.

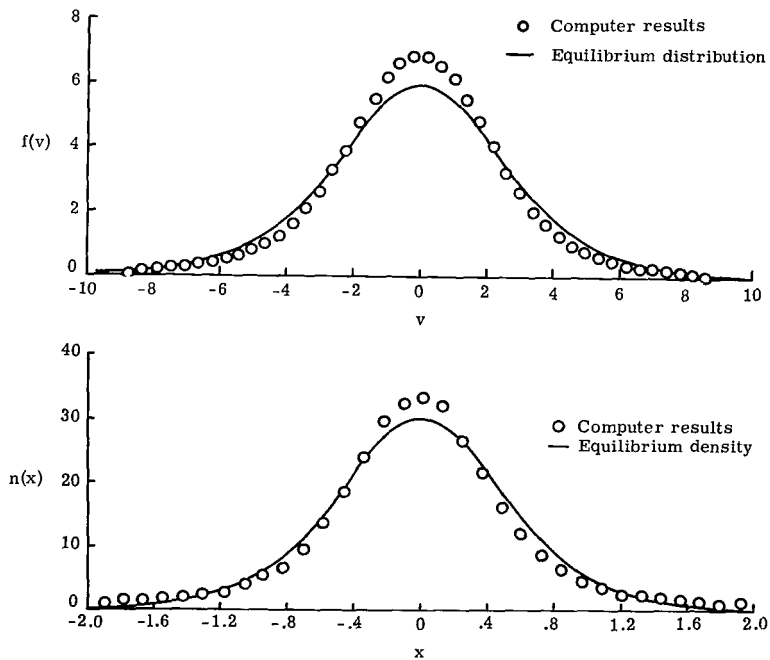


Figure 49.- Time-averaged density and velocity distribution for 40-particle system.

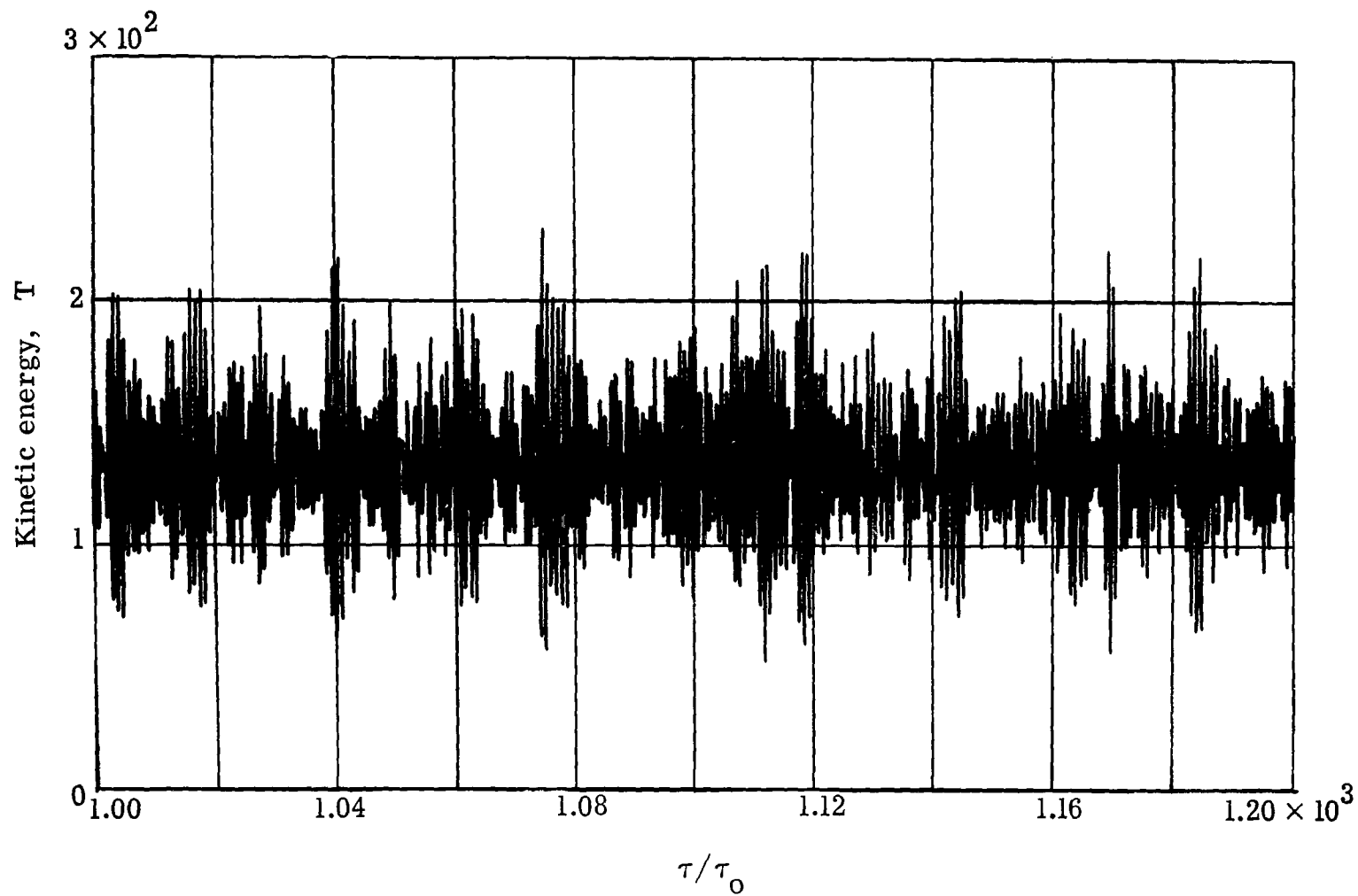


Figure 50.- Time variation of kinetic energy for 40-particle system.

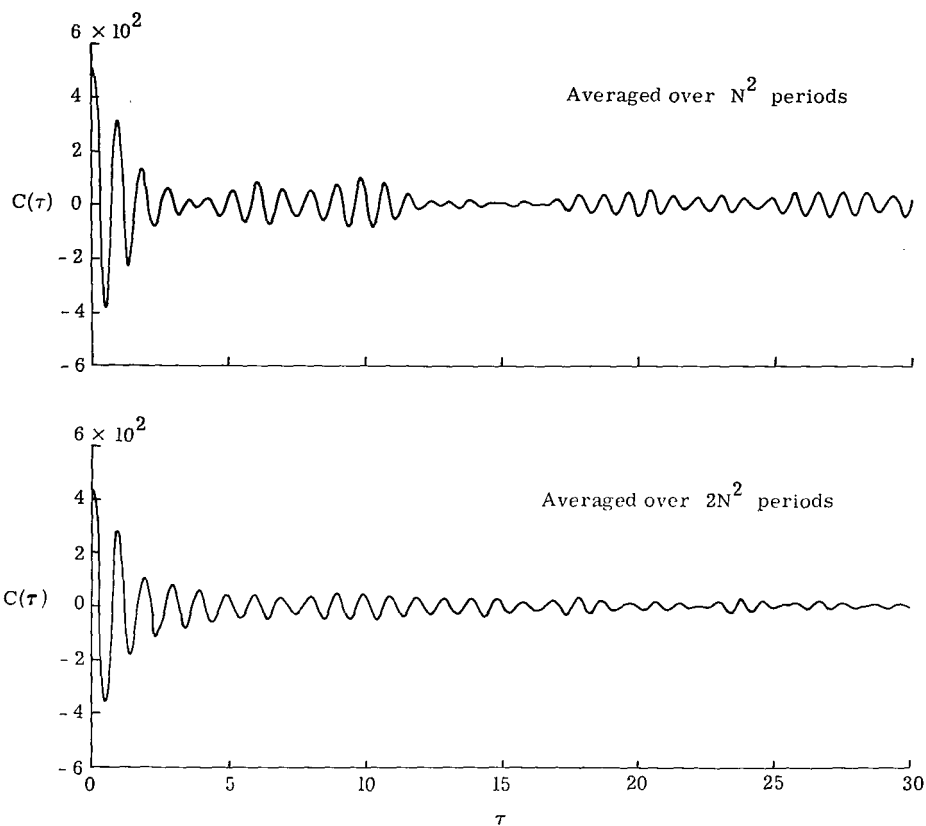


Figure 51.- Energy correlation function for 40-particle system.

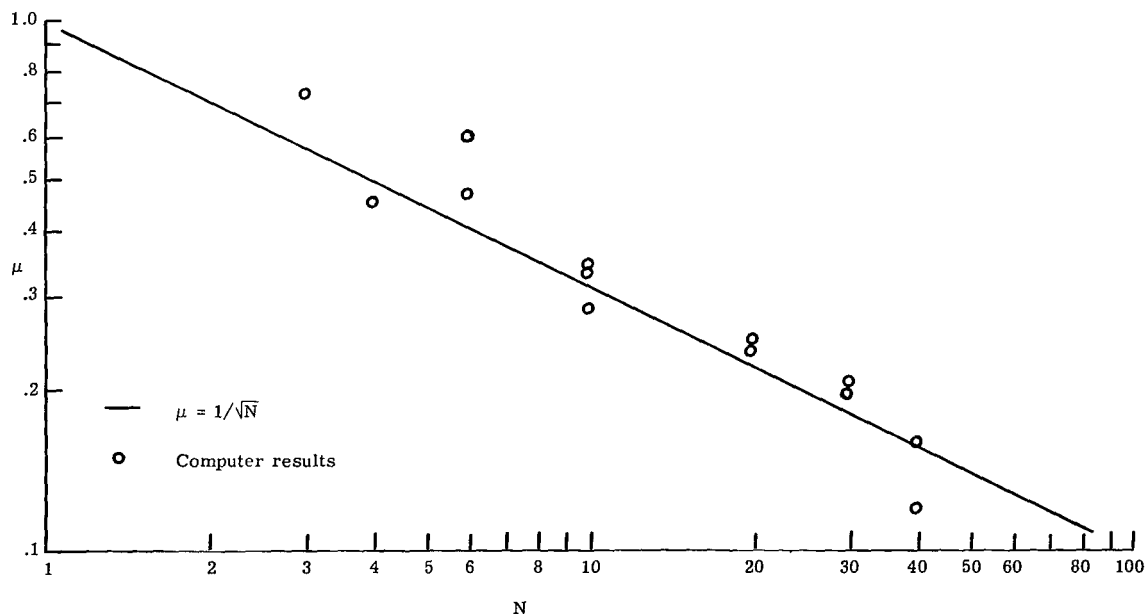


Figure 52.- Fluctuation in kinetic energy of system as function of number of particles.

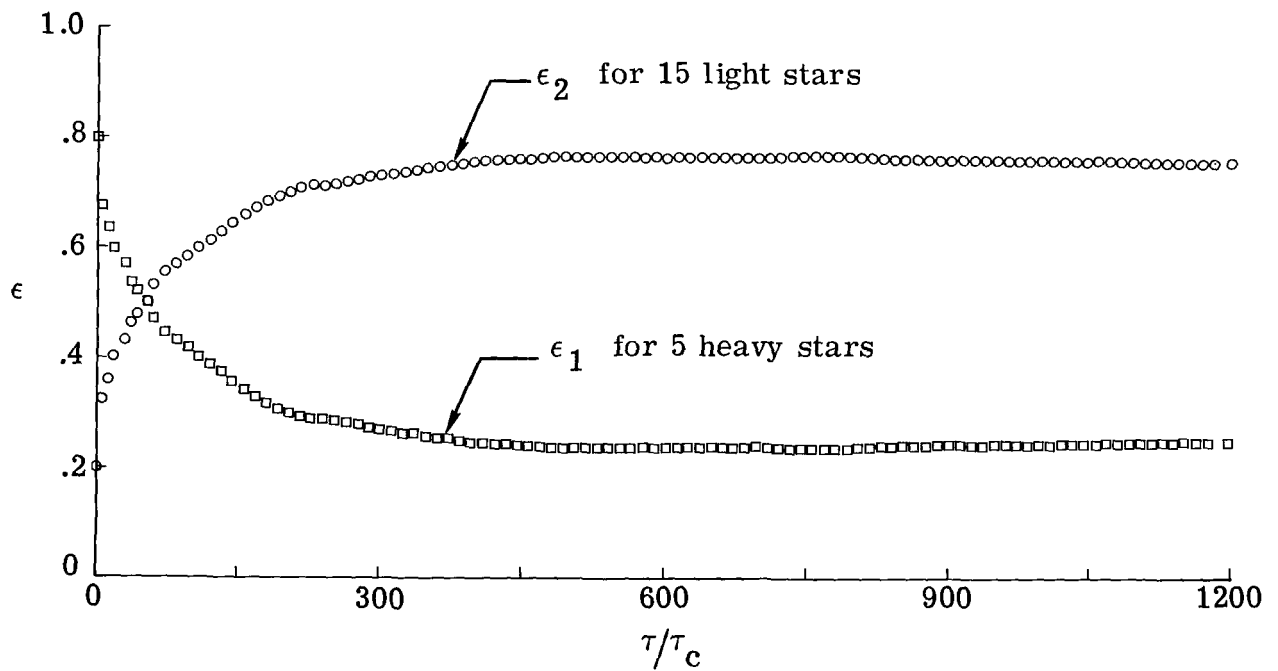
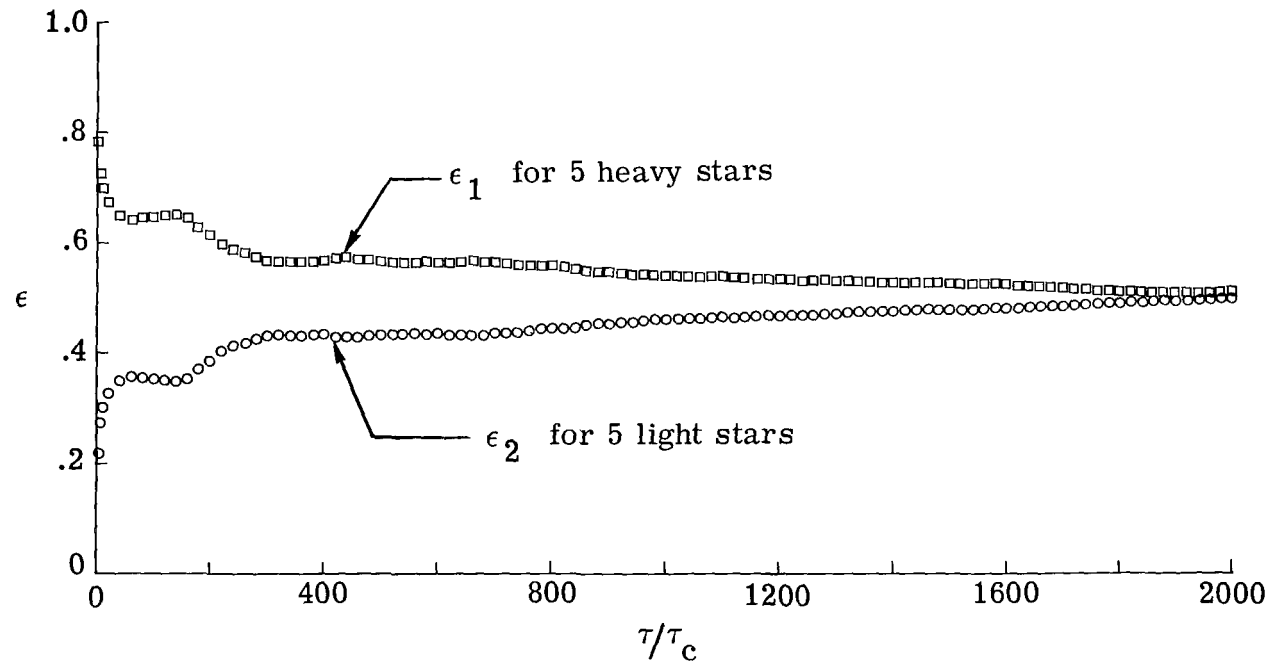


Figure 53.- Illustration of equipartition of energy.

POSTMASTER: If Undeliverable (Section 158
Postal Manual) Do Not Return

"The aeronautical and space activities of the United States shall be conducted so as to contribute . . . to the expansion of human knowledge of phenomena in the atmosphere and space. The Administration shall provide for the widest practicable and appropriate dissemination of information concerning its activities and the results thereof."

— NATIONAL AERONAUTICS AND SPACE ACT OF 1958

NASA SCIENTIFIC AND TECHNICAL PUBLICATIONS

TECHNICAL REPORTS: Scientific and technical information considered important, complete, and a lasting contribution to existing knowledge.

TECHNICAL NOTES: Information less broad in scope but nevertheless of importance as a contribution to existing knowledge.

TECHNICAL MEMORANDUMS: Information receiving limited distribution because of preliminary data, security classification, or other reasons.

CONTRACTOR REPORTS: Scientific and technical information generated under a NASA contract or grant and considered an important contribution to existing knowledge.

TECHNICAL TRANSLATIONS: Information published in a foreign language considered to merit NASA distribution in English.

SPECIAL PUBLICATIONS: Information derived from or of value to NASA activities. Publications include conference proceedings, monographs, data compilations, handbooks, sourcebooks, and special bibliographies.

TECHNOLOGY UTILIZATION PUBLICATIONS: Information on technology used by NASA that may be of particular interest in commercial and other non-aerospace applications. Publications include Tech Briefs, Technology Utilization Reports and Notes, and Technology Surveys.

Details on the availability of these publications may be obtained from:

SCIENTIFIC AND TECHNICAL INFORMATION DIVISION
NATIONAL AERONAUTICS AND SPACE ADMINISTRATION
Washington, D.C. 20546